Annual Summary Report
Contract AF 61 (052)-506

Research on Antennas

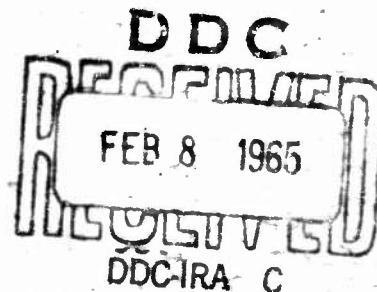I. Rod Antenna with Tunnel Diode
II. Scimitar Antennas

Prof. Dr. H. H. Meinke

Institut für Hochfrequenztechnik

der Technischen Hochschule München

Contract AF 61(052)-506

Annual Summary Report No.3

for the period 1.Sept. 1963 - 3o. Sept. 1964

Part I.   Rod antennas with integrated tunnel diode
Part II.   Scimitar antennas

Professor Dr.H.H.Meinke
Institut für Hochfrequenztechnik
Technische Hochschule
München (Germany)

Abstract

This annual report consists of two independent parts

I.   Rod antennas with integrated tunnel diodes

II. Scimitar antennas

Part I is concerned with the basic possibility to divide an antenna rod in 2 parts and to join these parts by help of a concentrated complex impedance with negative resistance. This complex impedance is produced by shunting a tunnel diode with a short circuited line of variable length.

$$b = \lambda/4$$

h_1

groundplane

feeder
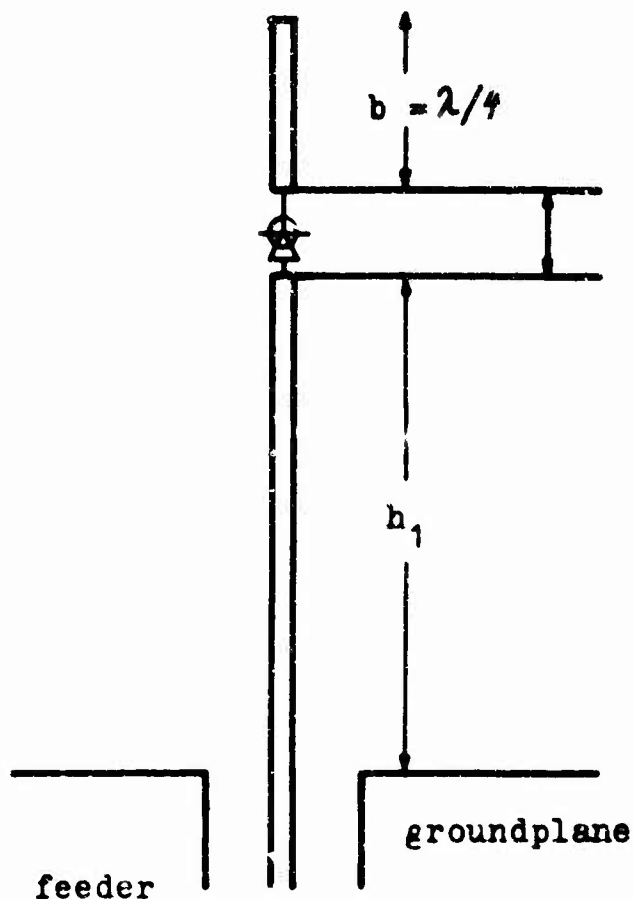
The upper part of the rod had an length of a quarter wavelength
to get an optimum effect of the negative resistance. The short
circuited line was housed in the interior of the upper part of
the rod. The length h_1 of the lower part of the rod was variable.
We investigated theoretically the current distribution on the
rod, the input resistance at the feeding point, the amplifica-
tion factor and the mutual coupling between 2 parallel rods of
this kind. We constructed such antennas and measured the input
impedance and the alternating voltage across the tunnel diode.
As stability problems arise with every application of negative
resistances we studied the stability of this arrangement in-
cluding the feeding system and found measures to avoid self
excitation. Basic methods for measuring the mutual coupling bet-
ween parallel rod antennas were developed.

Part II is concerned with a study on scimitar antennas, at first
scimitar antennas of conventional form, secondly of improved
form with broadband matching of the input impedance to the cha-
racteristic impedance of standard coaxial feeding cables. For
better understanding the complicated and frequency dependent
radiation diagram we measured the current distribution on the
scimitar antenna (amplitude and phase) and on the ground plane
in the near field. Further we measured the distribution of the
electrical field strength on the scimitar and on the ground
plane (amplitude and phase). This was done at many frequencies in
a range 1 : 4. We measured the accompaning radiation patterns for
these frequencies in both polarisation directions, vertical and
horizontal. We could explain the frequency dependent behaviour of
the radiation diagram by help of the near field measurements in
broad outline. The measured input impedances are around 2oo Ω,
except at low frequencies. To improve matching of the input for
the lower frequencies we insulated the scimitar from the ground
plane and put resistors between scimitar and ground plane. Thus
we had a better broadband matching, but of course some power loss
in these resistances at lower frequencies. To improve matching
to the characteristic impedance of standard feeding cables we

found a new form of scimitar antennas, whose input impedance is nearly 50Ω in a broad frequency range. To avoid some unwanted effects of the radiation patterns we tested a double scimitar antenna with 2 scimitars in opposite direction.

Table of contents

I. Rod antenna with integrated tunnel diode

Preface.

Conventional antennas constructed with passive elements show
some fundamental limitations concerning impedance behaviour
and radiation patterns. To overcome these limits there is some
hope to get new possibilities by integrating active elements
with antennas. Antennas with active elements have been dis-
cussed in various reports [1,2,3]. The object of this report is
the investigation of an antenna consisting of an unipole with
the total height of 3/4 wavelenths loaded with a tunnel diode
(TD) one quarter wavelength from its end. In particular sta-
bility against self excitation is discussed also the corres-
ponding impedance measuring equipment is described.

In [4] E.E. Altschuler reports about a similar antenna which con-
tains a normal resistor instead of TD. Altschuler showed experi-
mentally that by careful choice of the magnitude of this re-
sistance an essentially traveling-wave distribution of current
can be produced on the antenna and that mutual coupling effects
of such traveling-wave antennas are much less pronounced than
for conventional linear antennas. At first we study simple
structures integrated with one tunnel diode. To get an idea
what may be expected as effects of integrated negative resistan-
ces we calculate and measure input impedances, current dis-
tribution, radiation patterns and mutual coupling between parallel
antennas. In this time we do not look for special application,
but only for collecting general experience. Already in our
Final report of 30.April 1963 we described measurements of a
folded dipole with a tunnel diode interrupting the wire in the
vertex of the folded wire. In this new report we use a rod an-
tenna, the rod divided in 2 parts andjoined again by a complex
impedance with negative resistance. This complex impedance is
produced by a tunnel diode shunted by a short circuited line of
variable length. The effect of this negative resistance depends

on its position on the rod, expecially on the distance from the
end of the rod. The effect of the negative resistance is propor-
tional to the current flowing through the resistance. There-
fore in our fundamental experiments the tunnel diode was moun-
ted in a distance of a quarter wavelength from the open end of
the rod, i.e. in a point of maximum current, to assure maxi-
mum effect of the tunnel diode. To bring the d.c. voltage to
the upper end of the diode an additional wire is necessary,
which acts as a short circuited line at high frequencies. This
line is brought into a well defined coaxial form and provided
with a movable short circuit so that it produces a well defined
and variable reactance parallel to the tunnel diode resistance.
In this way the tunnel diode with the parallel line gives a vari-
able complex impedance and by varying the short circuit the
behaviour of the antenna can be widely changed for different
experiments. Further we can change the length of the upper part
of the rod and thus have two important variables in our antenna.
This may explain why we have chosen this special form of a rod
antenna for our research.

When using negative resistances the main problem is to avoid
self-excitation of the complete system at all freqquencies. The
stability of the circuits must be checked from very low fre-
quencies to very high frequencies. The demand for stability
excludes many favourable circuit forms and mostly imposes un-
wanted restrictions to the system. A negative resistance in
any circuit will always be an element which is to handle with
care and will not give to much freedom in the design of a system.

When estimating a possible progress of antenna characteristics
by using tunnel diodes the possibility of amplification seems
to be no special progress as in most cases a tunnel diode am-
plifier in the feeding point or at the input of the receiver may
produce the same amplification (or better) by more simple
arrangements. The same may happen with all ideas to change the
frequency dependence of the input impedance by an integrated
tunnel diode. Probably the same change of impedance mostly
may be found by simply using a twoport-network containing a

tunnel diode at the feeding zone. Certainly it is easier to
apply measuries of this kind at the feeding point than to apply
them at any other region of the antenna itself.

Therefore valuable applications of integrated tunnel diodes in
antennas will mostly be restricted to cases where the current
distribution will be favourably changed by the impedance of the
diodes. This may particularly refer to changes of radiation
pattern and to changing the mutual coupling between parallel
rods. We have not yet studied changes of radiation patterns,
as our test ground was occupied by other antenna measurements
this year. But we did extended work on the mutual coupling bet-
ween parallel rods, especially in the direction of eliminating
the coupling between parallel rods by changing the current dis-
tribution. This is a very important problem in modern antenna
technique.

We made basic experiments to find methods for measuring the
mutual coupling and to define a very general coupling factor.
Theoretical considerations and first measurements are discribed
in this report.

1. Principal Arrangement

The principal arrangement of the antenna to be investigated is shown in Fig. 1a.

Fig.1a   Fig.1b
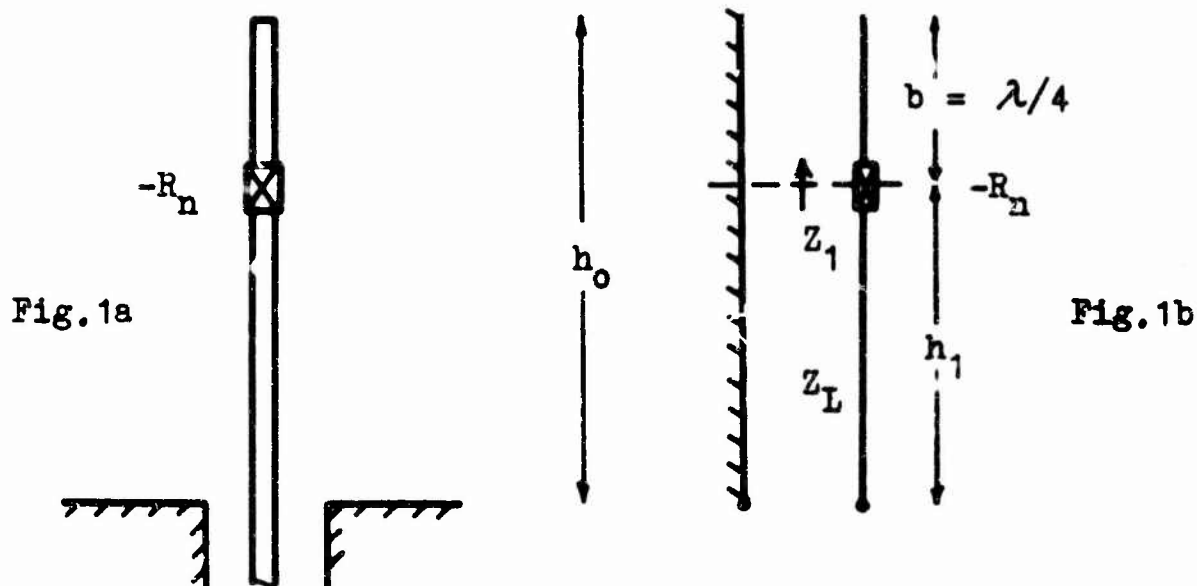
It consists of a conventional unipole, which is interrupted at the distance $b = \lambda/4$ from the open end by a negative resistance (TD). As a first approximation this antenna circuit can be replaced by an equivalent transmission line circuit as shown in Fig. 1b. According to transmission line theory the input impedance of an open circuited line with a length of $\lambda/4$ is very small. Therefore the arrangement acts as if the equivalent line is terminated at the height h_1 by the negative impedance $- R_n$ of the tunnel diode. In this report we are especially dealing with the case $R_n = Z_L$ (negative matching). If Z_1 is matched to the characteristic impedance Z_L of the equivalent line ($Z_1 = - Z_L$), a traveling wave runs down the antenna from $-R_n$ to the feeding point. On the quarter wavelength top of the antenna there remains a standing wave.

2. Negative Resistance of TDs

One of the simplest elements to produce a negative reistance is
a TD. Since many reports deal with TDs only their most important
properties shall be described. Feeding a TD with a suitable
bias voltage its ac-behaviour may be expressed by the equivalent
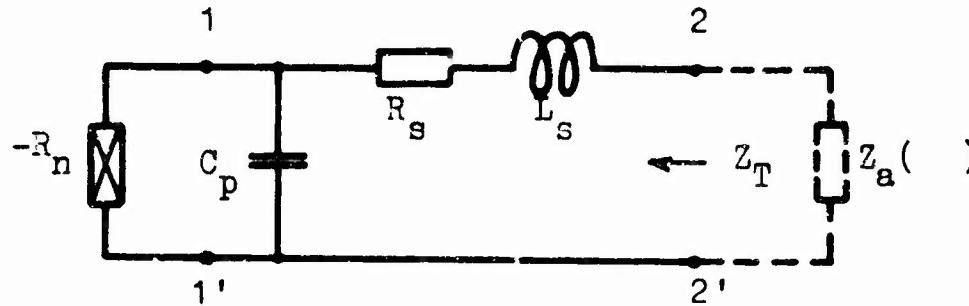network of Fig.2.

Fig.2

In parallel with the negative resistance $-R_n$ lies the capacity
C_p caused by the space charge of the blocking layer. In series
with this circuit is the resistance R_s (resulting from the ohmic
resistance of the connecting wire and the path resistance of the
semi-conductor crystal) and the inductance L_s (also caused by
the connecting wire).

The characteristic curve for the input impedance Z_T of the TD
is shown in Fig.3.

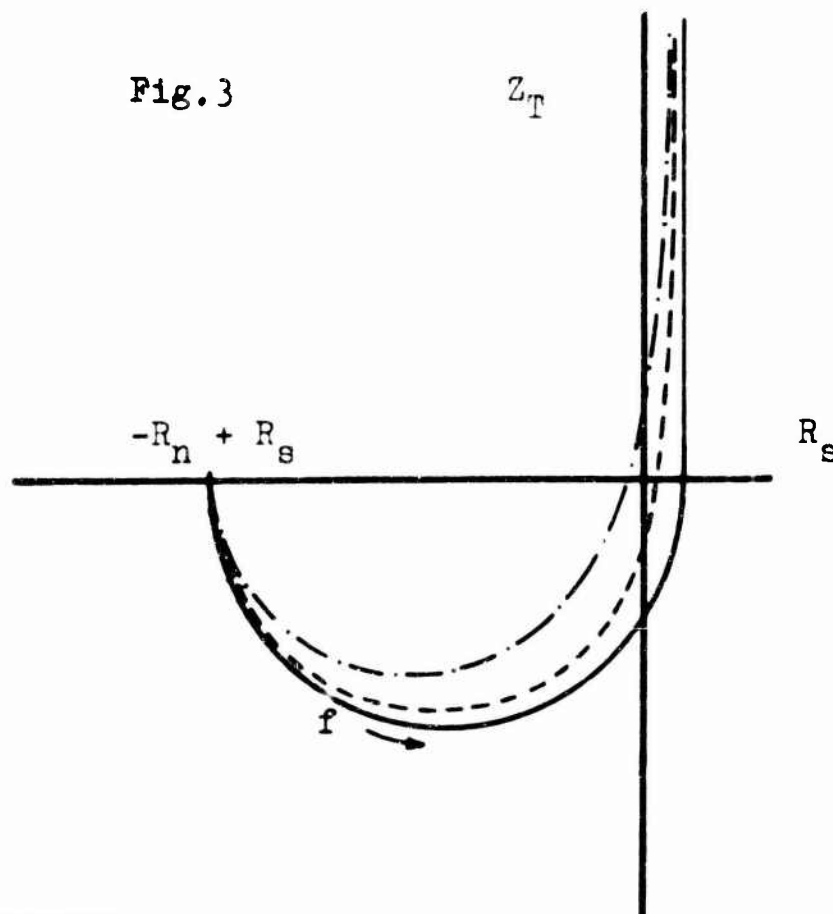

Fig.3

The solid curve is valid for $L_s = 0$, whereas the dashed curve and the dash dot curve represent the input impedances for different values of L_s.

Above that frequency, where the characteristic curve intersects the imaginary axis, an active behaviour of the TD is no more percebtible at the terminals 2-2'. The cut-off frequency defined this way results from the following equation:

$$f_g = \frac{1}{2\pi C_p R_n} \sqrt{\frac{R_n}{R_s} - 1}$$

(4)

3. Stability of Antenna Systems containing TDs

Because of its ability to deliver power into a passive network, a negative resistance always is in danger to produce a self-excitation. The decision about the stability of a circuit may be done by solution of a diffential equation or by the following method:

The negative resistance $-R_n$ is connected with the terminals A and B of a passive and linear network (Fig.4a).
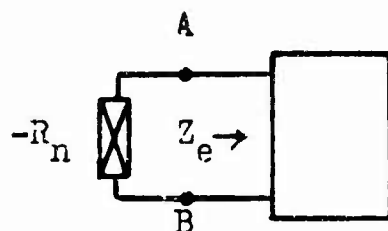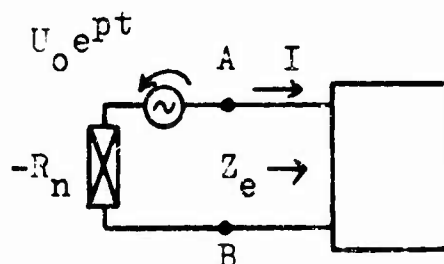

Fig.4a   Fig.4b

To test the stability of this circuit a disturbance generator is inserted as shown in Fig.4b. This generator consists of a source of electromotive force with the amplitude U_0 and the complex frequency $p = \delta + j\omega$; i.e.

$$u = U_0 e^{pt} = U_0 e^{\delta t} e^{j\omega t}$$

u represents a voltage oscillation with the real frequency ω that increases exponential with the time constant $1/\delta$. The resulting current I with the frequency p then is:

$$I = \frac{U_o}{Z_e(p) - R_n} \tag{5}$$

In this expression $Z_e(p)$ is the input impedance of the circuit $\overline{AB}$ for the complex frequency p. It results from the normal input impedance by simply replacing $j\omega$ by p.

The current I will become very great, if the denominator in equ. (5) becomes zero. The condition for this is:

$$Z_e(p) = R_n \tag{6}$$

$p = \delta + j\omega$ can be eliminated out of equ. (6). If there exists a solution $p_o = \delta_o + j\,\omega_o$ and $\delta_o > 0$, an oscillation of this frequency will excite itself out of a small disturbance. However, if there are only solutions with $\delta < 0$, all disturbances die away very soon - the circuit is stable. The elimination of p in equ. (6) generally is difficult and not necessary, because the accurate excitation frequency mostly is of little interest and the only assertion required is, whether the circuit is stable or not.

$Z_e(p)$ means a conformal mapping of the p-plane into the Z_e-plane. In particular the ω-axis of the p-plane is transformed into the characteristic impedance curve $Z_e(\omega)$. The area $\delta > 0$ on the right side of the ω-axis in the frequency plane p (running from $-\infty$ to $+\infty$) is mapped into the area on the right side of the characteristic impedance curve in the Z_e-plane. In addition with equ. (6) this leads to the following condition for stability [3] :

The circuit shown in Fig. 4a is stable, if the characteristic curve of the input impedance $Z_e(\omega)$ does not encompass the point R_n in such a manner that R_n lies on the right hand side of the characteristic curve. Assuming that the characteristic impedance curve to be discussed is steadily turning clockwise, and that the input impedance becomes very small at high frequencies (because of parallel capacities) it is allowed to simplify the Stability Criterion as follows: The circuit of Fig.4a is stable, if the characteristic input impedance curve does not intersect the real axis at values $R > R_n$. For the TD this means that at the terminals 1-1' (Fig.2), seen from $-R_n$, a real resistance greater than R_n must not appear.

At low frequencies

the stability is determined by the dc-voltage supply and one may neglect the fourpole of Fig.2. This circuit is shown in Fig.5.
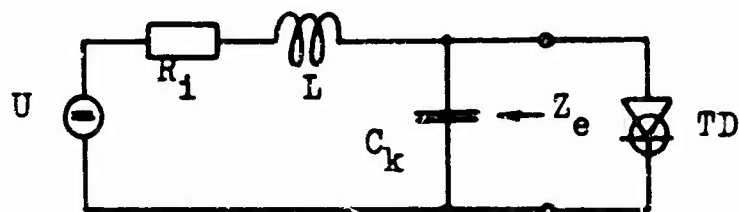

Fig.5

The diode is fed by a dc-voltage source with the internal resistance R_1 through a line whose inductance is represented by L. The capacitor C_k acts as a short circuit for high frequencies. The stability is determined by the input impedance Z_e:

$$Z_e(\omega) = \frac{R_i + j[\omega L(1-\omega^2 L C_k) - \omega C_k R_i^2]}{(1-\omega^2 L C_k)^2 + (\omega R_i C_k)^2} \qquad (7)$$

Real impedances appear at:

$$\omega_1 = 0 \ ; \quad Z_e(\omega_1) = R_i \ ,$$

$$\omega_2 = \sqrt{\frac{1 - C_k R_i^2/L}{L C_k}} \ ; \quad Z_e(\omega_2) = \frac{L}{C_k R_i}$$

The conditions for stability are: $\quad Z_e(\omega_1) = R_i < R_n \ ; \qquad (8)$

$$Z_e(\omega_2) = \frac{L}{C_k R_i} < R_n \ , \qquad (9)$$

If L is relatively great equ.(9) may not be fulfilled. It is possible then to enlarge the values of R_1 (regarding equ.(8) and C_k. By this means it is not difficult to avoid a low frequency self-excitation.

Considering the <u>stability at high frequencies</u>

the entire equivalent circuit of the TD (Fig.2) is valid. Since 2 and 2' are the terminals of the TD, only the impedance Z_a (see Fig.2) can be measured, whereas the impedance appearing at 1-1' must be calculated. This calculation is rather timewasting because it has to be done for all points of the characteristic curve. This can be avoided by the backward-diagram described in our Final Report No AF 61(052)-506, April 3o. 1963 (Fig.6.
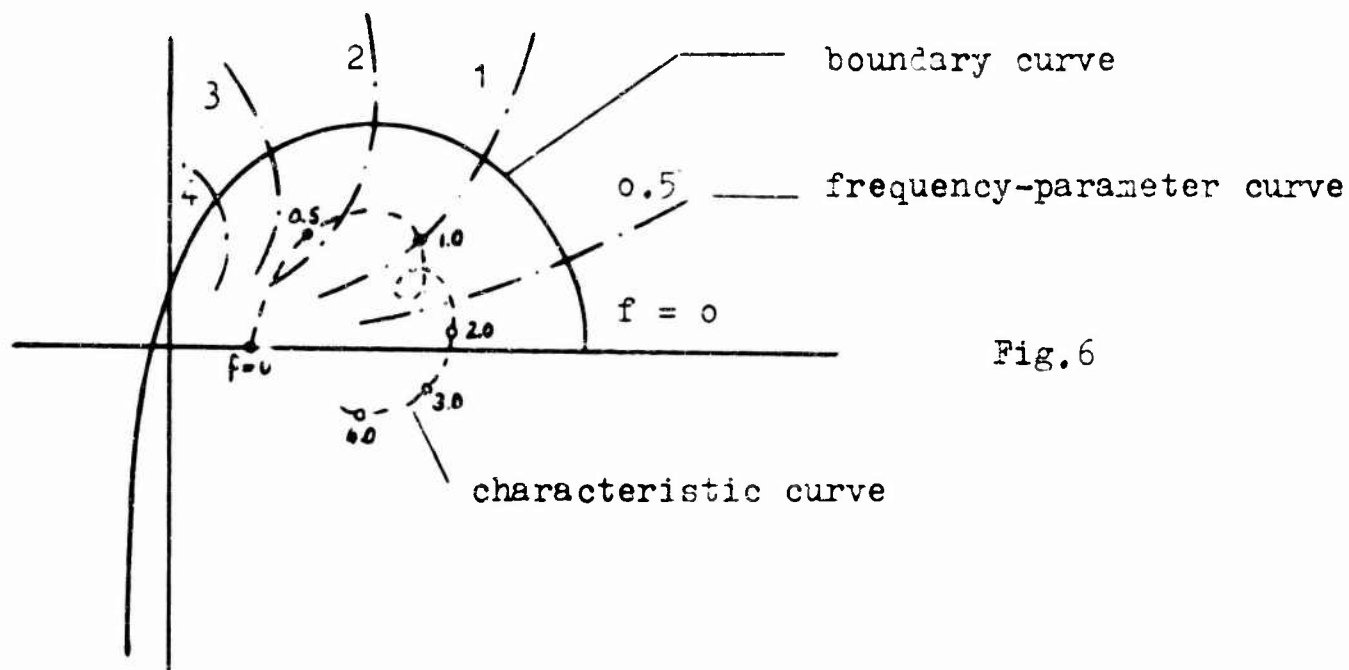

Fig.6

boundary curve

frequency-parameter curve

characteristic curve

Imaging the input impedance curve of the TD (Fig.3) at the origin, the boundary curve is obtained (Fig.6). This curve is the locus of all impedances Z_a which transform into the point R_n for the respective frequency-parameter. Constructing adequate curves for different values R_n' and linking the points of equal frequency, parameter-curves are obtained, which represent the complete backward-diagram together with the boundary curve (Fig.6).

A real impedance at 1-1' will only appear, if the characteristic impedance curve $Z_a(\omega)$ interesects a curve with equal frequency-parameter (for instance $f = 1$ in Fig.6). This point of inter-section being below the boundary curve, Z_a transforms into a real impedance $R < R_n$, the circuit is stable. The point of intersection however being above the boundary curve, the transformed resistance R is greater than R_n and the circuit therefore is instable.

To secure stability, the characteristic impedance curve has to be influenced so that it lies only below the boundary curve or that it has at least no points of intersection with parameter-curves of equal frequency above ist. Since stability at high frequencies was one of the main difficulties in designing the antenna with TD, this problem will be resumed in chapter 5.

If a network is in condition of self-excitation at a frequency far away from the measuring frequency, one would believe that this does only slightly affect the measurements. The following con-sideration shows that this is not true:
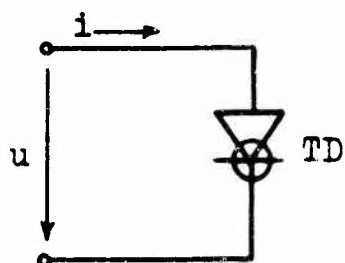

Fig.7

The non linear characteristic of the TD can be transformed into a power series. Regarding Fig.7 the following is valid:

$$i = I_0 + \Delta i = I_0 + S_1 \Delta u + S_2 \Delta u^2 + S_3 \Delta u^3 + \ldots \qquad (10)$$

where $\quad S_1 = \left(\dfrac{di}{du}\right)_{u = u_0} ; \quad S_2 = \dfrac{1}{2}\left(\dfrac{d^2 i}{du^2}\right)_{u = u_0} ; \quad S_3 = \dfrac{1}{6}\left(\dfrac{d^3 i}{du^3}\right)_{u = u_0} ,$

Choosing the operating point to be the point of inflexion, we find

$$S_1 = -\frac{1}{R_n} = -G_n ; \quad S_2 = 0 , \quad S_3 > 0 ,$$

The voltages u_1 and u_2 of the measuring frequency ω and of the self-excitation frequency Ω appear at the TD. Breaking off the series of equ.(1o) after the term of third order, Δi results as:

$$\Delta i = -G_n \left(U_1 \cos \omega t + U_2 \cos \Omega t\right) + S_3 \left(U_1 \cos \omega t + U_2 \cos \Omega t\right)^3,$$

According to well known formulas [5] the current i_1 of the frequency ω is:

$$i_1 = I_1 \cos \omega t = \left(-G_n U_1 + \tfrac{3}{4} S_3 U_1^3 + \tfrac{3}{2} S_3 U_1 U_2^2\right) \cos \omega t,$$

The input admittance G valid for the frequency ω therefore is:

$$G = \frac{I_1}{U_1} = -G_n + \tfrac{3}{4} S_3 \left(U_1^2 + 2U_2^2\right),$$

(11)

G depends as well on U_1 as on U_2. Therefore only at very low levels of U_1 and at $U_2 = 0$, i.e. stability, G is equal to $- G_n$ and reproduceable measurements are possible. As an example Fig.8 shows the input impedance of the antenna with TD at different levels of U_1. The relative level of 0 dB corresponds to a voltage U_1 of approximately 5 mV. Only below this level correct measurements can be performed.

4. Mechanical Antenna Design

As can be seen from Fig.9, 1o, and 11 the antenna consists of a rod over a conducting plane. The rod is mounted on the inner conductor of a measuring line, the latter being mounted below the conducting plane. This inner conductor as well as the antenna itself have been constructed as tubes, thus admitting wires to be drawn through the interior, which allow to supply the TD with bias voltage and to measure the rf-voltage at the diode. At the height h_1 the antenna is interrupted by a link of polystyrol, which contains the TD and some elements to measure the rf-voltage

Fig.   Input Impedance of the antenna-
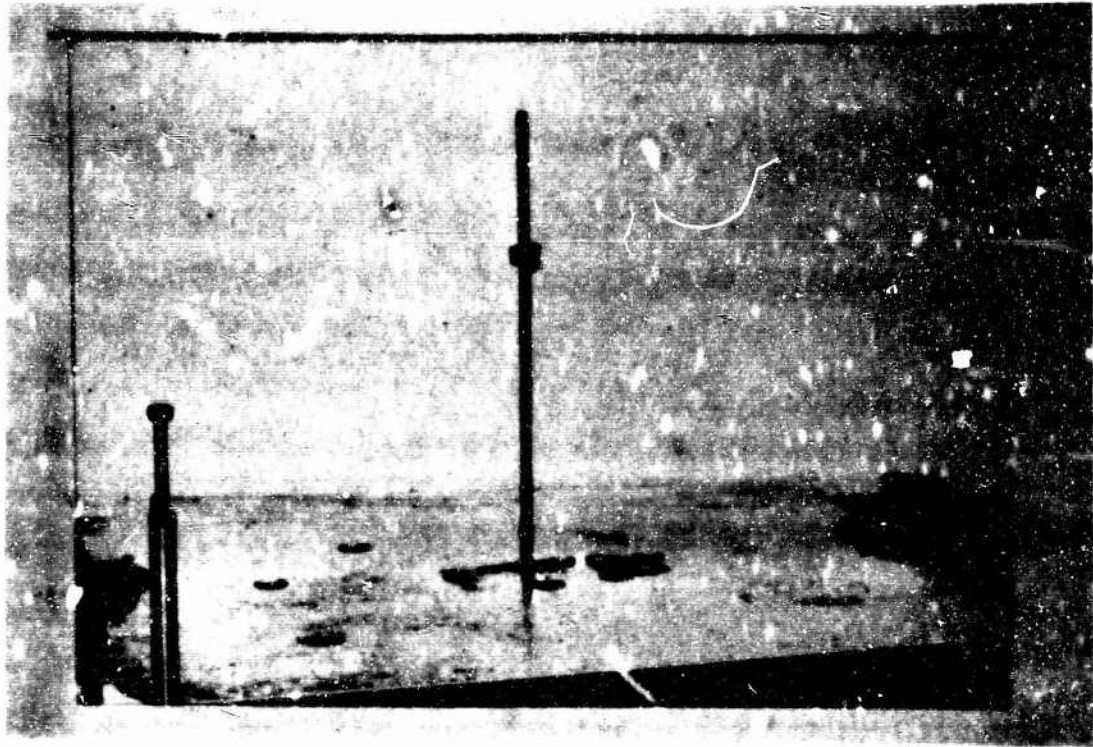circuit with TD at different
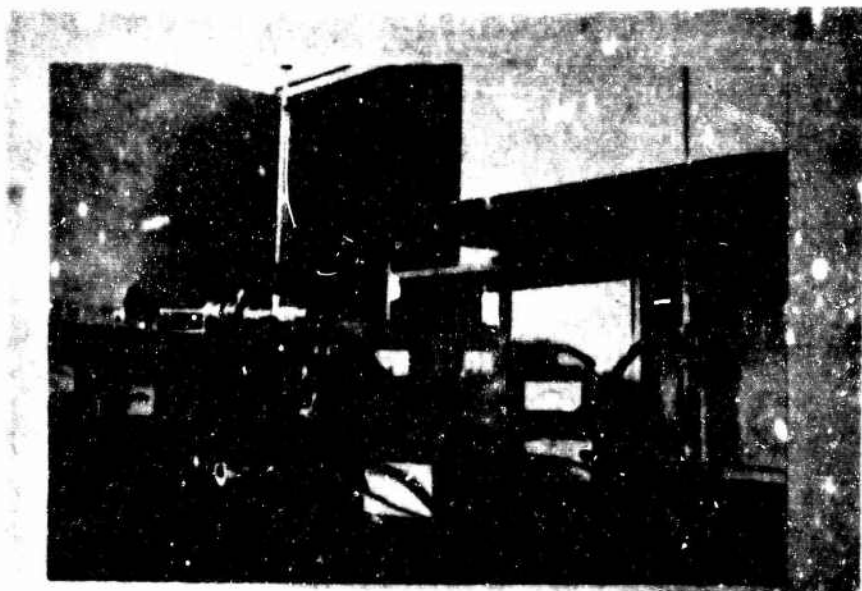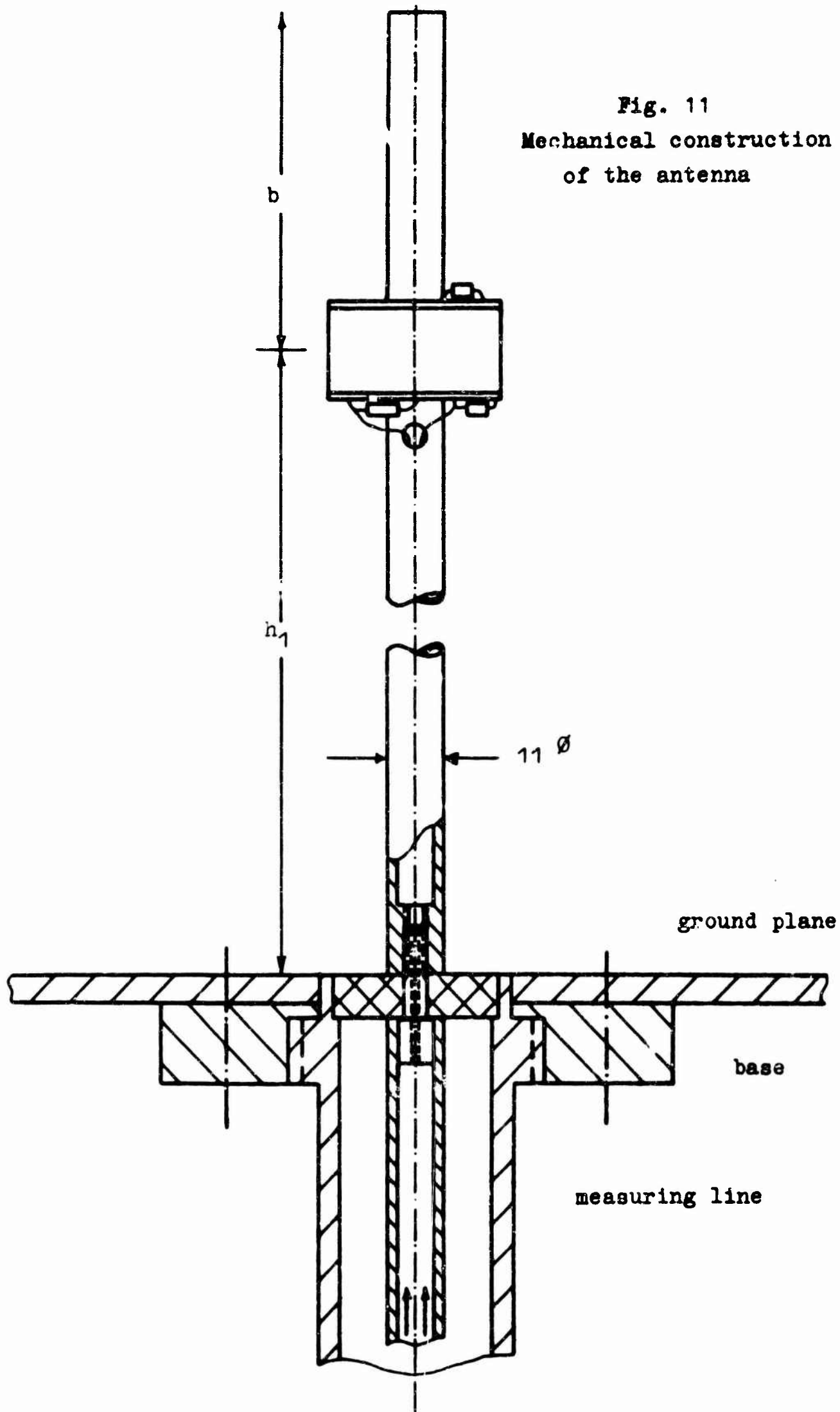levels of the voltage U_1
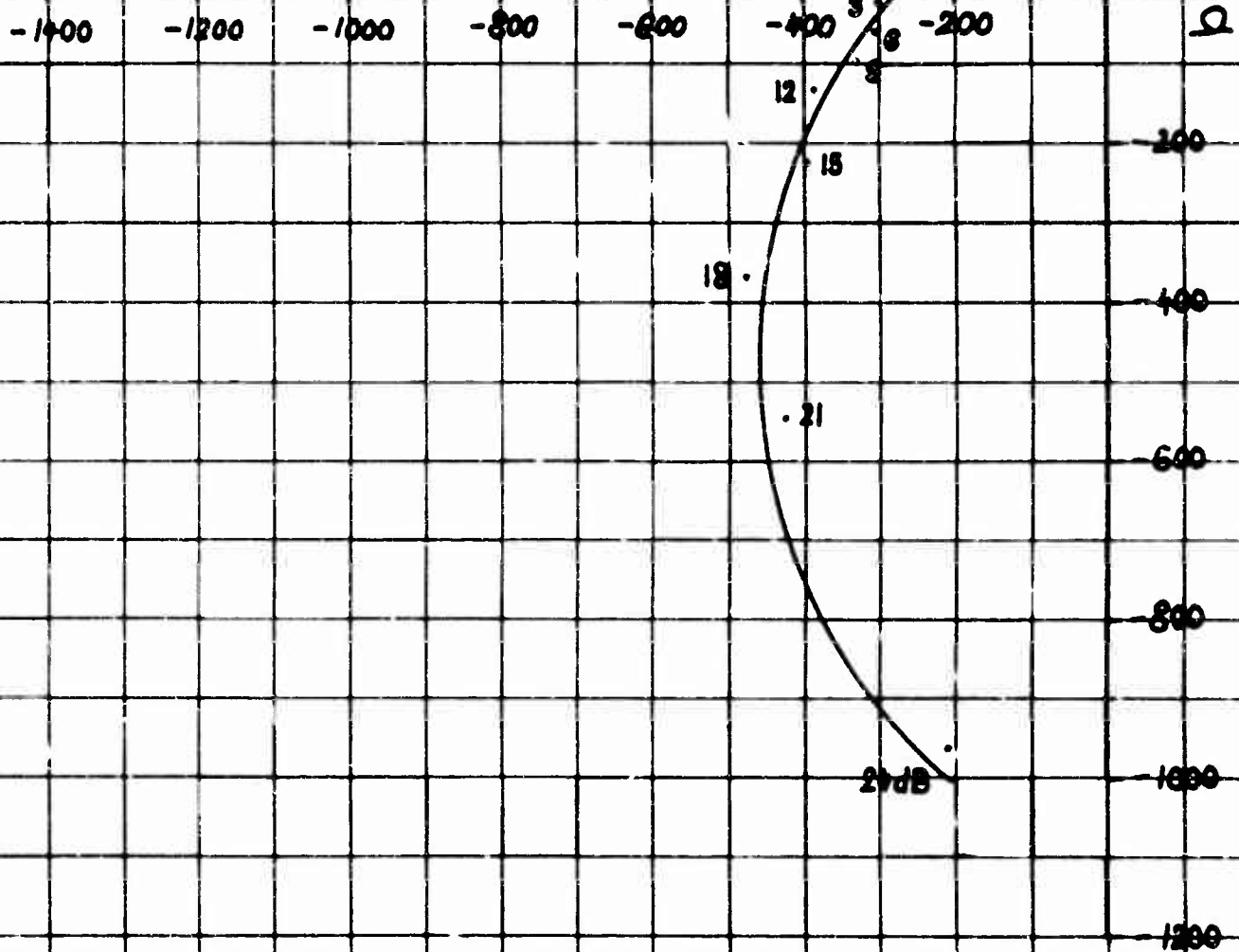
Fig. 9

Fig. 10

Fig. 11
Mechanical construction
of the antenna

b

h_1

11 ∅

ground plane

base

measuring line

at the diode. The highest part b (see Fig.11) of the antenna
contains an insulated inner conductor and serves at the same
time in addition with a sliding contact as a short circuited
line of variable length. Regarding high frequencies, the latter
is electrically in parallel with the TD. Fig.12 shows the con-
struction of the polystyrol link and the end of the antenna. In
Fig.11 and 12 no dimensions have been specified for h_1 and b
since these values could be varied. However mostly was h_1 = 338 mm,
b = 150 ... 225 mm.

5. Electrical Design

Fig.1o and 13 represent the spatial and schematic arrangement
of the impedance-measuring equipment. The power delivered from
the signal generator is coupled to the measuring line via a
variable attenuator. By means of a capacitive probe the distri-
bution of the voltage along the slotted line is measured and with
this the impedance of the antenna appearing at the input plane
is determined. Since the signal voltage at the probe was very
small, the input resistance of the used test receiver has been mat-
ched to the internal resistance of the probe.

The upper part of Fig.13 shows the circuitry of the link between
the two antenna parts. For better understanding the short cir-
cuited line in the upper antenna end is sketched as if it was a
two wire line and seperated from the antenna. The TD lies with
C_k in series to the antenna and gets its bias voltage from a
stabilized power supply. The dc feeding current flows over the
inner conductor of the measuring line, over the antenna rod and
the short-circuited line to the TD and flows backover an insula-
ted wire in the interior of the inner conductor. Two resistors of
30 Ω prevent the short-circuiting of the measuring line for rf by
the 2 power supply wires. The two resistors must not have great
values since they are in series with the internal resistance
of the dc-supply and have to fulfil the stability conditions
of equ. (8).

According to chapter 3 the rf-Voltage at the TD must be kept small.
Therefore ist is necessary to measure it. The dc-current, origi-
nating at the measuring diode, flows over a resistor of 1o kΩ
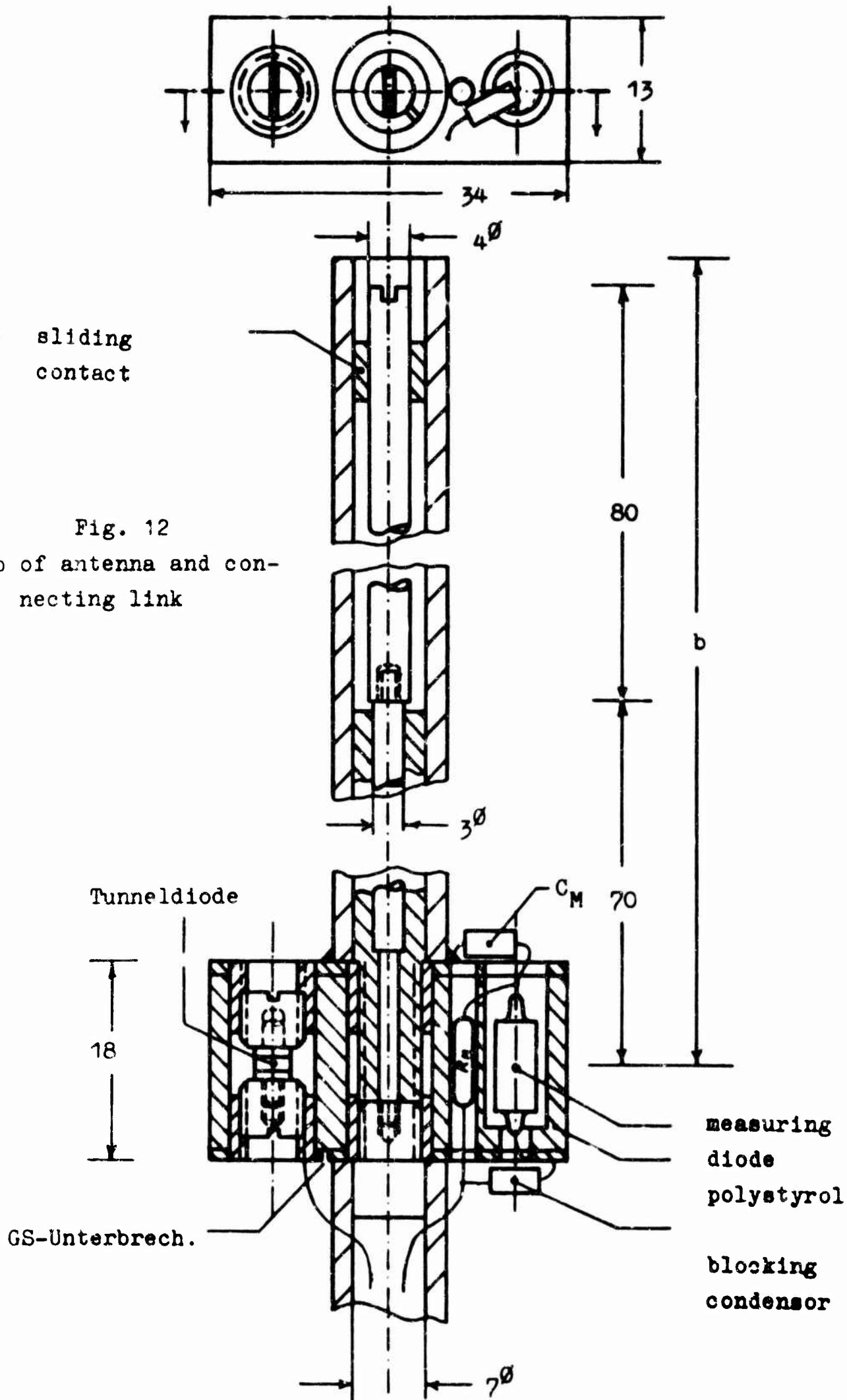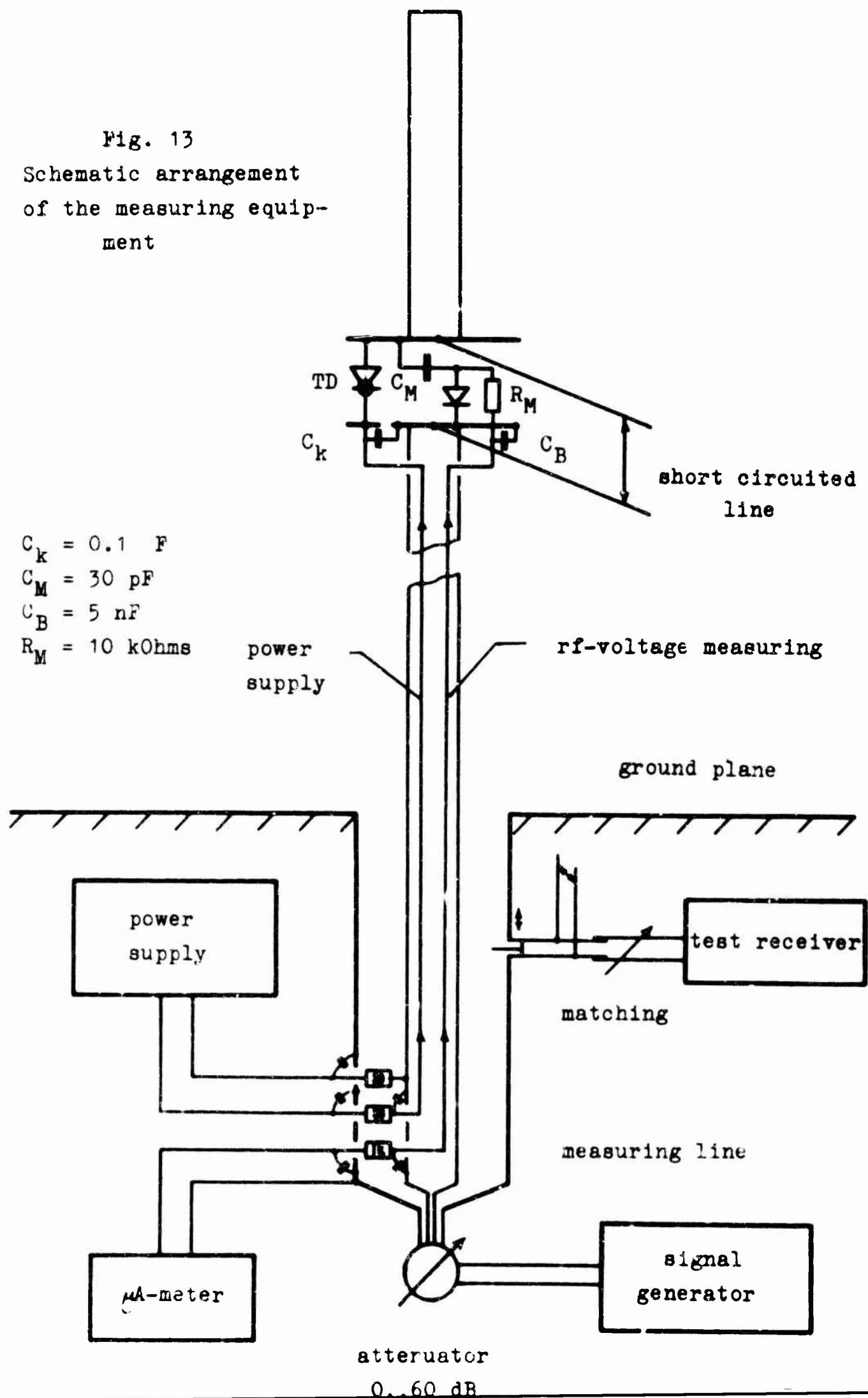R_M, over a wire in the interior of the inner conductor and over

Fig. 12
Top of antenna and con-
necting link

Fig. 13
Schematic arrangement
of the measuring equip-
ment

$C_k = 0.1$ F
$C_M = 30$ pF
$C_B = 5$ nF
$R_M = 10$ kOhms

short circuited
line

power
supply

rf-voltage measuring

ground plane

power
supply

test receiver

matching

measuring line

μA-meter

signal
generator

atteruator
0..60 dB

a resistor of 1 kΩ respectively over the inner conductor itself, the internal resistance of the signal generator (60Ω), and the outer conductor of the measuring line to a micro-amp-meter where it is measured. The 1 kΩ resistor again is necessary to avoid a short circuit of the measuring line. See Fig. 13

The antenna was designed on account of two conditions:

1. electrical stability

1. generation of a traveling wave on the lower part

According to part I.1 of this report the existance of a traveling wave depends on the value of the negative resistance. Approximately R_n has to be:

$$R_n = Z_L$$

Z_L is a function of the antenna dimensions [6u] :

$$Z_L = 60 \ln \left(1.15 \frac{h_1 + b}{D} \right) \quad ohms \tag{12}$$

D = diameter of the antenna rod = 1.1 cm. h_1 and b mostly have been: h_1 = 33.8 cm, b = 18.7 cm. Then Z_L is equal to 240 Ω. Therefore we need approximately R_n = 240 Ω. The impedance measurement gives a criterion for this condition.

The most difficult problem of the antenna design was the stability of the circuit. Therefore the considerations of chapter 3 shall be resumed.

To fulfil the stability conditions for low frequencies a capacity C_k = 0.1 μF (Fig. 5) proved to be sufficient. The admissible inductance then is with R_n= 200Ω and R_i = 60 Ω according to equ. (9)

$$L = R_n R_i C_k = 12 \ mH$$

The stability at high frequencies is determined by the mutual positions of the boundary curve and the characteristic impedance

curve in the backward-diagram. Since the boundary curve can be derived from the input impedance of the TD, it is sufficient to consider Fig.3. The value of the series inductance L_s (Fig.2) being sufficiently great (dash dot curve), the impedance curve intersects the real axis at negative values. This means for the backward-diagram that the point $Z_a = 0$ lies above the boundary curve and self-excitation is possible - the TD has no short-circuit stability. Since L_s mostly cannot be lowered, short-circuit stability can only be attained by enlarging R_s (Fig.2), i.e. by inserting a series resistor R'_s. Such a resistor, which can be mounted directly on the TD is shown in Fig.14. It consists of a polystyrol hat painted with conducting lac and contact surfaces painted with conducting silver.
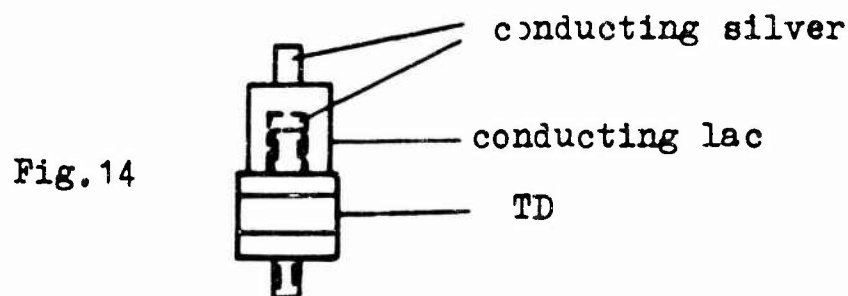

Fig. 14

The diasdvantage of a series resistance consists in the lowering of the cut-off frequency according to equ.(4). In some cases however, stability could not be attained without this series resistance.

The value of the negative resistance $-R_n$ determines the size of the boundary curve in the backward-diagram. R_n being great, the area below the boundary curve is great and therefore the probability is great that the characteristic impedance curve Z_a takes its course only in this area: i.e. with regard to stability TDs with great negative resistances are advantageous. Since for a traveling wave antenna R_n has to be approximately equal to Z_L, in the present case TDs with $R_n \approx 200\Omega$ are used. Of course it is possible to apply diodes with lower negative resistances by connecting in parallel an ohmic resistance R_p. Since this can mostly be done only over additional connecting wires the first case is

easier to survey and only small stability-corrections should be
made by this shunting.

Apart from the boundary curve, whose position in the complex im-
pedance plane is only a property of the TD applied, the position
of the characteristic input impedance curve at the TD is impor-
tant too. Since the shape of this curve neither could be measured
nor could be constructed with adequate accuracy, the solution of
the stability problem had to be tried by help of theoretical
approximations and experimental stability investigations. A crude
survey about the shape of the characteristic curve can be attained
by applying transmission line theory to the antenna. The equivalent
circuit is shown in Fig.15. Z_a consists of the series arrangement
of two impedances Z_x and Z_y. Z_x is the input impedance of the
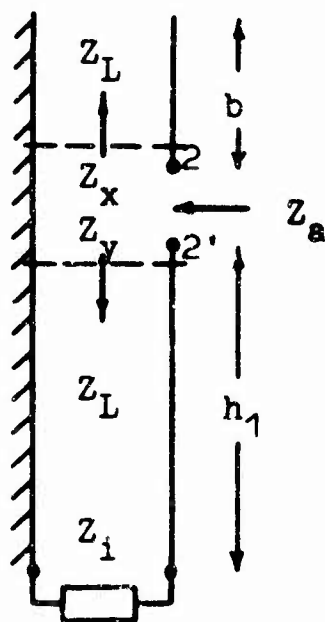
Fig. 15

open circuited line with the length h, Z_y is the feeding resistan-
ce Z_i, transformed by the line with the length h_1. Z_i is caused
by the internal resistance of the signal generator and the resis-
tors of 30 Ω and 1 kΩ. It was measured at f_o = 400 Mc/s:
Z_i = 148 - j42 Ω.

A small input impedance Z_a at 2-2', which is desired to get favorable stability conditions, can be attained at the operation frequency f_o by making $h_1 = \lambda/2$, $b = \lambda/4$, Z_x then being very small and $Z_y = Z_i$. At frequencies different from f_o however, very unfavorable stability conditions result. For instance: f being twice the operation frequency f_o, Z_x becomes very great and with this the probability of self-excitation becomes great too. Therefore it is necessary to influence the characteristic impedance curve at frequencies $f = f_o$ thus that only small impedances appear. This can be done by a tank-circuit with the resonance frequency $f_R = f_o$ connected in parallel with the terminals 2-2' (Fig.15). At $f = f_o$ it does not affect the impedance Z_a, at $f = f_o$, by connecting in parallel great susceptances, small input impedances result.

In practice however parallel resonant circuits do not function very well at high frequencies. In the present case therefore the tank-circuit was replaced by a short circuited line of the length $\bar{a} = \lambda/4$. This short circuited line behaves like a parallel resonant circuit.

Z_{LK} = characteristic impedance of the short circuited line.

Concerning stability it is desirable that already by little detuning great susceptances appear. This can be attained by choosing a small characteristic impedance Z_{Lk} of the short circuited line. The dimensions of the considered line are shown in Fig.12, Z_{Lk} being 33 Ω. The lower part of the line is filled with polystyrol to lengthen it electrically and to hold the inner conductor mechanically. By shifting the sliding contact, the resonance frequency can be varied. At $f = 3f_o$ (f_o = operating frequency) the input impedance of this line circuit again is very great. To avoid self-excitation it is necessary to apply a TD with a cut-off frequency lower than $3f_o$ (eventually by inserting a series resistor as shown in Fig.14).

Another possibility to influence the stability is a variation of the internal resistance Z_i, which appears at the feeding point of the antenna. In the present case this possibility has not been utilized because it produces great constructional trouble.

According to the preceding considerations the equivalent
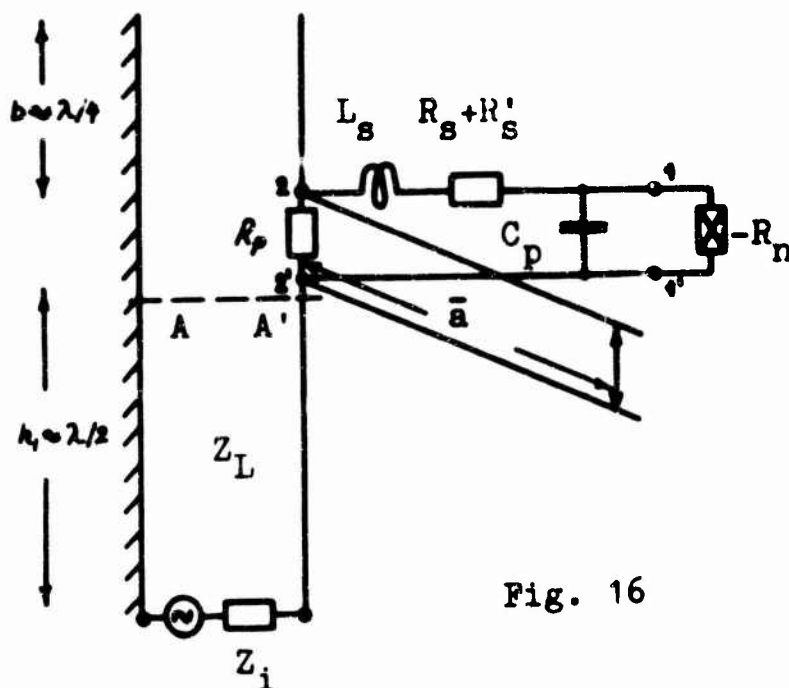rf-circuit of the antenna results as shown in Fig.16.

Fig. 16

The difficulties, which arose constructing the antenna, were
based on the fact that not only stability conditions had to
be considered, but that also a certain input impedance (corres-
ponding to a traveling wave distribution) had to be attained.
Considering stability the impedance appearing at the terminals
1-1' (seen from $-R_n$) is of importance, whereas considering mat-
ching the impedance at 2-2' respectively at A-A' is important.

By careful adjustment of R_p, $\bar{a}$ and b it is possible to match
any value of $-R_n$ to the characteristic impedance of the antenna
line. At the same time however, the stability conditions chan-
ge, if R_p, $\bar{a}$ and b are varied. Therefore it was the problem of
the experimental investigations to find an adjustment where
both conditions are fulfilled.

6. Amplification

Since a TD is able to deliver power into a passive network, the
described antenna arrangement also acts as an antennafier. There

are many possibilities to define an amplification factor of
an antenna with integrated TD. It seems reasonable however to
derive such a factor by comparison with the unloaded antenna.
For the reception case its behaviour as seen from the recei-
ver may be expressed by the equivalent network of Fig.17a,
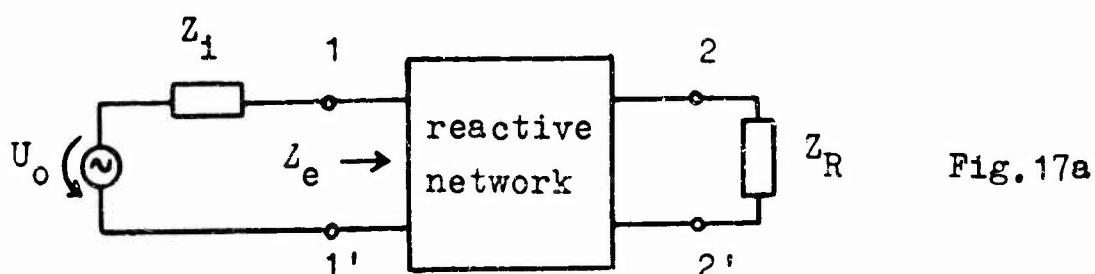where U_o means the electromotive force, which is caused by an

Fig.17a

incoming wave; Z_i is the internal resistance of the antenna
and Z_R is the load resistance as for example the input impe-
dance of a receiver. In order to get maximum power from the
antenna into the load Z_R is transformed by the reactive net-
work 1-1', 2-2' into an impedance Z_e, which is equal to the
conjugate complex value of Z_i; $Z_e = Z_i^*$. The real power P_{w1}
then delivered to the load is:

$$P_{w1} = \frac{1}{2} \frac{|U_o|^2 Re(Z_i^*)}{|Z_i + Z_i^*|^2} \tag{13}$$

where $R_e(Z_i^*)$ means the real part of Z_i^*.

Replacing the antenna by the loaded type, the equivalent net-
work of Fig.17b is attained. Assuming that the radiation pat-
tern of the antenna does not change by loading the antenna
with a TD, the electromotive force U_o' of Fig. 17b is equal to
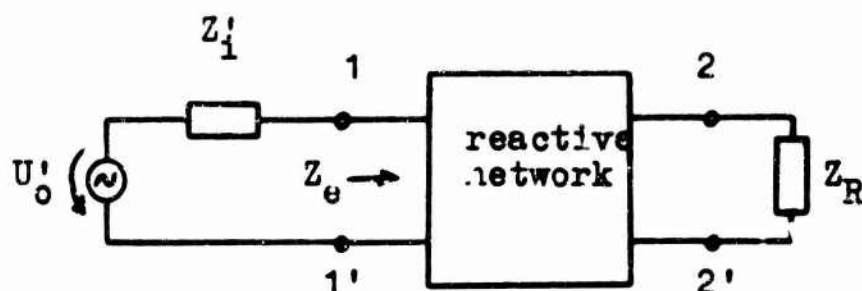U_o of Fig.17a, only the internal resistance Z_i' has changed.

Fig.17b

With the antenna to be discussed here, this assumtion is not true, since the TD alters the current distribution on the antenna and with this its pattern. Therefore to get the entire amplification, the power delivered to the load should be related in both cases to an equal value of the electric field strength of the intrinsic wave. This however is a rather difficult thing for calculation. Therefore we seperate the gain of the antenna, caused by the variation of U_o according to the variation of the radiation pattern, from a factor which we call the amplification and which only depends on the variation of Z_i and can be computed by assuming that $U_o = U_o'$.

The input impedance Z_e being unchanged ($Z_e = Z_i^*$), we get for the real power now delivered to the load:

$$P_{W2} = \frac{1}{2} \frac{|U_o|^2 \cdot Re(Z_i^*)}{|Z_i' + Z_i^*|^2} \tag{14}$$

Consequently the power amplification g_p is:

$$g_p = \frac{P_{W2}}{P_{W1}} = \frac{|Z_i + \bar{Z}_i^*|^2}{|Z_i' + Z_i^*|^2} = \frac{4 Re(Z_i)}{|Z_i' + Z_i^*|^2} \tag{15}$$

Example:
For the unloaded unipole with a length of $3\lambda/4$ according to [4] is: $Z_i = 70 + j27 \ \Omega$.

For the PD-loaded unipole according to Fig. 29
$Z_1' = - 60 + j42 \, \Omega$ can be attained. Then $g_p = 4.05$.

Since with the TD-loaded antenna the internal resistance contains a negative real part, it is always possible to transform Z_R via the reactive network thus that $Z_e = - Z_i'$. Then the power delivered to Z_R is infinite. Because of stability conditions this can not be obtained however.

It should be statet very clearly that there are many possibilities to define an amplification factor for an antenna with integrated TD. We could also compare for example the loaded antenna with an arbitrary unloaded one of equal or smaller height, which should be ommi_directional and give maximum power to the receiver. Since however, the quality of an antenna_fier is not only determined by its amplification factor but also by its noise behaviour, all these definitions seem to be rather arbitrary. To qualitf an antenna with active element, perhaps a factor is more appropriate, which considers noise behavior too, for instance the field sensitivity strength (FSS). The FSS is the value of the power density of the incoming wave, which produces a signal to noise ratio equal to 1 at the output of the antenna [7].

7. Transformation of Negative Resistances by Homogeneous Transmission Lines

In the preceding chapters Transmission-Line Theory has been applied to antennas containing negative resistances. This chapter dealt with the transformation of impedances with negative real parts along homogeneous transmission lines. The input impedance Z_1 of a homogeneous line of length a' and characteristic impedance Z_L, terminated by the impedance Z_2 is [66]:

$$Z_1 = Z_L \frac{Z_2/Z_L + \tanh \gamma a'}{1 + (Z_2/Z_L)\tanh \gamma a'} \tag{16}$$

$$\gamma = \alpha + j\beta \tag{17}$$

In this the real part of Z_2 may be positive or negative.

The numerical evaluation of equ. (16) generally is complicated. In case of $\alpha = 0$, i.e. regarding lossless transmission lines the input impedance simply is obtained from the circle diagram in the complex plane or from the Smith-Chart. These charts mostly exist only for impedances with positive real parts and have to be extended for impedances with negative real parts. The complete circle diagram with rectangular coordinates is shown in Fig.18, the extended Smith-Chart is shown in Fig.19. Since for $Z_2 = - Z_L$ the reflection coefficient becomes infinite, the Smith-Chart is not well suited for negative resistances in the proximity of the characteristic impedance of the line.

In case of lossy transmission lines the relative input impedance can be obtained from the charts too. Now the transformation does not follow circles but spirals, because the standing wave ratio (VSWR) changes along the line (in the following $m = 1/VSWR$ will be employed, because this factor is limited between 0 and 1). Being $m = m_2$ at the end of the line, m_1 at the input of the line of length a' is:

$$ m_1 = \frac{m_2 + \tanh \alpha a'}{1 + m_2 \tanh \alpha a'} \qquad (18) $$

m_1 as a function of m_2 and $\alpha a'$ can be taken from Fig.20.

According to [66] the input impedance Z_1 of a lossy transmission line can now be found as follows: For a special value of Z_2/Z_L, a_2/λ and m_2 are taken from the impedance or Smith-chart. For a special attenuation $\alpha a'$, m_1 is obtained from Fig. 20 and a_1/λ from the simple equation $a_1/\lambda = a_2/\lambda + a'/\lambda$. With these values the relative input impedance can be attained from the circle diagram or from the Smith-chart.

The impedance curve of a dissipative transmission line $(\alpha\lambda = 0.8)$ terminated with a negative resistance $Z_2 = - 0.65 Z_L$ as a function of the length of the line a' is plotted in Fig.18. At first

Extended Circle Diagram

Fig 18

Extended Smith Chart

Fig. 19
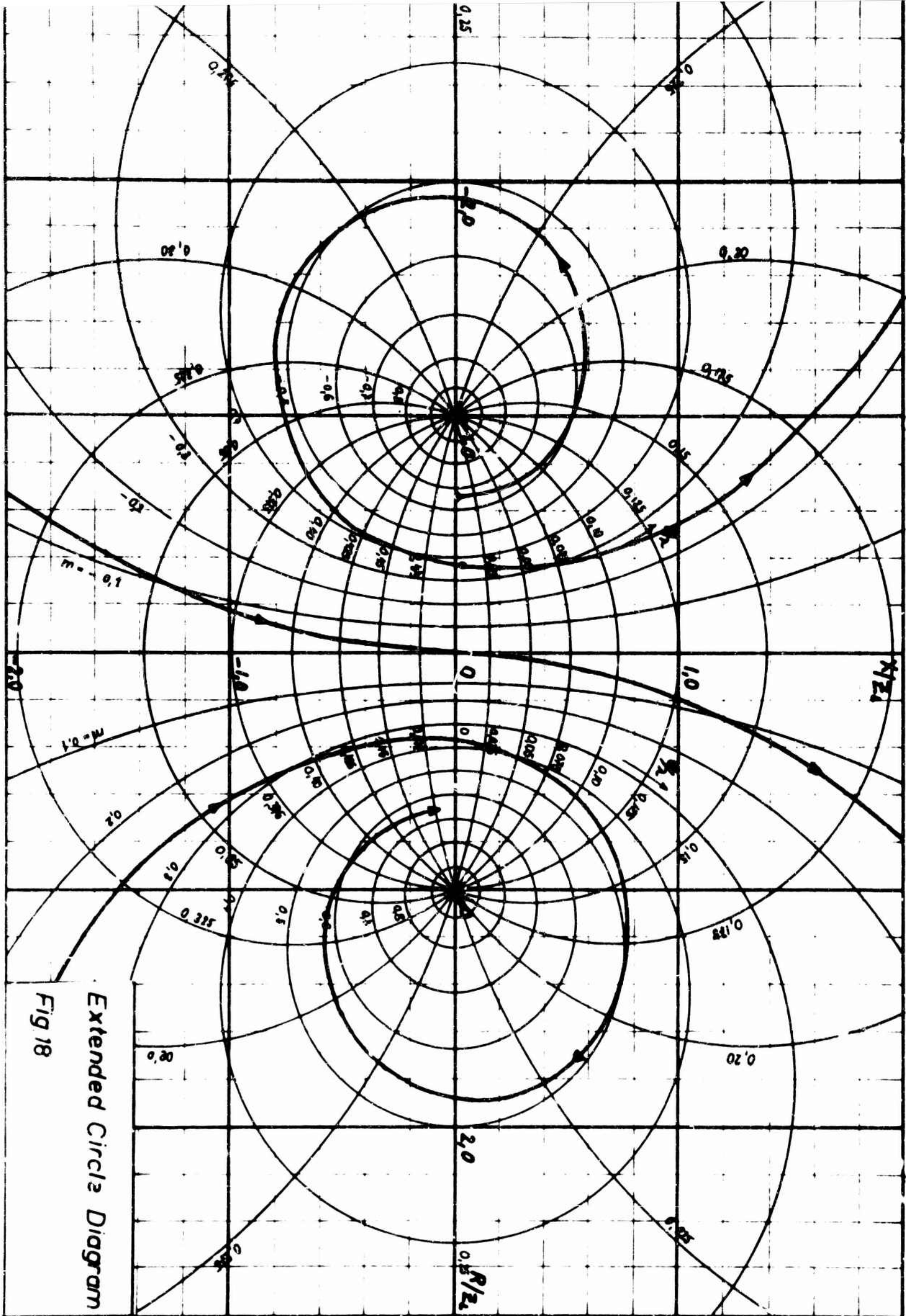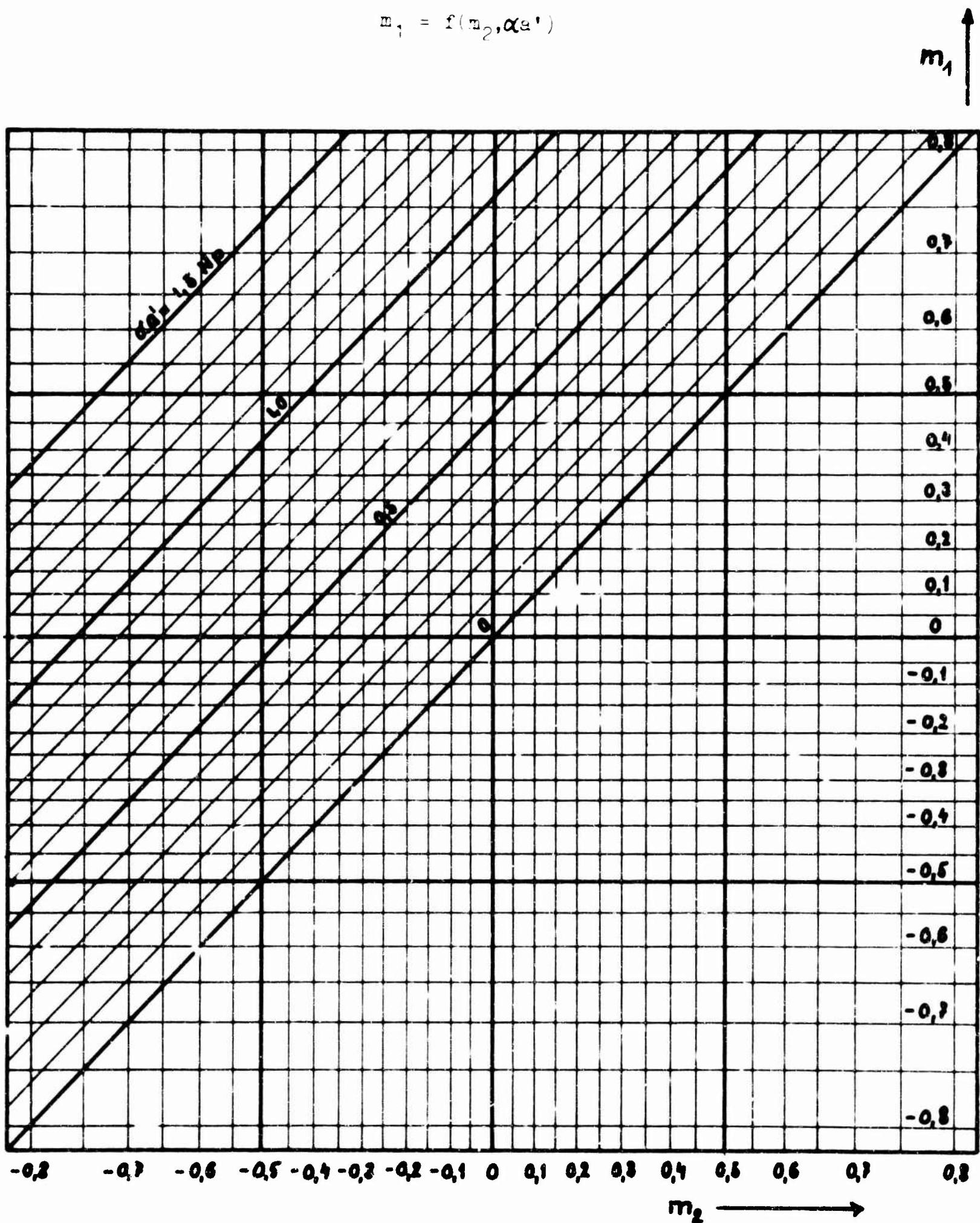
$$m_1 = f(m_2, \alpha a')$$

Fig. 20

the negative resistance transforms on an extending counter-
clockwise turning spiral till it reaches the imaginary axis
(the point of intersection will generally not be the origin);
then the curve runs on a now contracting clockwise turning
spiral, which, the length of the line being sufficient, ends
at the point $Z_2/Z_L = +1$. Only if Z_2 is exactly equal to $-Z_L$
(matching), the input impedance remains constantly $-Z_L$ inde-
pendent of the length of the line. Since already small in-
homogeneities bring a disturbance to this matching, the input
impedance of a dissipative transmission line always strives
for the point $+Z_L$. For this reason the realization of a tra-
veling wave antenna with negative term'nating resistance, is
difficult and not possible for great antenna hights h_1. There
is still another physical reason for this: exact negative
matching of a long lossy line would mean that the voltage
along the line increases exonential from the input to the ne-
gative terminating resistance. Since negative resistances are
always nonlinear, only small voltages may appear at their
terminals i.e. the voltage at the input of the line must be
very small and with very long lines would become smaller than
the noise.

In the Smith-chart the impedance curve is an always clock-
wise turning contracting spiral, since the changing of m
according to equ. (18) corresponds to a change of the reflec-
tion coefficient r according to equation (19).

$$ |r_1| = |r_2| e^{-2\alpha a'} \tag{19} $$

8. Discrimination of Impedances with Positive and Negative

Real Parts

The impedance measuring arrangement (see Fig.13) has been des-
cribed in chapter I.5. Since the input impedance is measured
by the voltage distribution along the measuring line, it is
not possible to decide, if the measured impedance contains

a positive or negative real part. For this decision a further
measurment is necessary. For instance, by means of directional
couplers the reflection coefficient on the line could be de-
termined. If it is less than 1, the line is terminated by a
positive resistance, if it is greater than 1, the line is
terminated by a negative resistance. Because of constructional
reasons this method could not be applied. Another procedure
will be described, which allows to distinguish between impe-
dances with positive and negative real parts by measuring the
ratio $q = U_{max\ 2}/U_{max\ 1}$, where $U_{max\ 1}$ is the maximum voltage,
which appears on the measuring line, if it is terminated by a
short circuit, $U_{max\ 2}$ is the maximum voltage on the measuring
line, if it is terminated by the impedance Z_2 to be measured.
Fig.21 gives the situation:

measuring line (Z_L)
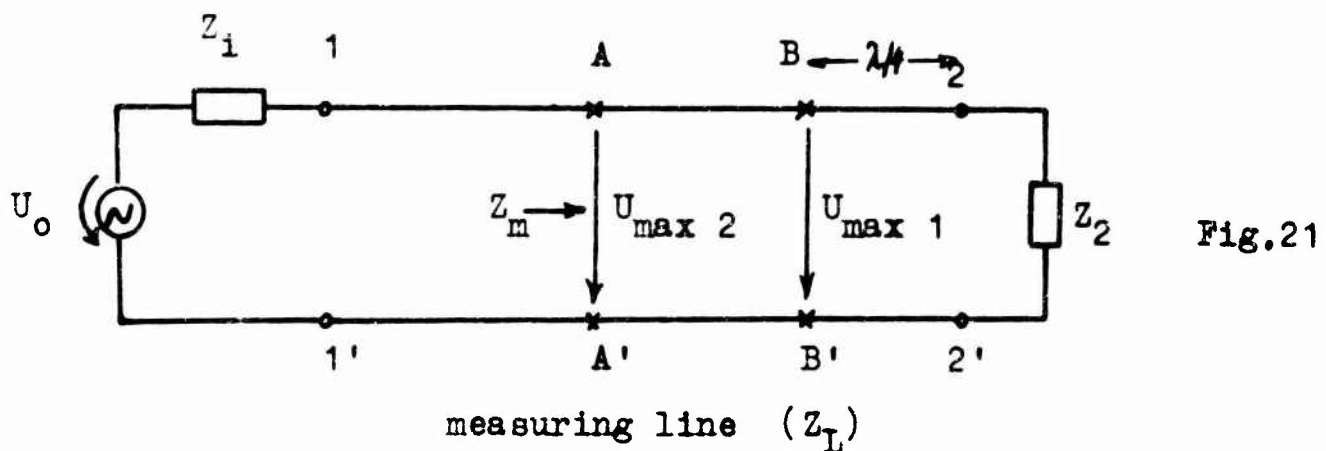
Simple conditions are obtained in case of

$$\underline{Z_i = Z_L}$$

If the terminating impedance Z_2 is different from Z_L, a certain
VSWR appears on the line. At the place A-A' ot the voltage
maximum, the input impedance is real and equal to $\frac{Z_L}{m_2}$, where
m_2 ($= 1/VSWR$) is positive, if the real part of Z_2 is positive,
and m_2 is negative, if the real part of Z_2 is negative.

The voltage source U_0 and the internal resistance Z_i can be
transformed to the terminals A-A'. This gives the equivalent
circuit of Fig.22.
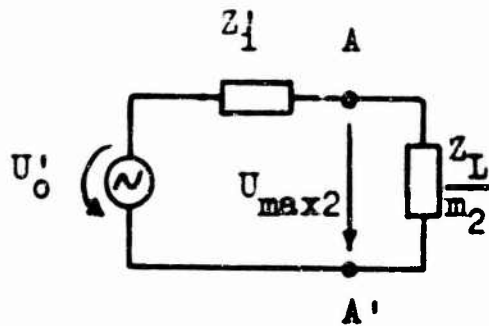
Fig.22

In case of $Z_1 = Z_L$, Z_1 transforms into $Z_1' = Z_L$.
$U_{max\,2}$ then is

$$U_{max\,2} = \frac{U_o' \frac{Z_L}{m_2}}{Z_L + \frac{Z_L}{m_2}} = \frac{U_o'}{1 + m_2}$$

If the line is terminated with a short circuit, i.e. $Z_2 = o$,
$Z_1 = Z_L$ we get from transmissionline theory

$$U_{max\,1} = U_o'$$

(In general $U_{max\,1}$ does not appear at A-A'). Consequently

$$q = \frac{U_{max\,2}}{U_{max\,1}} = \frac{1}{1 + m_2} \qquad (20)$$

m_2 being greater than zero (i.e. Z_2 contains a positive real
part) q is less than 1. If m_2 is less than zero (Z_2 with negative
real part), q is greater than 1. Therefore by measurement of q
it can be decided, whether the impedance Z_2 contains a positive
or negative real part.

In case of $$Z_1 = Z_L$$

the foregoing criterion is not valid, since the reactive com-
ponents of Z_1 and Z_2 can produce a resonance effect.

Consequently as well for positive as for the negative terminating
resistances q can be less or greater than 1. Therefore applying
the preceding criterion, always Z_1 has to be made equal to Z_L.
On account of the 30 Ω bushing resistances (Fig.13) this was
not possible in the present case.

It has therefore been tried to extend the foregoing method for the case of $Z_1 = Z_L$. In general the value of q for the impedance $Z_2 = R_2 + jX_2$ with positive real part is different from the value of q for $Z_2^n = -R_2 + jX_2$ with negative real part. Z_1 is measured and a known complex value. Calculating q for both cases and comparing these values with the measured one, it can be decided whether R_2 has a positive or negative sign. In practice this calculation is not done refering to the impedance Z_2 but directly to the measured values of m_2 and a_2/λ (see Fig. 23). a_2 is the distance between the position of the voltage minimum on the line and the input of the line.
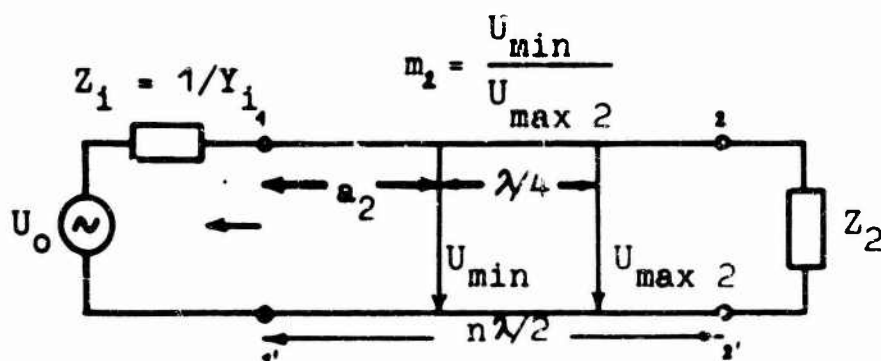
Fig. 23

According to transmission line theory is

$$q = \frac{1}{\left| \cos 2\pi a_2/\lambda + j Y_i Z_L \sin 2\pi a_2/\lambda + m_2 \left(Y_i Z_L \cos 2\pi a_2/\lambda + j \sin 2\pi a_2/\lambda \right) \right|} \qquad (21)$$

Not to impede the impedance measurements unnecessarily by this calculation, a table was computed from which the required values easily could be taken by interpolation. For this purpose equ. (21) was programed on an electronic computer. The program can be applied to different values of the relative internal admittance $Y_1 Z_L = y_1 = g_1 + jb_1$. In the present case the calculation was done with $g_1 = 0.374$ and $b_1 = 0.1o6$, which was the relative internal admittance for our physical arrangement at 400 Mc/s. q was computed for $m_2 = -1 \ldots +1$ in steps of 0.1 and $a_2/\lambda = 0 \ldots 0.5$

in steps of 0.01. As an example Fig.24 shows a confrontation of
the computed values of q for $m_2 = -0.3$ and $m_2 = +0.3$. According
to the preceding considerations an impedance measurement was
performed as follows: At first the measuring line was short cir-
cuited at the ground plane and the voltage maximum on the mea-
suring line was noted. Then the short circuit was taken away
and the antenna was mounted on the input of the measuring line.
The measured value of the voltage maximum was noted. The quotient
of both maxima gives q. Next we measured m_2 and a_2 on the slotted
line. With these values of m_2 and a_2/λ , q can be taken out of
the table for positive and negative sign of m_2 and be compared
with the measured value of q. Thus in almost all cases the sign
of the real part of the measured impedance could be decided.
Only at values of m_2 in the proximity of 0 (VSWR = ∞) this
decision became uncertain. This disadvantage however cannot be
avoided by other methods either.

9. Experimental Results

The final arrangement of the antenna (Fig.11) was made according
to the considerations of chapter I.5. Since the wavelength λ of
electro-magnetic waves on rod antennas is smaller than the wave-
length λ_o in free space, h_1 was not chosen equal to $\lambda_o/2$, but
a shortening factor was taken into consideration

$$h_1 = 0.458 \, \lambda_o = 338 \, mm \quad for \, f = 400 \, Mc/s .$$

b was vaiable between $0.2 \, \lambda_o$ = 150 mm and $0.3 \lambda_o$ = 225 mm.
From several TDs we chose the following, the data of which proved
to be best suited to achieve stability: R_n = 200 Ω, C_p = 5.8 pF,
R_s = 2.25 Ω.

The impedance measurements were performed at a frequency of 400
Mc/s. Varying the length $\overline{s}$ of the short circuited line, the
resulting input impedance of the antenna follows a circle in the
complex impedance plane. Fig.25 shows the input impedance for
$b = 0.2 \lambda_o$, R_p = 500 Ω and R_s' = 6.4 Ω. The parameters on tne

Fig. 24
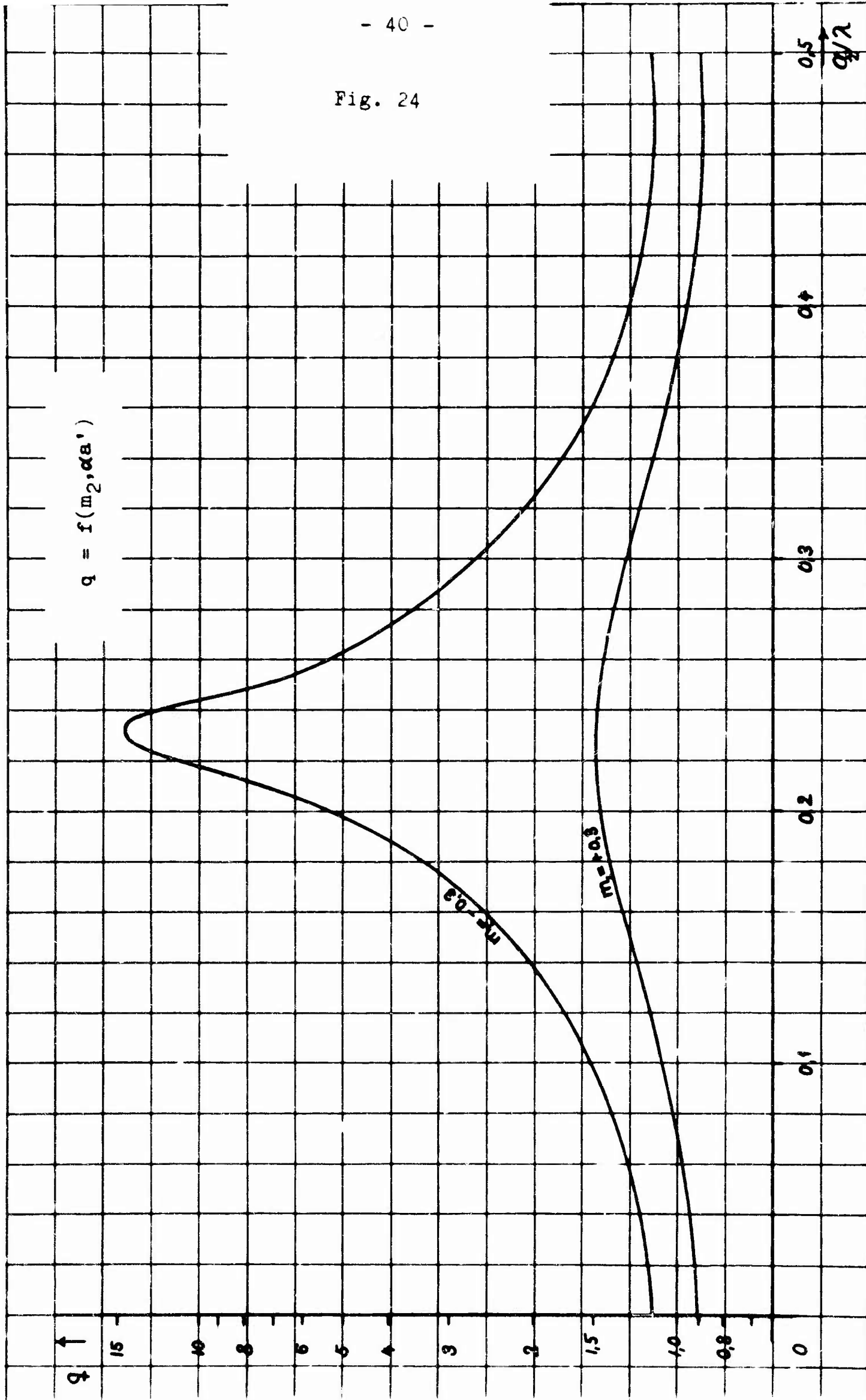
Fig. 25   Antenna-input impedance at different values of $\bar{a}$. $h_1 = 338$ mm, $R_s' = 6.4\Omega$, $R_p = 500\Omega$; $b = 0.2\lambda_o$.
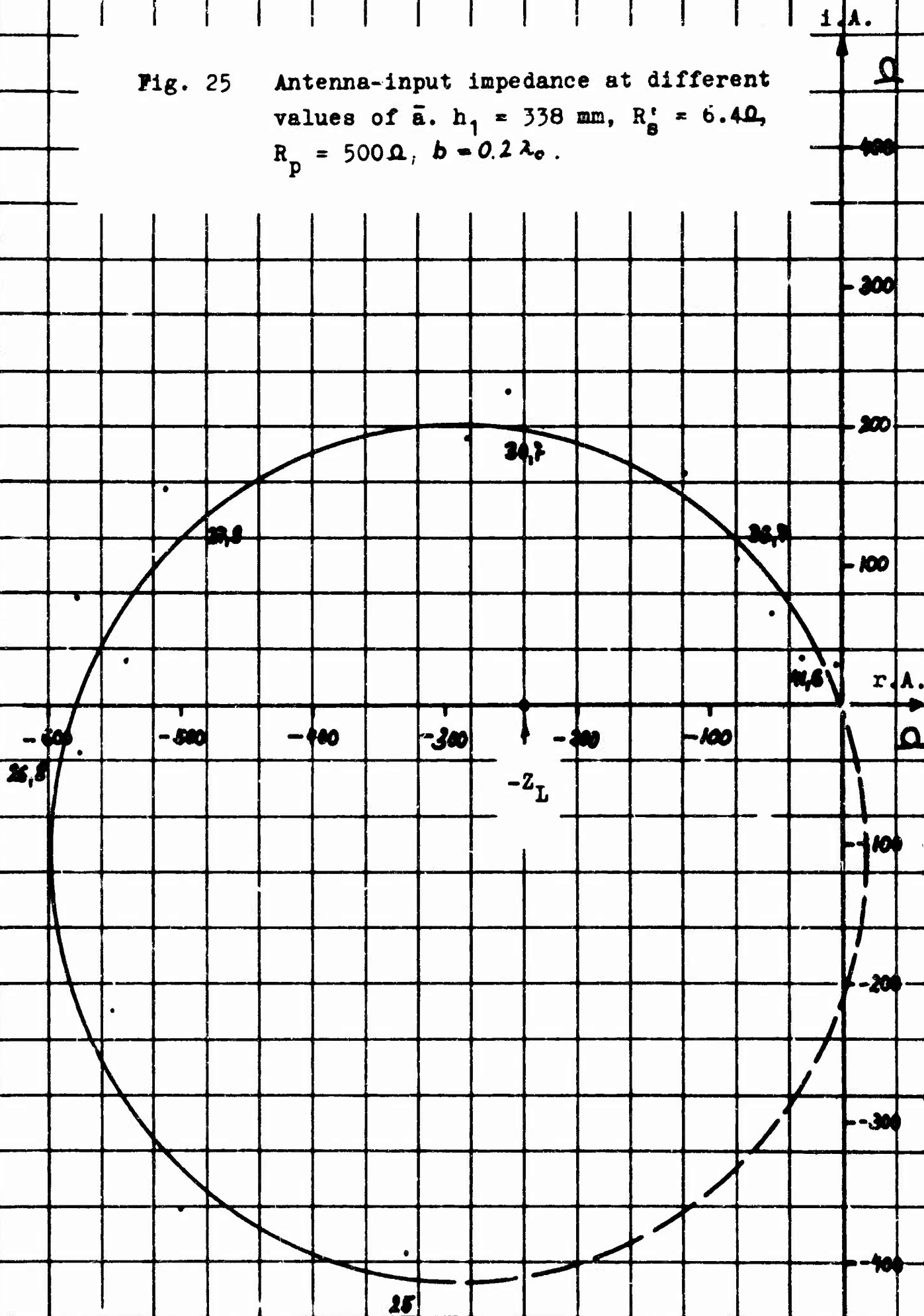
circle represent the susceptance B in mMho, which at the respective impedance point is generated by the short circuited line at the terminals 2-2' (see Fig.16). The dashed section of the circle indicates input impedances, which because of constructional or stability reasons could not be attained by varying $\bar{a}$. These measured values of the input impedance are now compared with calculated values. In Fig.26-R_n = 200 Ω is the negative resistance of the tunnel diode used and C_p = 5.8 pF is the parallel capacity,
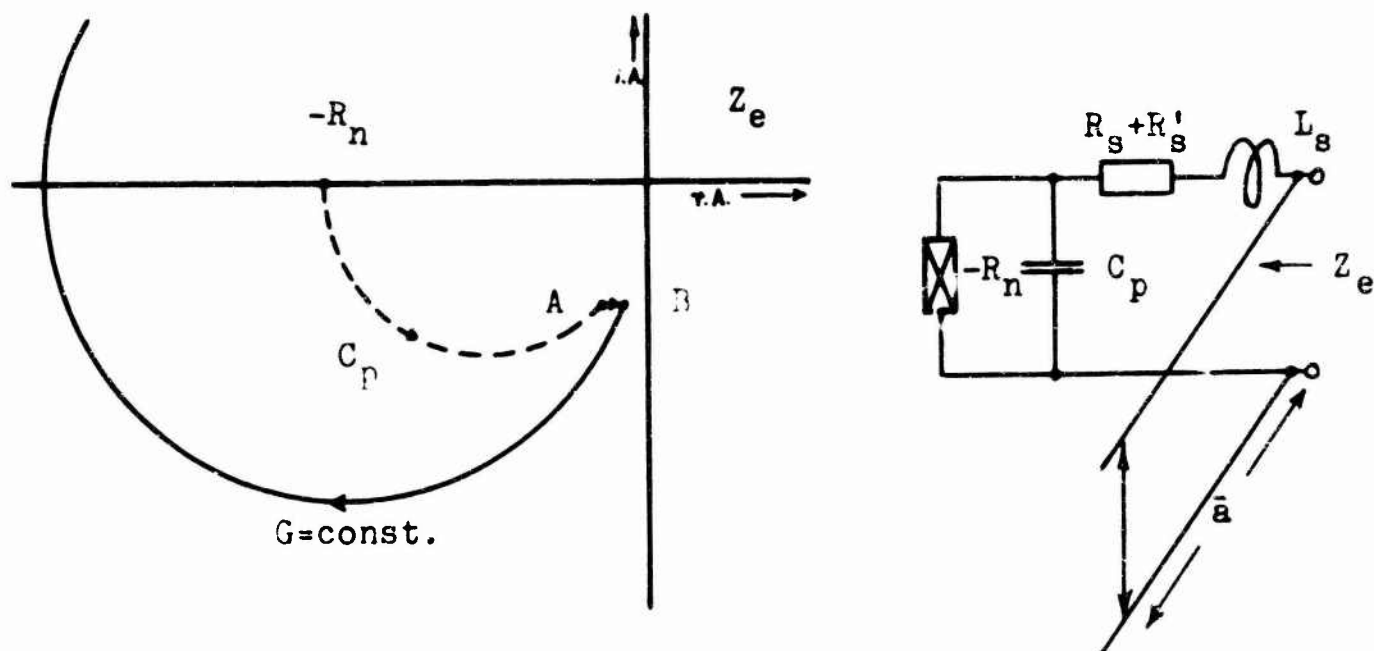
Fig. 26

which at the frequency f = 400 Mc/s transforms -R_n on a circle of constant conductance to the point A of the impedance plane in Fig.26 (L_s is neglected). By the additional series resistance $R_s +$ R_s' this impedance is transformed to the point B and by the susceptance of the short circuited line B is further transformed on a circle of constant conductance (G = const.). This circle has a great diameter because B ist very close to the imaginary axis. Finally the relatively small radiation resistance of part b of the antenna must be added to this impedance shown in Fig.26.

and the sum must be transformed from the locus of the TD to the feeding point, for receiving the input impedance of the antenna (R_p has been neglected). According to chapter 5 the antenna, shows only then a traveling wave behaviour, if the feeding point impedance lies near $-Z_L = -240\Omega$. Therefore the series resistor R_s' could not be applied.

Fig.27 shows the input impedance for $b = 0.2\lambda_0$, $R_p = 500\ \Omega$. $R_s' = 0$. The approach of the circle to the point $-Z_L$ is better than with the conditions of Fig.25 but seems not yet to be sufficient. Better results are obtained by varying the length b of the top of the antenna. According to Fig.16 a lengthening of b corresponds to a series connection of a positive reactance, i.e. by this lengthening the impedance circle of Fig.27 is shifted up.

Fig.28 and 29 are valid for $b = 0.25\lambda_0 = 187.5$ mm and $b = 0.3\lambda_0$ = 225 mm, the remaining parameters being unchanged. With $B = 19.4$ mMho, the circle of Fig.29 is very near to $-Z_L$. In this case probably a traveling wave distribution of current exists on the antenna. With accuracy this condition can be tested by probing the current distribution and by minimizing the VSWR on the antenna through variation of b and $\bar{a}$. On account of the results received by measurement this should be possible with the test conditions of Fig.28 and 29.

10. Evaluation of the Radiation Impedance

a. Physical Principle

The radiation impedance Z_{s1} of a single antenna is defined by

$$P_S = \frac{1}{2}|I_a|^2 Z_{s1} \qquad \text{respectively} \qquad Z_{s1} = \frac{2P_s}{|I_a|^2} \qquad (22)$$

where P_s is the entire (complex) power which is radiated from the antenna and I_a is the antenna current at a special reference point. Since Z_{s1} depends on the location of this reference point, in the following always the current at the feeding point of the antenna will be used as reference term.

Fig. 27   Antenna-input impedance at different values of $\bar{a}$. $h_1 = 338$ mm, $b = 0.2 \lambda_o$ = 150 mm, $R_S' = 0$, $R_p = 500 \Omega$
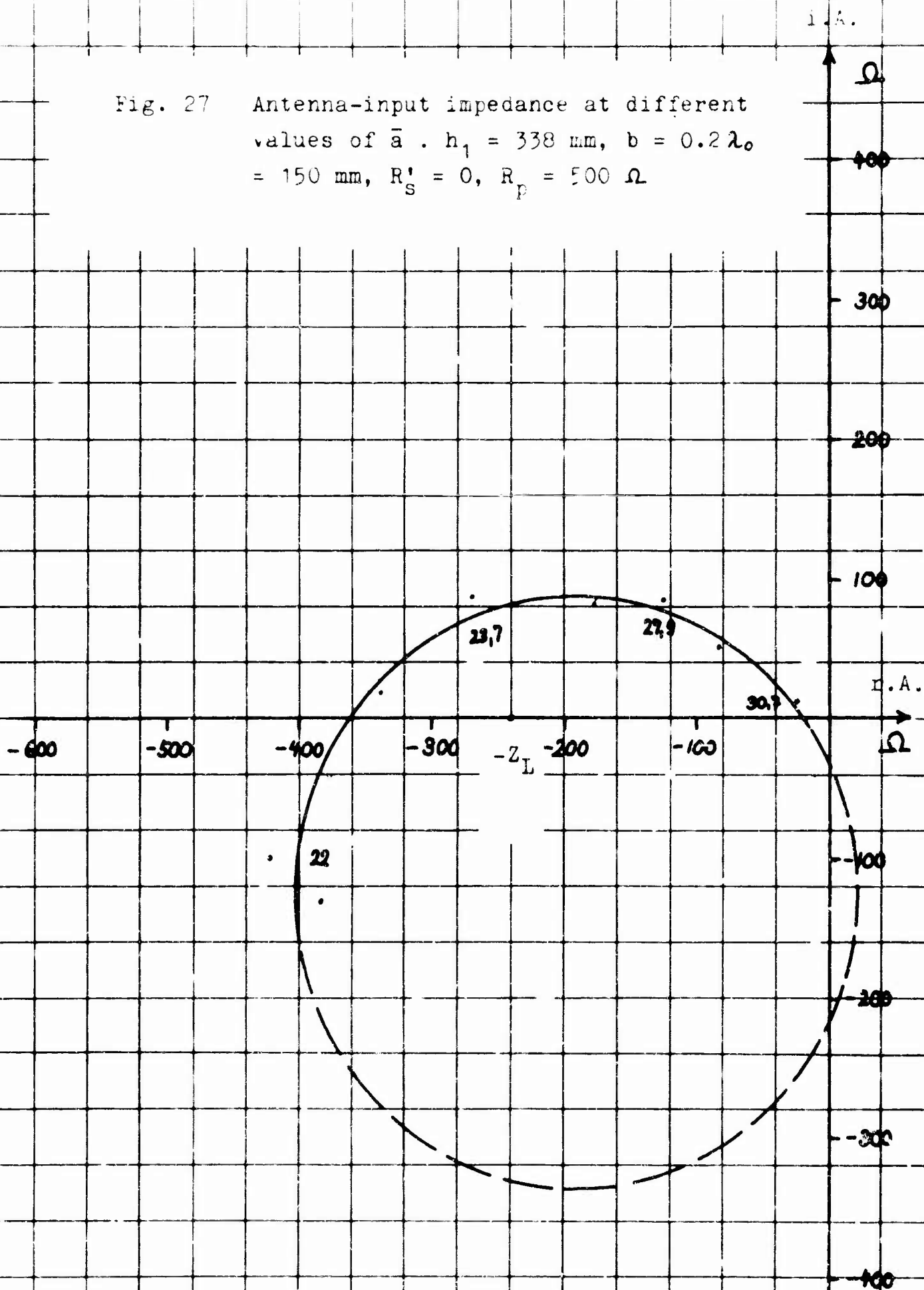
Fig. 2   Antenna-input impedance at different values of $\bar{a}$. $h_1 = 338$ mm, $b = 0.25\lambda = 187.5$ mm, $R_s' = 0$, $R_p = 500.\Omega$.
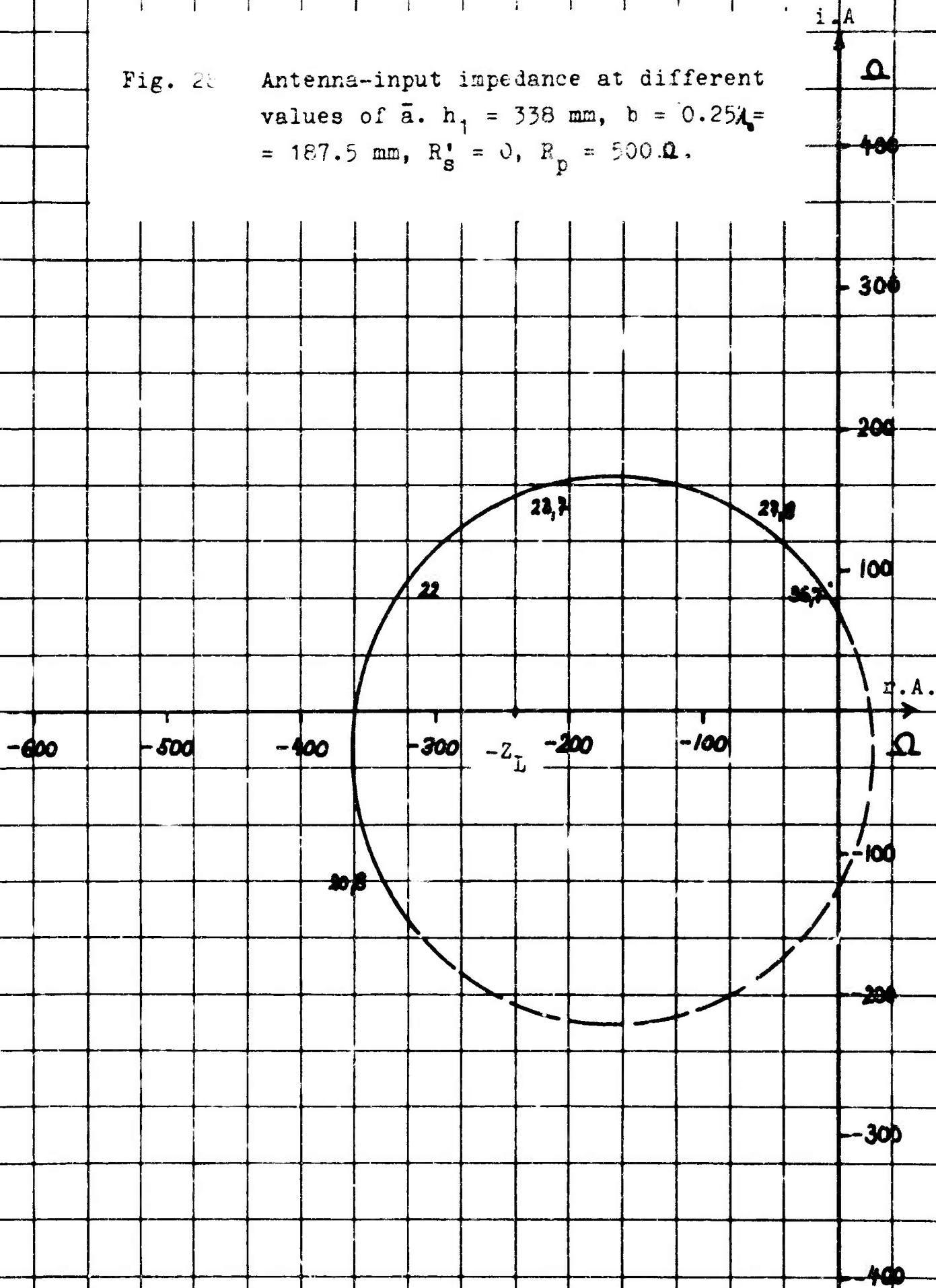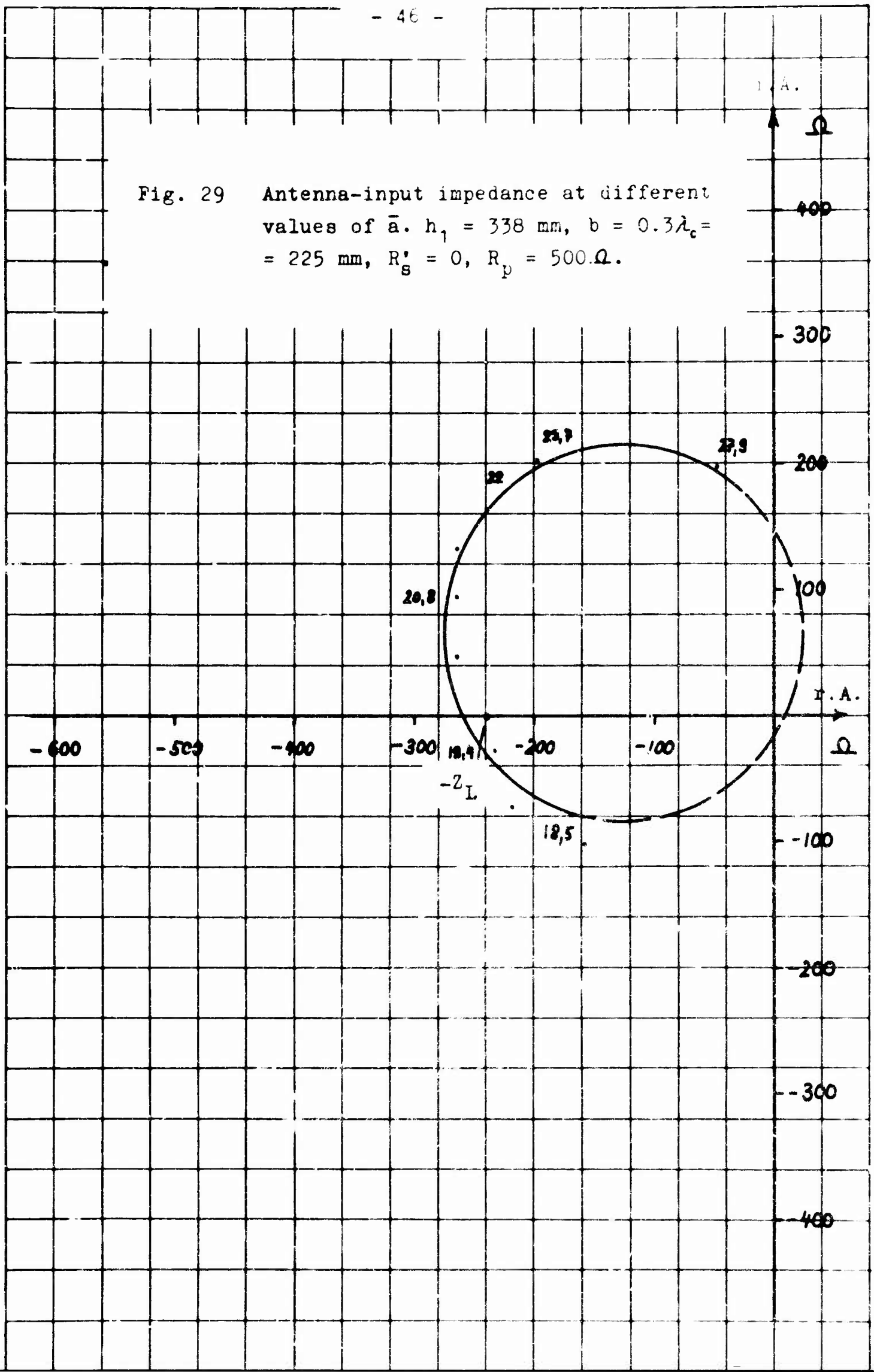
Fig. 29 Antenna-input impedance at different values of $\bar{a}$. $h_1 = 338$ mm, $b = 0.3\lambda_c = 225$ mm, $R_s' = 0$, $R_p = 500.\Omega$.

According to [6a] P_s can be found by integration of Poynting's vector over the surface A of the antenna.

$$P_S = -\frac{1}{2} \int\limits_{(A)} [EH^*]\, da, \tag{23}$$

where da = surface element of the antenna.

Regarding rod-antennas equ. (23) may be replaced by the simpler relation (24).

$$P_S = -\frac{1}{2} \int\limits_{(l_o)} E_z I^*\, dz \tag{24}$$

E_z means the component of the electric field strength in direction of the conductor element dz of the rod, I^* is the conjugate complex value of the antenna current.

Considering an arrangement of two rod antennas as shown in Fig.30,
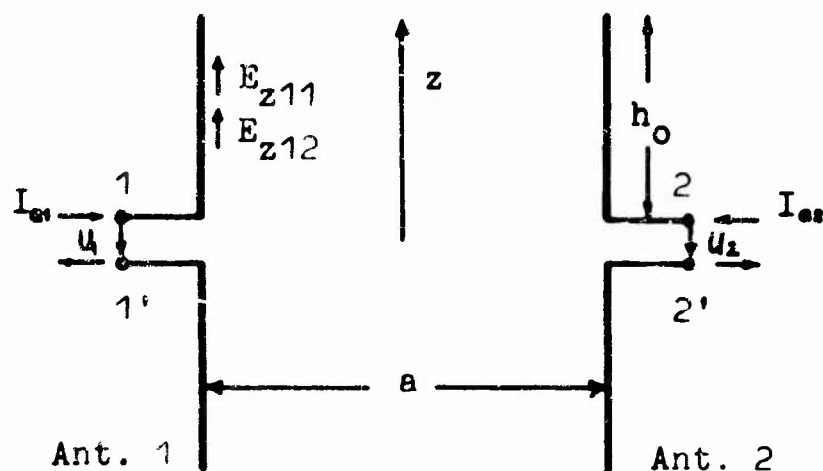
Fig. 30

the inherent radiation resistance Z_{s1} of one rod is not sufficient to describe the radiated power. According to equ. (24) the entire complex power which is radiated by antenna 1 is:

$$P_{s1} = -\frac{1}{2} \int\limits_{-h_o}^{h_o} (E_{z11} + E_{z12})\, I_1^*\, dz =$$

$$= -\frac{1}{2} \int\limits^{h_o} E_{z11} I_1^*\, dz - \frac{1}{2} \int\limits^{h_o} E_{z12} I_1^*\, dz =$$

$$= P_{S11} + P_{S12} \tag{25}$$

E_{z12} means the z-component of the electric field strength at the locus of antenna 1, produced by antenna 2, whereas E_{z11} is produced by antenna 1 itself. The power P_{s11} corresponds to an inherent radiation resistance Z_{s11}, the power P_{s12} to the mutual radiation impedance Z_{s12}.

$$P_{S11} = -\frac{1}{2} \int_{-h_o}^{h_o} E_{z11} I_1{}^* \, dz = \frac{1}{2} I_{a1}^* I_{a1} Z_{S11} \tag{26}$$

$$P_{S12} = -\frac{1}{2} \int_{-h_o}^{h_o} E_{z12} I_1{}^* \, dz = \frac{1}{2} I_{a1}^* I_{a2} Z_{S12} \tag{27}$$

where I_{a1} and I_{a2} are the feeding point currents of the respective antennas. Then

$$Z_{S1} = -\int_{-h_o}^{h_o} \frac{\bar{E}_{z11} I_1{}^*}{I_{a1} I_{a1}{}^*} \, dz$$

$$Z_{S12} = -\int_{-h_o}^{h_o} \frac{E_{z12} I_1{}^*}{I_{a2} I_{a1}{}^*} \, dz \tag{29}$$

Analog to equ. (26, 27) also for antenna 2 the powers P_{s22} and P_{s12} and with this the radiation resistances Z_{s22} and Z_{s21} may be defined.

Considering only arrangements of identical antennas, as will be done in the following, we have

$$Z_{s11} = Z_{s22} \tag{30}$$

Because of reciprocity for all used antennas:

$$Z_{s12} = Z_{s21} \tag{31}$$

On the premises of equ. (3o), reducing the distance a of the two antennas to zero, results

$$E_{z1} = E_{z12} = E_{z21} = E_{z22}$$

Consequently equ. (28, 29) give

$$Z_{s11} = Z_{s22} = \lim_{a \to 0} Z_{s12} = \lim_{a \to 0} Z_{s21} \tag{32}$$

It is sufficient therefore to evaluate the mutual radiation impedance Z_{s12} as a function of a. The inherent radiation impedance Z_{s11} then is attained by equ. (32). The resulting value of Z_{s11} at first is only valid for a = 0. Since however, Z_{s11} for thin antennas is nearly independent of a, the result of equ. (32) may be applied for our antennas to different distances a too.

In general the radiation impedances Z_{s11}, Z_{s12}, Z_{s21}, Z_{s22} are not identical with the parameters of the impedance matrix of the fourpole 1-1', 2-2' in Fig.30. This can be derived by considering the power conditions. The fourpole equations are:

$$U_1 = I_{a1} Z_{11} + I_{a2} Z_{12}$$
$$U_2 = I_{a1} Z_{21} + I_{a2} Z_{22} \tag{33}$$

By these equations we define impedances Z_{11}, Z_{12}, Z_{21} and Z_{22}. The power input P can be found by multiplying the equations with $\frac{1}{2} I_{a1}^*$ or $\frac{1}{2} I_{a2}^*$ respectively

$$P_1 = \frac{1}{2} U_1 I_{a1}^* = \frac{1}{2} I_{a1}^* I_{a1} Z_1 + \frac{1}{2} I_{a1}^* I_{a2} Z_{12} = P_1 + P_{12}$$

$$P_2 = \frac{1}{2} U_2 I_{a2}^* = \frac{1}{2} I_{a2}^* I_{a1} Z_{21} + \frac{1}{2} I_{a2}^* I_{a2} Z_{22} = P_{21} + P_{22} \;,$$

Z_{11} and Z_{12} (resp. Z_{21} and Z_{22}) are then and only then iden-
tical with Z_{s11} and Z_{s12} (Z_{s21}, Z_{s22}), if the complex powers
P_{11} and P_{12} (P_{21}, P_{22}) are identical with the complex <u>radiation</u>
powers P_{s11} and P_{s12} (P_{s21}, P_{s22}). This happens only, if the
entire complex power input of the antennas is transformed into
radiation power; i.e. neither my power be consumed nor be ge-
nerated in the antenna. Furthermore the phase of the current
must not change along the line. For this reason and because
of the impedance W, the simplifications of former theories are
not valid with our antennas. Only for the case of $W = 0$, we
find:

$$Z_1 \approx Z_{s1} \;, \quad Z_{12} \approx Z_{s12}, \quad Z_{21} \approx Z_{s21}, \quad Z_{22} \approx Z_{s22} \;; \qquad (34a)$$

b. <u>Sequence of Calculation</u>

On account of equ. (29) now the mutual radiation impedance Z_{s12}
of two identical traveling wave antennas approximately shall be
evaluated by means of an electronic computer.

The antennas are shown in Fig.31. They consist of rods with the
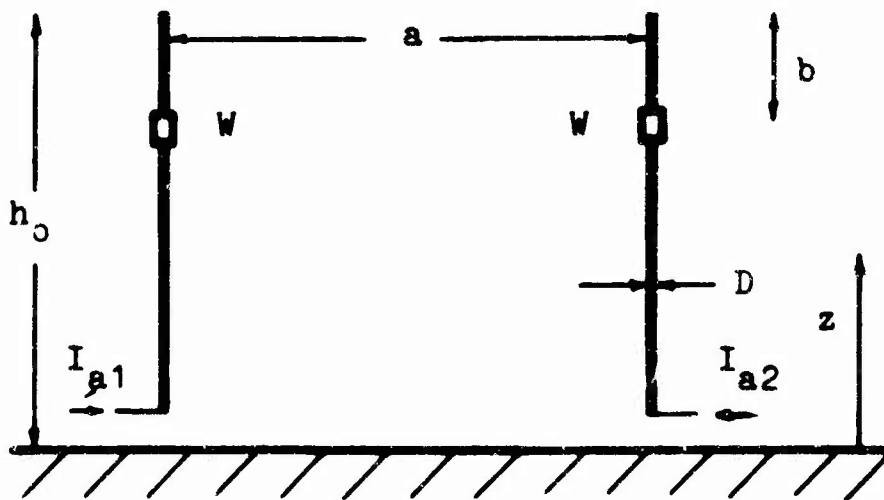
Fig. 31

length h_0, which are mounted vertically over a large well con-
ducting plane. One quarter wavelength from their ends the im-
pedance W is inserted.

To evaluate Z_{s12} from equ. (29) it is necessary to know the current distribution on the antennas. By a first approximation it can be stated that on thin rod antennas the current distribution is equivalent to that on a homogeneous transmission line with the characteristic impedance Z_L.

$$Z_L = 60 \ln \left(1.15 \frac{h_0}{D} \right) \tag{12}$$

The equivalent circuit of the antenna (Fig. 31) is shown in Fig. 32.
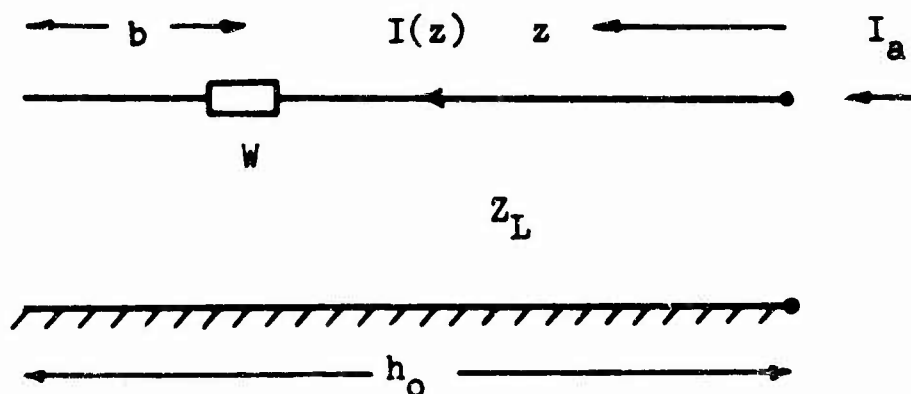
Fig. 32

By means of transmission line theory the following equations can be derived, which are valid for both antennas:

if $h_0 \geqslant z \geqslant h_0 - b$ then

$$\frac{I(z)}{I_a} = \frac{\sin \beta (h_0 - z)}{\sin \beta b \left[\cos \beta (h_0 - b) + \cot \beta b \cdot \sin \beta (h_0 - b) + j (W/Z_L) \sin \beta (h_0 - b) \right]} \tag{35}$$

if $h_0 - b \geqslant z \geqslant 0$ then

$$\frac{I(z)}{I_a} = \frac{\cos \beta (h_0 - b - z) + \cot \beta b \cdot \sin \beta (h_0 - b - z) + j (W/Z_L) \sin \beta (h_0 - b - z)}{\cos \beta (h_0 - b) + \cot \beta b \cdot \sin \beta (h_0 - b) + j (W/Z_L) \sin \beta (h_0 - b)} \tag{36}$$

where $\beta = 2\pi/\lambda$ (37)

In case of $b = \lambda/4$ and $h_0 = 3\lambda/4$, equ. (35) and (36) become much simpler:

if $h_0 \geqslant z \geqslant h_0 - b$ then

$$\frac{I(z)}{I_a} = \cos \beta z \; ; \tag{35a}$$

if $h_0 - b \geqslant z \geqslant 0$ then

$$\frac{I(z)}{I_a} = \cos \beta z - j \, (W/Z_L) \sin \beta z . \tag{36a}$$
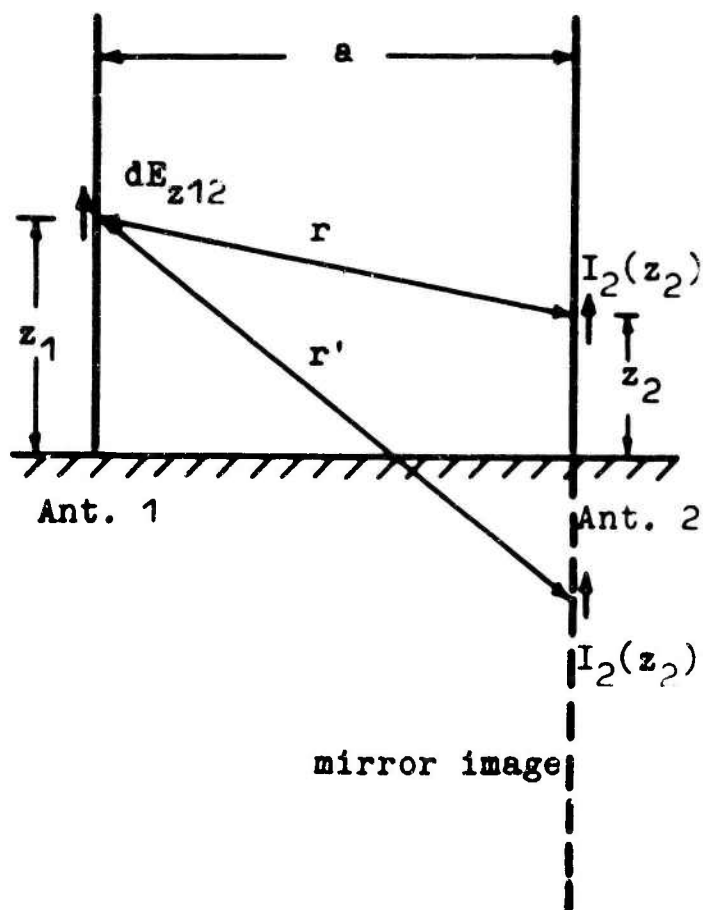
Fig. 33

To evaluate E_{z12} (Fig.33) antenna 2 is completed by its mirror-image. The calculation is done by decomposing the antenna into a series of small Hertz oscillators and by superposition of the originating electric fields. Here the assumption is made, that the radiation field of antenna 2 propagates as if antenna 1 was removed and vice versa. Further it is assumed that the physical extensions of the impedances W are small compared with the antenna dimensions.

According to [8] the increase dE'_{z12} of the electric field strength at the point z_1 of antenna 1, which originates from the Hertz oscillator with the current $I_2(z_2)$ and the length dz_2 at the point z_2 of antenna 2 is:

$$dE'_{z12} = \frac{Z_0 \, dz_2}{4\pi \, \lambda^2} I_2(z_2) \, e^{-j2\pi r/\lambda} \left[\frac{2}{(r/\lambda)^2} - \frac{3(a/\lambda)^2}{(r/\lambda)^4} + \right. \quad (37)$$
$$\left. + j\left(\frac{3(a/\lambda)^2}{2\pi(r/\lambda)^5} - \frac{1}{\pi(r/\lambda)^3} - \frac{2\pi(a/\lambda)^2}{(r/\lambda)^3} \right) \right]$$

with $Z_0 = 120\pi \ \Omega$ and

$$r/\lambda = \sqrt{(a/\lambda)^2 + (z_1/\lambda - z_2/\lambda)^2} \qquad (38)$$

The contribution of the mirror image can also be attained according to equ. (37) if r/λ is replaced by r'/λ

$$r'/\lambda = \sqrt{(a/\lambda)^2 + (z_1/\lambda + z_2/\lambda)^2} \qquad (39)$$

Substituting

$$V = e^{-j2\pi r/\lambda} \left[\frac{2}{(r/\lambda)^2} - \frac{3(a/\lambda)^2}{(r/\lambda)^4} + \right. \qquad (40)$$
$$\left. + j\left(\frac{3(a/\lambda)^2}{2\pi(r/\lambda)^5} - \frac{1}{\pi(r/\lambda)^3} - \frac{2\pi(a/\lambda)^2}{(r/\lambda)^3} \right) \right]$$

respectively writting v'(r') for the mirror image, the total
differential component of the field strength dE_{z12} can be
expressed by equ. (41).

$$dE_{z12} = \frac{Z_0}{4\gamma} I_2(z_2) \cdot (v + v') \frac{dz_2}{\lambda^2} \qquad (41)$$

Consequently:

$$E_{z12}(z_1, z_2) = \frac{Z_0}{4\gamma} \int_0^{l_0} I_2(z_2) \cdot (v + v') \frac{dz_2}{\lambda^2} \qquad (42)$$

In addition with equ. (29) Z_{s12} can be expressed as follows:

$$Z_{s12} = -\frac{Z_0}{4\gamma} \int_0^{l_0}\int_0^{l_0} \left[\frac{I_2(z_2)}{I_{a2}} (v + v') \frac{dz_2}{\lambda} \right] \frac{I_1^*(z_1)}{I_{a1}^*} \frac{dz_1}{\lambda} \qquad (43)$$

where I_1^* and I_{a1}^* means the conjugate complex value of I_1 or
I_{a1} respectively.

Z_{s12} was calculated from equ. (29) - (43) by means of an
electronic computer. The calculation was done for $W_1/Z_L = 1$,
$W_2/Z_L = 0$, $W_3/Z_L = -1$ and $a/\lambda = 0.05$ to $a/\lambda = 1.00$ in steps
of 0.05. $W_1/Z_L = 1$ corresponds to the traveling wave antenna
as described by E. Altschuler [4] . $W_2/Z_L = 0$ is valid for a con-
ventional unloaded unipole with a length of $3\lambda/4$ and $W_3/Z_L = -1$
corresponds to an antenna, according to Fig.31 loaded with a
negative resistance, as described in part I.1.

c. Results

The dashed curves of Fig.34 show the calculated real and
imaginary part of the mutual radiation impedance Z_{s12} for
two unloaded unipoles ($W_2/Z_L = 0$) as a function of the distan-
ce a. The solid curves are taken from [9] , where they have
been calculated from integral functions. With the exception
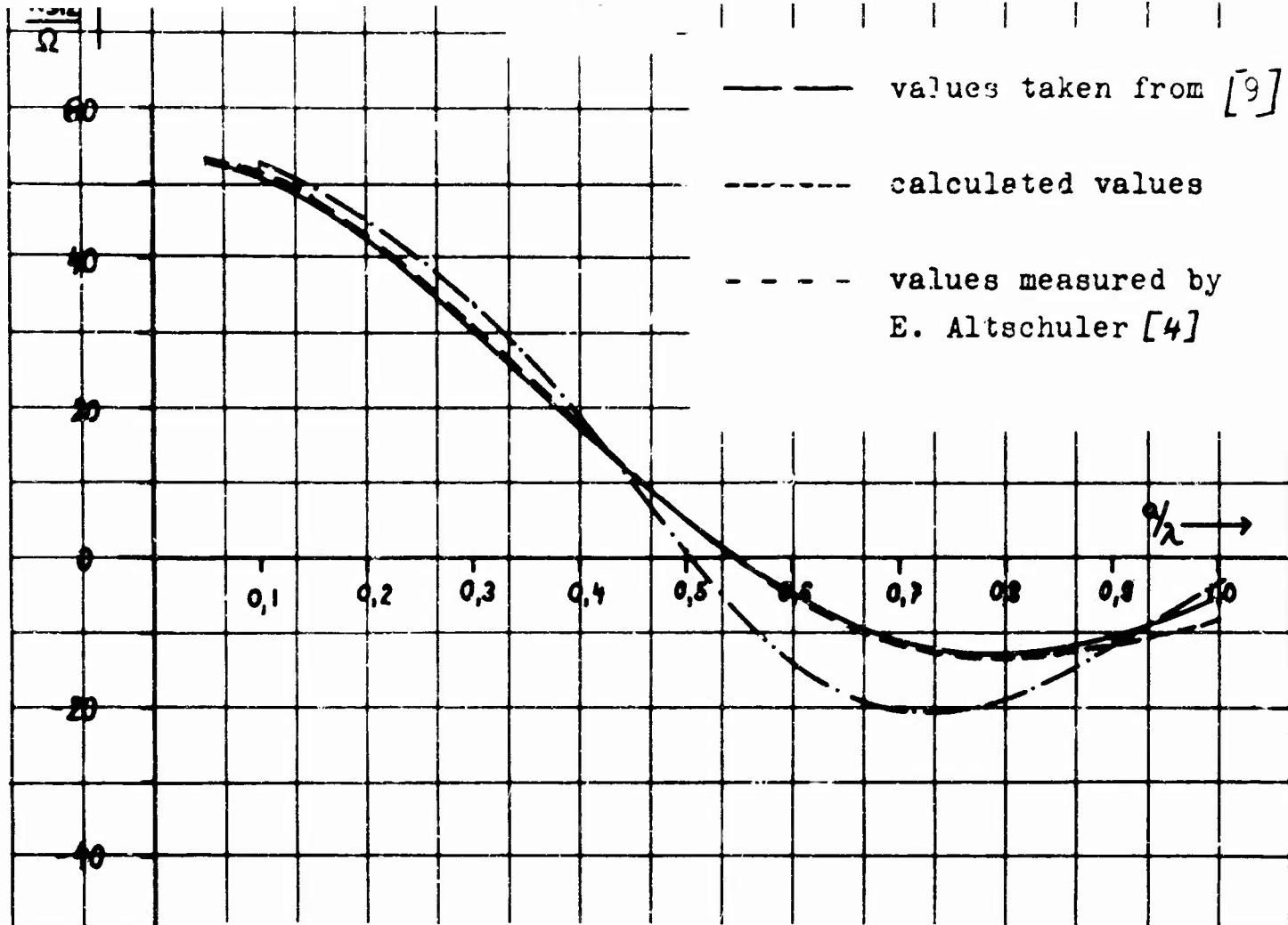
Fig. 34   Mutual radiation impedance $Z_{s12} = R_{s12} + jX_{s12}$ of unloaded unipoles with $h_o = 3\lambda/4$.
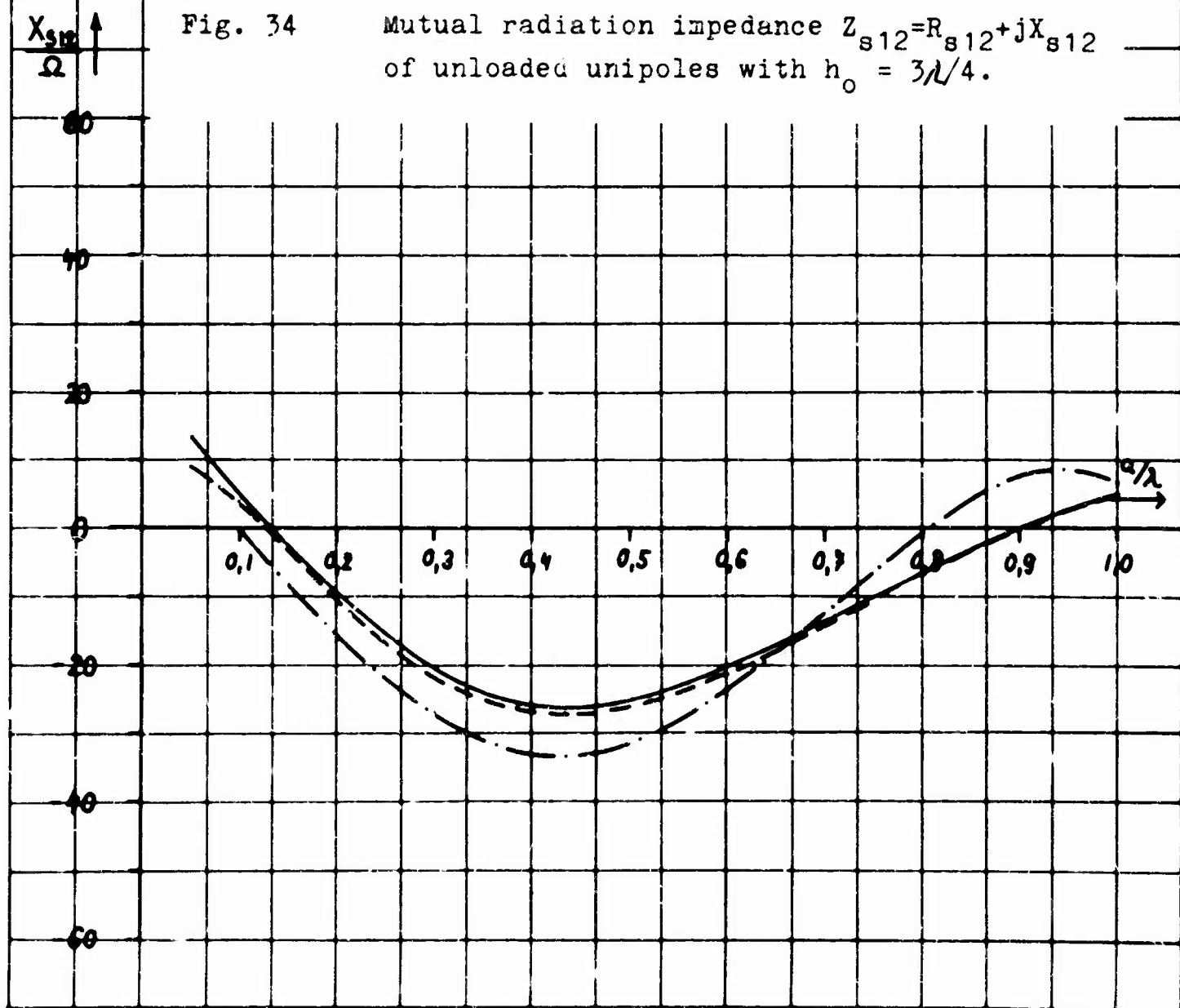
of little deviations, both curves are identical. These deviations probably could be avoided by improving the numerical method by which equ. (43) was evaluated. The dash-dot curves show the result of measurings, which have been performed by E. Altschuler at unipoles with $h_o/D = 70$ (Fig.31). In consideration of the many simplifying assumptions on which the calculation is based, the agreement of the calculated and measured curves seems to be satisfactory. Fig.35 shows the real and imaginary part of the calculated radiation impedance of two identical antennas according to Fig.31 ($h_o = 3\lambda/4$). For antennas with negative resistances $-W$ exactly the same results were obtained as for antennas with positive W, if $|-W|$ was equal to $+W$. According to equ. (32) the inherent radiation impedance was attained by extrapolation:

$$Z_{s11} = R_{s11} + jX_{s11} = 153 + j73\Omega$$

Comparing Fig.35 with Fig.34, it can be seen, that the radiation impedance of a traveling wave antenna (Fig.31) is twice to three times greater than the radiation impedance of a standing wave antenna of comparable size. This means, supposing an equal feeding current that a traveling wave antenna radiates more than an unloaded antenna.

11. Determination of the Mutual Coupling

a. Sequence of Calculation and Deductions

The coupling coefficient of two identical antennas can be defined as

$$k = \frac{|Z_{12}|}{|Z_{11}|} \tag{44}$$

where Z_{11} and Z_{12} are parameters of the impedance matrix of the fourpole 1-1', 2-2' (see Fig.30, 31). Because of equ. (34a), the coupling of standing wave antennas approximately can be determined by evaluation of the radiation impedance Z_{s11} and Z_{s12}. Regarding traveling wave antennas $Z_{11} \neq Z_{s11}$ and $Z_{12} \neq Z_{s12}$; therefore the evaluation of the coupling coefficient requires the calculation of Z_{11} and Z_{12}.
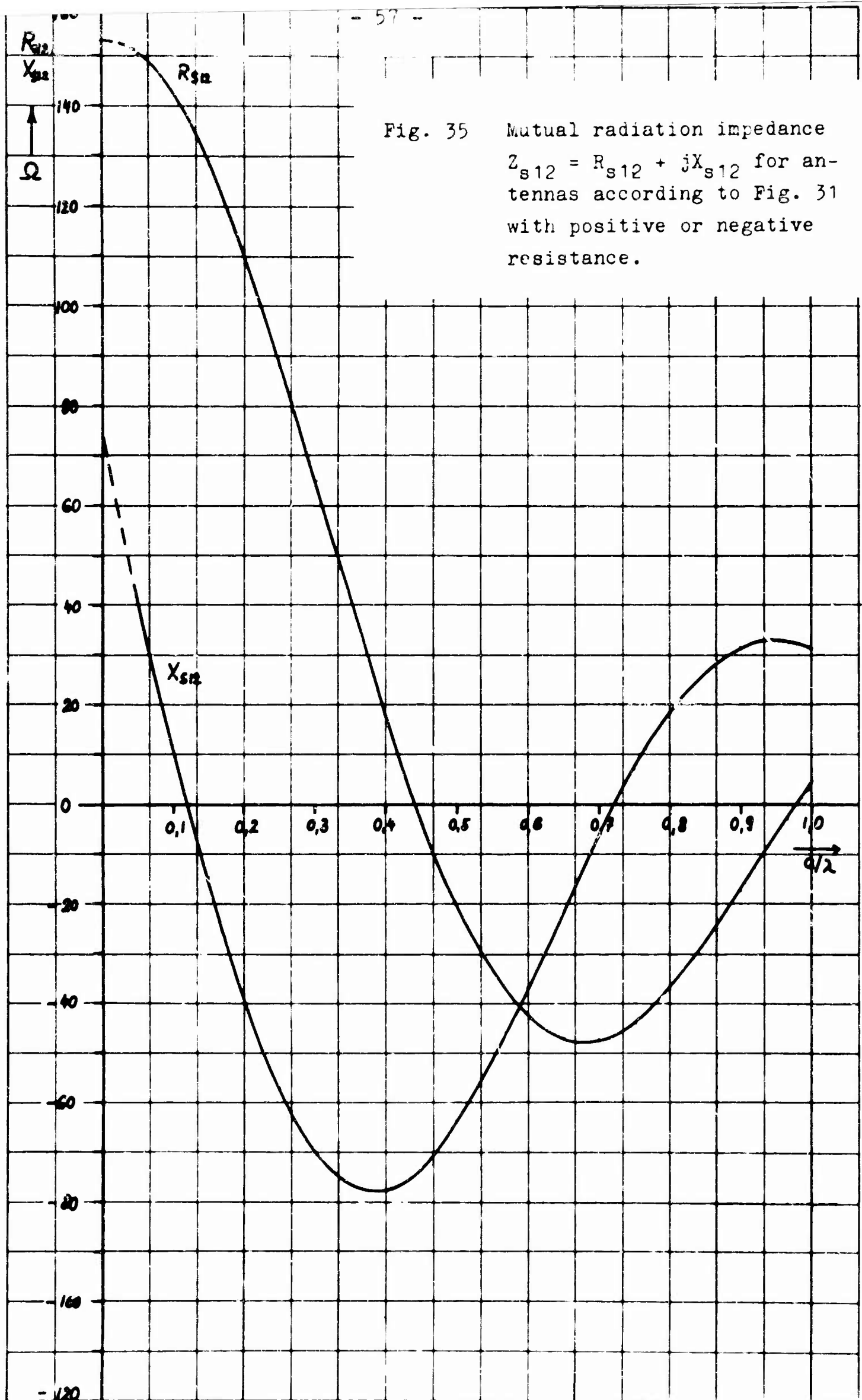
Fig. 35 Mutual radiation impedance
$Z_{s12} = R_{s12} + jX_{s12}$ for an-
tennas according to Fig. 31
with positive or negative
resistance.

By first approximation Z_{11} and Z_{12} can be determined by the following considerations:

Because of reciprocity and on the premises of Z_{11} being equal to Z_{22}, equ. (33) may be written:

$$U_1 = I_{a1} Z_{11} + I_{a2} Z_{12}$$
$$U_2 = I_{a1} Z_{12} + I_{a2} Z_{11} \tag{45}$$

Case A

Both antennas are fed by identical currents, i.e.

$$I_{a1} = I_{a2} = I_a ; \quad U_1 = U_2 = U ;$$

In addition with equ. (45) the input impedance of antenna 1 then is:

$$Z_{1A} = U_1 / I_{a1} = U / I_a = Z_{11} + Z_{12} \tag{46}$$

Case B

The feeding now is done anti-symmetrically, i.e.

$$I_a = I_{a1} = - I_{a2}; \quad U = U_1 = - U_2$$

The input impedance of antenna 1 is now:

$$Z_{1B} = U_1 / I_{a1} = U / I_a = Z_{11} - Z_{12} \tag{47}$$

In addition with equ. (46) consequently

$$Z_{11} = \frac{1}{2} (Z_{1A} + Z_{1B}) \tag{48}$$

$$Z_{12} = \frac{1}{2} (Z_{1A} - Z_{1B}) \tag{49}$$

The impedances Z_{1A} and Z_{1B} can be calculated approximately by applying transmission line theory to antenna 1 (see Fig.32) and considering the radiated power.

In **case A** according to equ. (2€, 27) the power radiated by antenna 1 is:

$$P_{S1A} = \frac{1}{2}|I_a|^2 (Z_{S11} + Z_{S12})$$

(50)

In **case B:**

$$P_{S1B} = \frac{1}{2}|I_a|^2 (Z_{S11} - Z_{S12})$$

(51)

The radiated **real** power in case A or B respectively is:

$$P_{SW1A,B} = \frac{1}{2}|I_a|^2 (R_{S11} \pm R_{S12})$$

(52)

This radiated real power can be described by a constant series resistance per unit length along the equivalent transmission line. Based on the current distribution according to equ. (35a, 36a) and with the assumption that this distribution is not essentially changed by the attenuation, the resis ance per unit length can be derived from the following equation:

$$\frac{1}{2}\int_0^{h_o} |I(z)|^2 R'_{A,B}\, dz = P_{SW1A,B}$$

(53)

With $b = n\lambda /4$ (n = 1, 2, 3, 4 ...)

$$R'_A = \frac{R_{S11} + R_{S12}}{h_o - b/2} \quad ; \quad R'_B = \frac{R_{S11} - R_{S12}}{h_o - b/2}$$

(54)

In analogy with this, the reactive power can be considered by an additional series reactance $\Delta X'$ per unit length. From this consideration results

$$\Delta X'_A = \frac{X_{S11} + X_{S12}}{h_o - b/2} \quad ; \quad \Delta X'_B = \frac{X_{S11} - X_{S12}}{h_o - b/2} \quad ,$$

(55)

The influence of $\Delta X'$ on the input impedance is less pronounced however than the influence of R' on the input impedance. The values of R_{s11}, R_{s12}, X_{s11} and X_{s12} are known from Fig.35 and equ. (32).

In case of $R'_{A, B} \ll Z_L$, the appearing attenuation by radiation can be expressed by the following approximate formula

$$\alpha_A = \frac{R'_A}{2Z_L} \quad , \quad \alpha_B = \frac{R'_B}{2Z_L} \tag{56}$$

Regarding an isolated antenna $(R_{s12} = X_{s12} = 0)$

$$R' = \frac{R_{s11}}{h_0 - b/2} \quad and \quad \alpha = \frac{R'}{2Z_L} \tag{57}$$

Evaluating R_{s11}, R_{s12}, X_{s11}, X_{s12} in chapter I. 10b equ. (35a, 36a, 43), the attenuation has been neglected. An approximation of second order can be attained therefore, by basing a new calculation of the radiation impedances on the current distribution, which is obtained by consideration of the attenuation according to equ. (56, 57). Through this iteration method a continuous improvement of the values of the radiation impedances and of the current distribution is possible. In the present case the approximation of first order was thought to be sufficient however.

The fact that the current distribution on such antennas changes with the mutual coupling, probably affects the radiation patterns too.

On account of the preceding considerations the input impedances Z_{1A} and Z_{1B} can now be calculated by means of the equ. (54-56) on the base of the equivalent transmission line circuit of Fig.32. An example is given in section b.

Regarding the case of wave antennas with according to Fig.31 with positive resistances, W has to be chosen thus that the impedance appearing at $z = h_0-b$ is matched to the characteristic impedance of the antenna line. Then $Z_{11} \approx Z_L$. According to equ. (44) the coupling coefficient is then

$$k = \frac{|Z_{12}|}{|Z_L|} \tag{58}$$

In equ. (58) $\left| Z_L \right|$ appears in the denominator. Since $\left| Z_{12} \right|$ is not much depending on the value of Z_L, the fact can be stated, that by increasing $\left| Z_L \right|$ the coupling decreases. On the other hand bandwidth and efficiency η decline too, if Z_L is raised.

η is attained from the equation

$$\eta = 1 - P_v / P_e$$

where P_v means the loss of real power in the resistor W (other losses are neglected) and P_e is the total real power input of the antenna. Approximately

$$P_e = \frac{1}{2} \left| I_a \right|^2 Z_L , \qquad P_v = \frac{1}{2} \cdot \left| I (h_0 - b) \right|^2 W$$

Since

$$W \approx Z_L \quad and \quad \left| I (h_0 - b) \right| \approx \left| I_a \right| \bar{e}^{\,\alpha (h_0 - b)}$$

and with equ. (57)

$$\eta = 1 - exp \left(- \frac{R_{s\parallel} (h_0 - b)}{Z_L (h_0 - b/2)} \right) \tag{59}$$

Z_L being great, η is small. This means that in practice a good compromise between equ. (58) and equ. (59) must be sought.

Since negative resitances mean amplification, equ. (59) is _not_ valid for antennas according to Fig. 31 with negative resistances. An increase of the characteristic impedances of such antennas and with this a decrease of the mutual coupling however is also combined with a reduction of the bandwidth. In this chapter the coupling was described according to equ. (44). This is a well known and often applied definition. However, we think, that dealing with antennas containing negative resistances this factor is not much appropiate and we should use a more general definition. We shall deal with this problem in one of our next reports.

b. Results

Z_{11} and Z_{12} have been calculated in chapter 11a by assuming that the characteristic impedance Z_L is constant along the antenna. In reality however this condition is not fulfilled. Therefore not unimportant deviations between calculated and measured values are obtained. Considering the coupling coefficient

$$k = \frac{|Z_{12}|}{|Z_{11}|} = \frac{|Z_{1A} - Z_{1B}|}{|Z_{1A} + Z_{1B}|} \qquad (60)$$

these mistakes are smaller, because the main effect of an inhomogeneous line consists in the impedance transformation. Since both impedances, in the numerator and in the denominator, are transformed, the mistakes are compensated.

The evaluation of Z_{11}, Z_{12} and k according to equ. (48, 49) first of all was done for the case of two antennas according to Fig.31 with positive resistances as investigated in [4]. The given values are:

$h_o = 3\lambda/4 = 37.5$ cm, b $= \lambda/4 = 12.5$ cm, D $= 0.635$ cm, f $= 600$ Mc/s, W $= 240$ Ω.
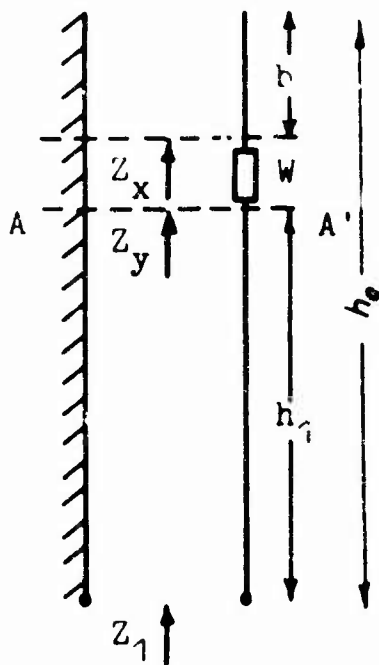
Fig. 36

The sequence of calculation is explained by the following example, a/λ being 0.7.

Concerning antenna 1, the equivalent circuit of Fig.36 is valid. According to equ. (12) the equivalent characteristic impedance of the antenna without radiation losses is equal to 253 Ω, respectively according to [66] :

$$L' = 8.43 \; nH/cm \;, \qquad C' = 0.132 \; pF/cm \;;$$

or

$$X'_L = 2\pi f L' = 31.8 \; \Omega/cm \;,$$

$$B'_C = 2\pi f C' = 0.498 \; mMho/cm \;,$$

where L' is the inductance, C' the capacity, X'_L the reactance and B'_C the susceptance per unit length of the equivalent line. From Fig. 35 we find: $R_{s11} = 153 \; \Omega$, $R_{s12} = -47.4 \; \Omega$, $X_{s11} = 73 \; \Omega$, $\lambda_{s12} = -6.4 \; \Omega$.

In case A, according to equ. (54, 55) then

$$R'_A = 3.38 \; \Omega/cm; \quad X'_A = 2.15 \; \Omega/cm$$

The constants of the equivalent line (see Fig.36) therefore are:

$X'_t = X'_L + \Delta X'_A = 33.95 \; \Omega/cm; \quad B'_{Ct} = B'_C = 0.498 \; mMho/cm.$

$R'_t = R'_A = 3.38 \; \Omega/cm.$

According to well known formulas

$$Z_{L1} = 261.5 - j \; 13.0 \; \Omega, \; \alpha = 0.00646 \; 1/cm$$

$$\beta = 0.131 \; 1/cm \;.$$

In this, Z_{L1} means the characteristic impedance of the lossy equivalent line, α is the attenuation- and β the phase constant.

The input impedance of the open circuited line of length b = 12.5 cm is according to transmission line theory

$$Z_x = 21.2 - j1.05 \; \Omega$$

At A-A' (see Fig.36) then the impedance

$$Z_y = Z_x + W = 261.2 - j1.05 \ \Omega$$

appears. As has been said before, the characteristic impedance $Z_L(h)$ is not constant along the antenna. At the place A-A', which is important for matching, the real characteristic impedance $Z_L(h_1)$ differs from the average characteristic impedance Z_{L1}. This can be considerd by inserting an ideal transformer, which transforms $|Z_L(h_1)|$ into $|Z_{L1}|$ or Z_y into $\overline{Z}_y$ respectively.

$$|Z_{L1}| = |Z_L(h_1)| \ / n^2$$

respectively

$$\overline{Z}_y = Z_y \big/ n^2$$

n can be determined by assuming that with the experimental ascertained value of W, (regarding the isolated antenna i.e. $R_{s12} = X_{s12} = 0$), Z_y must be matched to the line (that means $\overline{Z}_y = |Z_{L1}|$ or $Z_y = |Z_L(h_1)|$:

$$n = \sqrt{\frac{|Z_y|}{|Z_{L1}|}} = 1.016$$

Consequently for the present case

$$\overline{Z}_y = Z_y \big/ \ n^2 = 253 - j1.02 \ \Omega$$

Z_{1A} finally is attained by transformation of $\overline{Z}_y$ over the line of length $h_1 = 25 \, cm$. This transformation can be performed according to chapter I,7.

$$Z_{1A} = 257.0 - j3.4 \ \Omega$$

In analogy to this, Z_{1B} can be obtained by replaxing R_A' and $\Delta X_A'$ by R_B' and $\Delta X_B'$. The result is

$$Z_{1B} = 270.5 - j15.2 \ \Omega$$

Consequently

$$Z_{11} = \tfrac{1}{2}(Z_{1A} + Z_{1B}) = 263.5 - j\,9.3\ \Omega$$

$$Z_{12} = \tfrac{1}{2}(Z_{1A} - Z_{1B}) = -6.75 + j\,5.9\ \Omega$$

$$k = \frac{|Z_{12}|}{|Z_{11}|} = 0.0341$$

The results for Z_{12} which were obtained according to the principles, described above, are shown in Fig.37. The solid curves represent R_{12} and X_{12} as a function of the distance a/λ. For comparison with measured values these curves are not appropriate because their shape depends much on the quality of the matching at A-A' (see Fig.36). Less dependent on these conditions is the coupling coefficient k, shown in Fig.38. The dashed curve represents the calculated coupling coefficient as a function of a/λ. The solid curve shows values, which were measured by E.Altschuler [4]. Considering the many approximations on which the calculation is based, the agreement of both curves seems to be sufficient.

Therefore this method of calculation was applied to antennas (according to Fig.31) with negative resistances too. The sequence of calculation corresponds exactly to that with the antennas containing positive resistances, if " is replaced by $-R_n$. The value of R_n can be obtained from the condition that the impedance appearing at A-A' (Fig.36) must be matched to the line. Therefore $R_n = 301\ \Omega$.

The dash dot curve of Fig.38 shows the coupling coefficient of two antennas with negative resistances - $R_n = W = -Z_L$. It can be seen that, regarding small distances a/λ, the coupling coefficient is greater than for the antennas with positive resistances. This is due to the fact that negative

Fig. 37 R_{12} and X_{12} for an array of two antennas according to Fig. 31 ($h_o = 3\lambda/4$, $b = \lambda/4$)

——— with positive resistances

- - - - with negative resistances
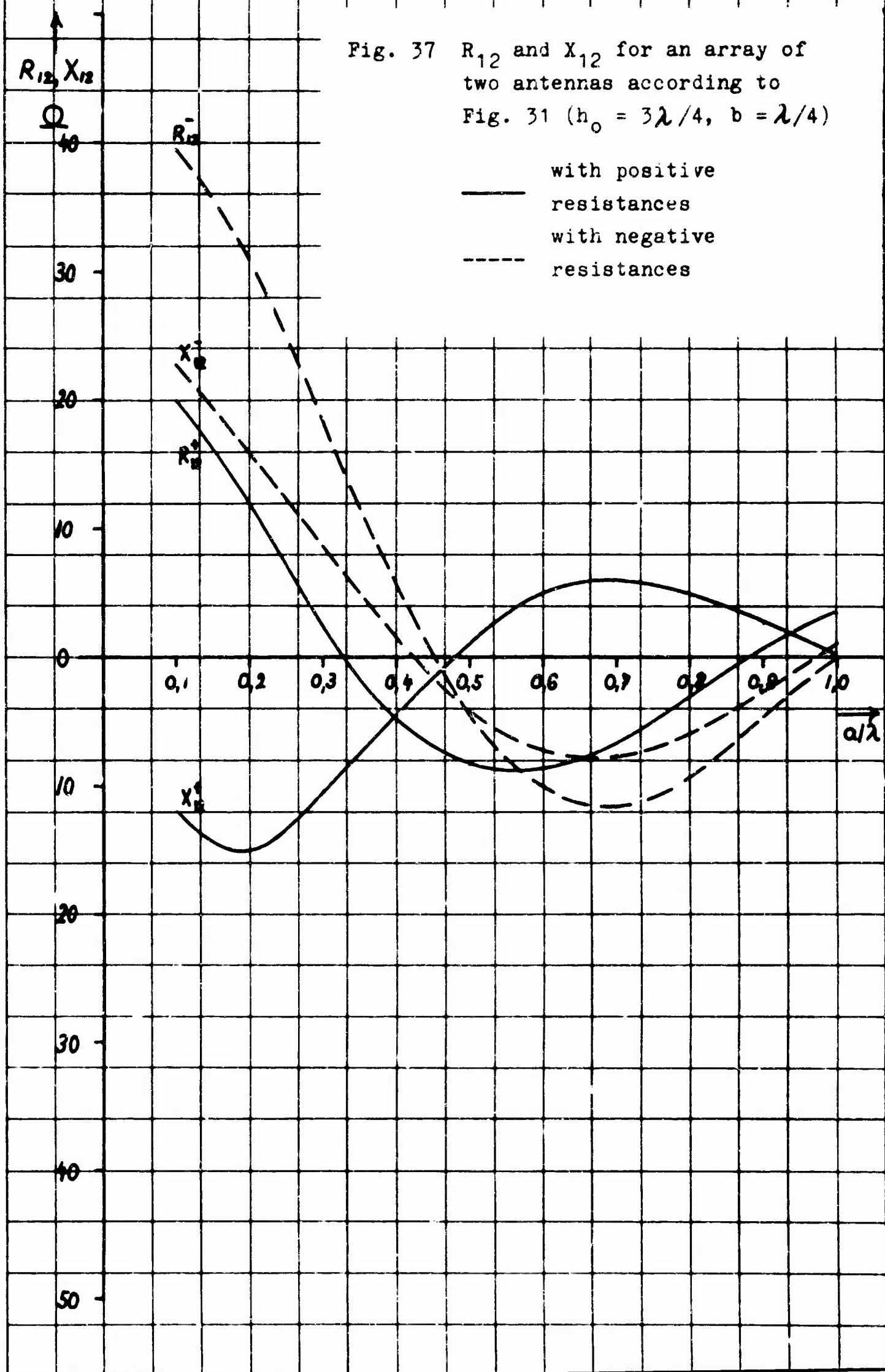
Fig. 38   coupling coefficient for an array
of two antennas according to
Fig. 31 ($h_o = 3\lambda/4$, $b = \lambda/4$)

------   calculated values

———   measured values

—·—   calculated values
          in case of $W = -Z_L$

unloaded unipoles

unipoles with $W = -Z_L$

unipoles with $W = +Z_L$
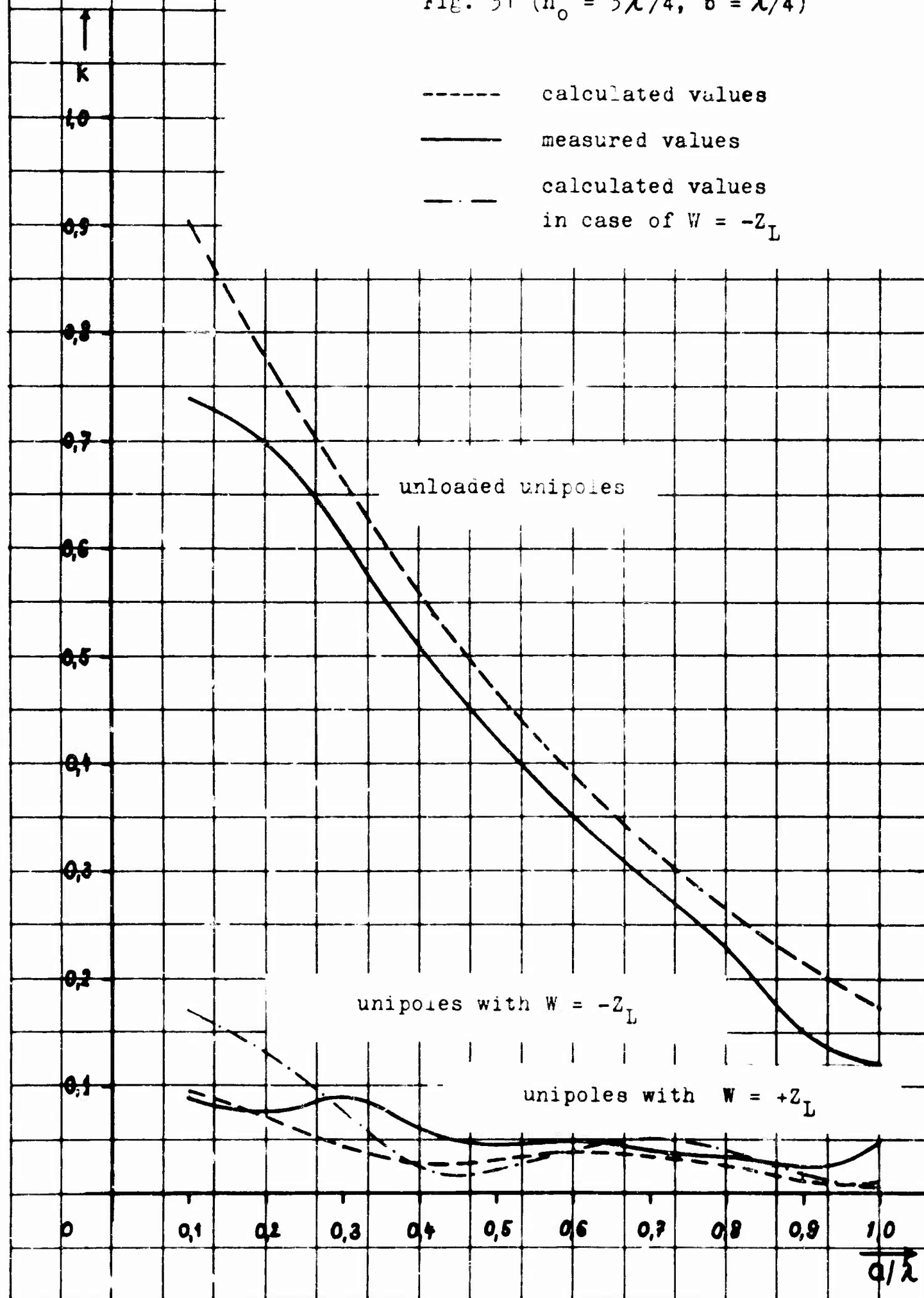
resistances, terminating a dissipative transmission line, transform on enlarging spirals as described in chapter I.7.

For comparison Fig.38 also shows the measured and calculated values of the coupling coefficient of unloaded antennas ($h_o = 3\lambda_o/4$.) With these antennas the coupling coefficient is considerably greater than with the antennas according to Fig.31.

In spite of the small coupling factor which we found for antennas with a traveling wave distribution, we do not think these antennas to be well suited for arrays, since their good property, i.e. low coupling, is only pronounced for great heights. Then however, their radiation is concentrated in the direction of the rod. Furthermore, regarding antennas according to Fig.31 with positive resistances, we get poor efficiency, replacing the resistor by a TD the bandwith of the circuit becomes very small (the amplification effect can easier be attained by a TD-amplifier at the input of the antenna). Therefore we shall investigate other antennas with integrated active elements, which we hope to have a low mutual coupling factor without the disadvantages of the antennas described in the foregoing.

12. Measurement of the Mutual Coupling of Antennas

To understand and to measure the coupling between parallel rod antennas we developed methods which we described in our administrative reports No. 9, 1o, 11.

For measuring the current distrubution along a rod antenna, a small loop with rectifier and indicator is moved along the rod. This arrangement is combined with a method for measuring the coupling between this rod and a parallel rod antenna in the near field of the first dipole.

According to Fig.39 the second rod is terminated by a coaxial line with movable short, i.e. terminated by a variable reactance. The impedance of the first rod is measured.

If the short is moved the impedance of the first rod antenna is changed and the amount of impedance change is dependent on the amount of coupling between the 2 rod antennas. In the
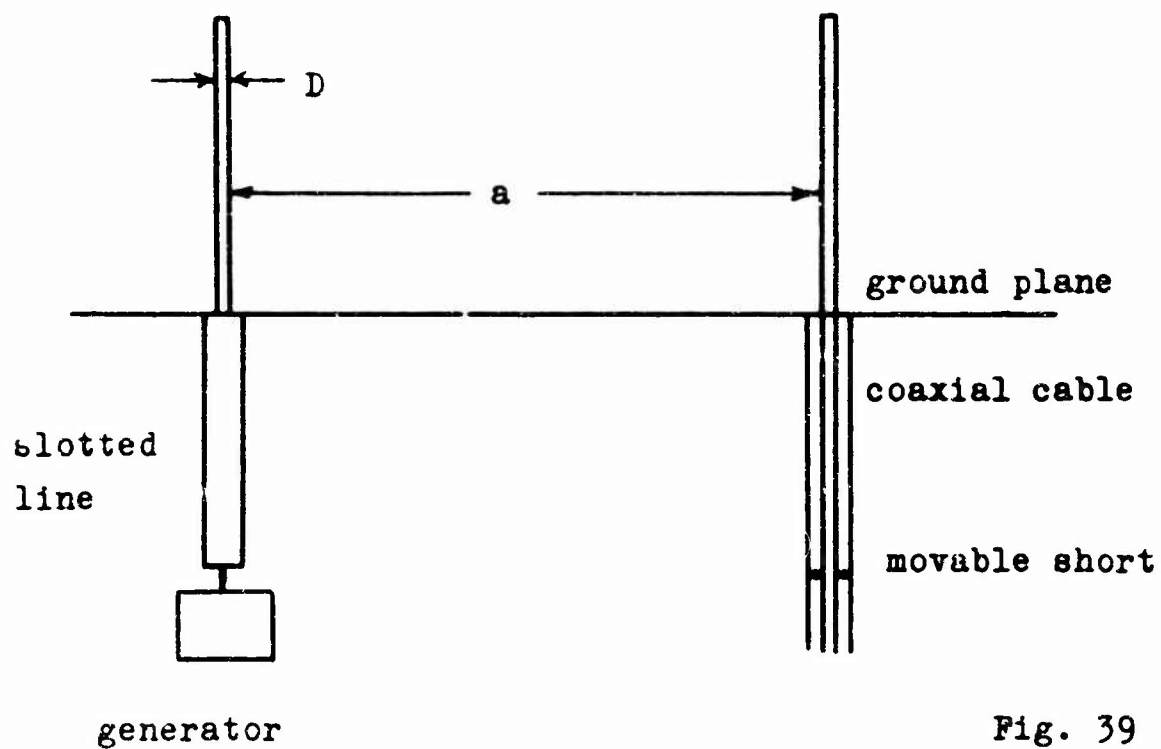
Fig. 39
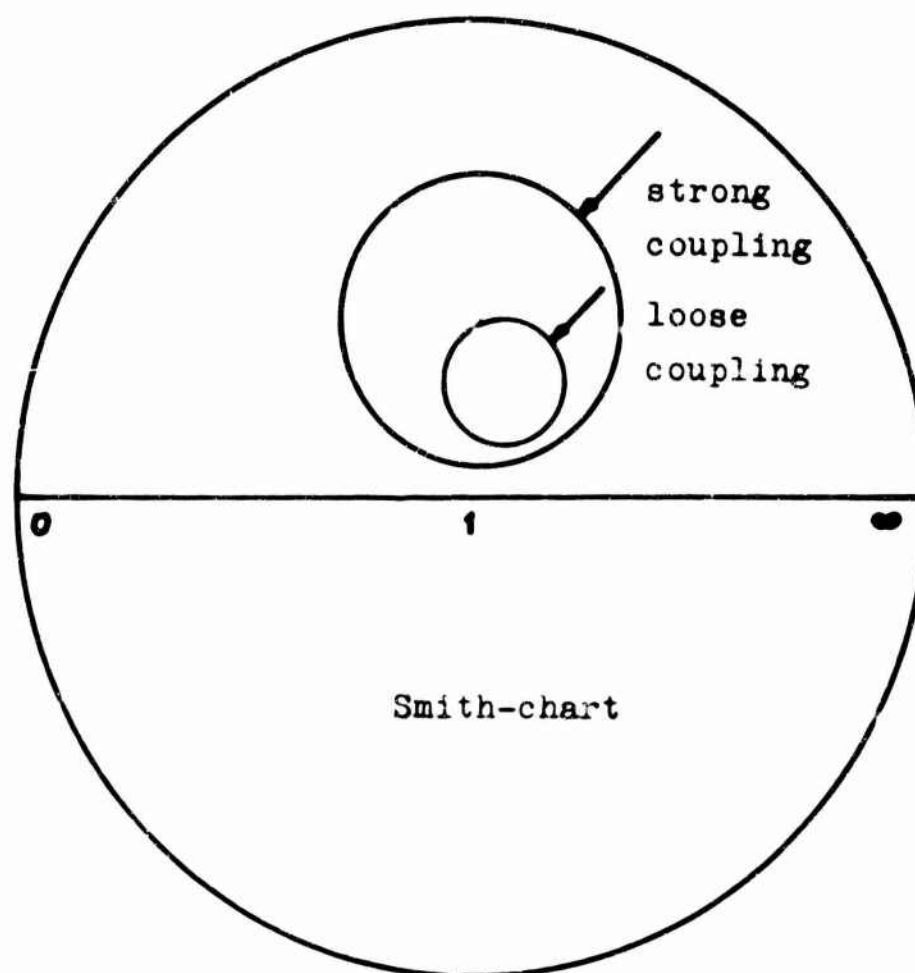
Smith-chart

Fig. 40

complex impedance plane the measured impedance runs around a
circle, when the short is moved. Fig.40 shows in a Smith chart
two of these circles, the larger one for rods with strong
coupling, the smaller circle for rods with loose coupling. The
size of this circle is a good indicator for the amount of coup-
ling between the 2 rods. The 2 rods may be regarded as a two-
port-network, whose input is the feeding point of the first rod
and whose output is the feeding point of the second rod (see
Fig.41).
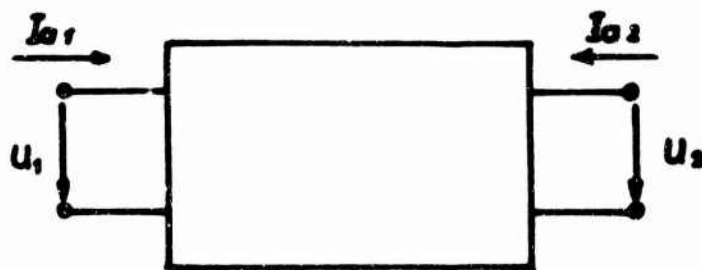
Fig. 41

Then the following is true

$$U_1 = Z_{11}I_{a1} + Z_{12}I_{a2}$$
$$U_2 = Z_{21}I_{a1} + Z_{22}I_{a2}$$

(61)

with the coupling impedance for reciprocal twoports

$$Z_{12} = Z_{21}$$

(62)

Z_{11} is the primary open circuit impedance, Z_{22} the secondary
open circuit impedance.

For identical antennas (arrays) we have

$$Z_{11} = Z_{22}$$

(63)

If we take the terminating reactance X_a of antenna 2

$$\frac{U_2}{I_{a2}} = -j X_a$$

(64)

We get with eq. (62), (63) and (64) from eq. (61) the input impedance Z_e of antenna 1:

$$Z_e = Z_{11} - \frac{Z_{12}^2}{Z_{11} + jX_a} \qquad (65)$$

Fig. 42 shows this transformation of X_a to the input of antenna 1 in the complex plane. Fig. 42a shows the function $Z_{11} + jX_a$; Fig. 42b shows the inversion $\dfrac{1}{Z_{11} + jX_a}$; Fig. 42c shows the rotated and stretched expression

$-\dfrac{Z_{12}^2}{Z_{11} + jX_a}$; Fig. 42d shows the shifted expression

according to eq. (65).

As can be seen from Fig. 42d the diameter D' of the circle is

$$D' = \frac{|Z_{12}|^2}{R_{11}} \qquad \Omega \qquad (66)$$

or

$$Z_{12} = \sqrt{D' R_{11}} \qquad \Omega \qquad (66a)$$

We can also see from Fig. 42d that the angle α of $|Z_{12}| e^{j\alpha}$ is the angle between a diameter of the circle intersecting the point $jX_a = \infty$ and a straight line parallel to the real axis. In this way $Z_{12} = |Z_{12}| e^{j\alpha}$ can be found by measuring the circle in the complex impedance plane and marking the point on the circle that belongs to $jX_a = \infty$.

The quality of the results is tested by measuring common rod antennas, whose current distribution and whose coupling is known by theory. Fig. 43 shows the coupling impedance $Z_{12} = R_{12} + jX_{12}$ of two rod antennas of the height $h_o = \lambda/4$ which is 15 cm at the measuring frequency of 600 Mc/s. The distance a/λ of the two antennas was variable. The diameter
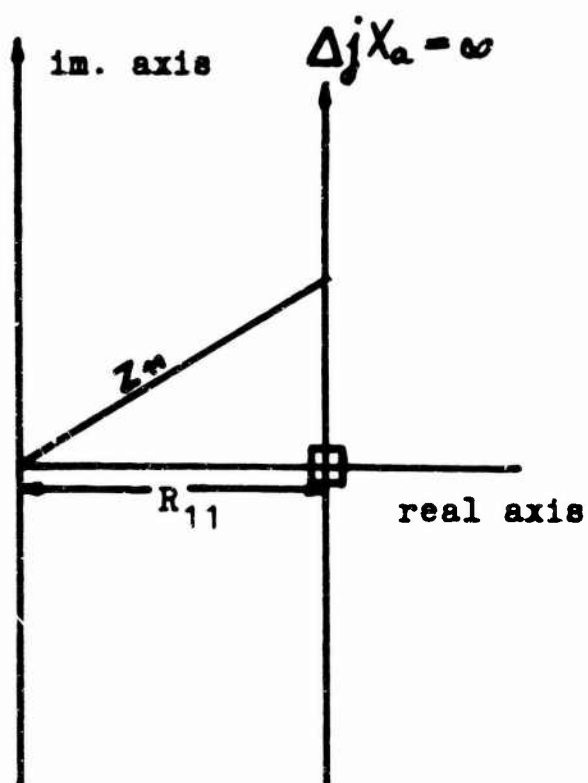
Fig. 42a
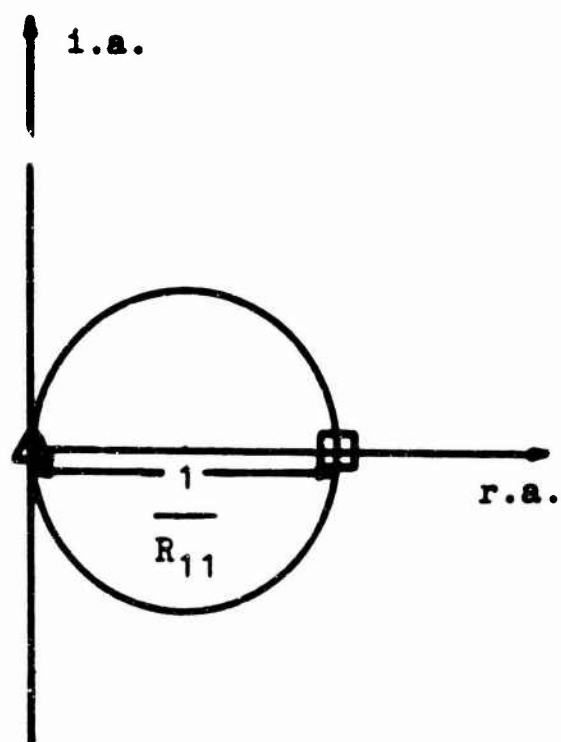
Fig. 42b
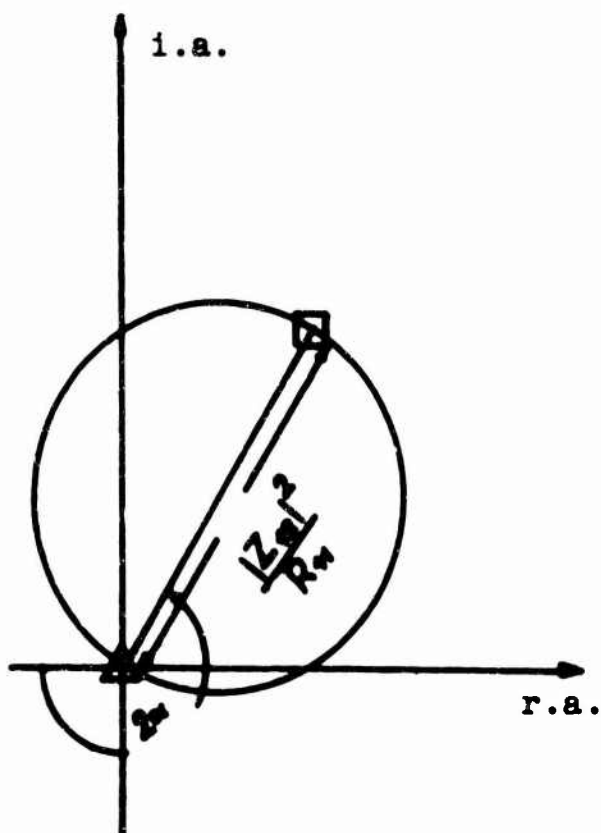
Fig. 42c
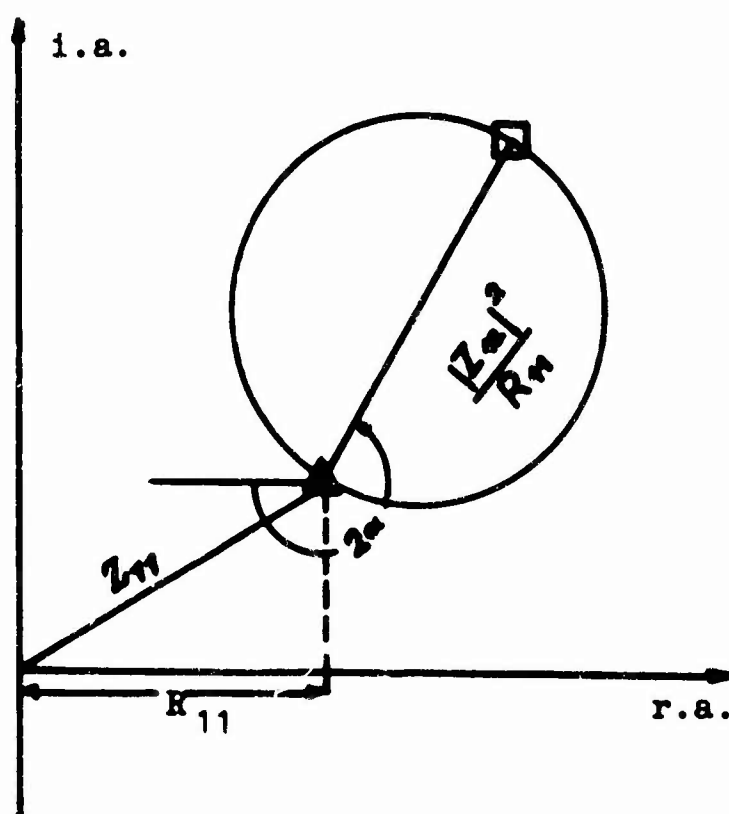
Fig. 42d
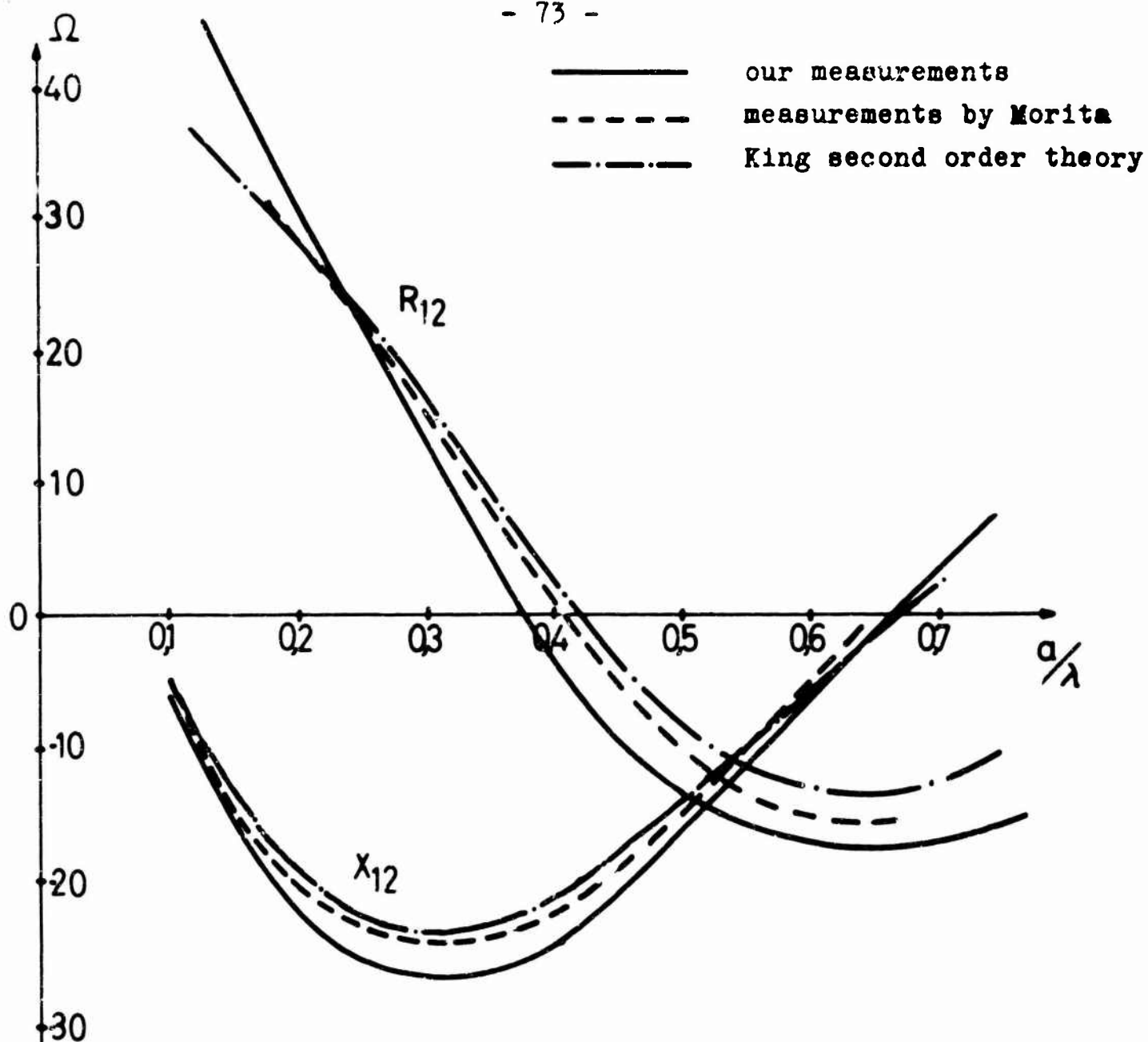
Fig. 43   Coupling impedance $Z_{12} = R_{12} + jX_{12}$
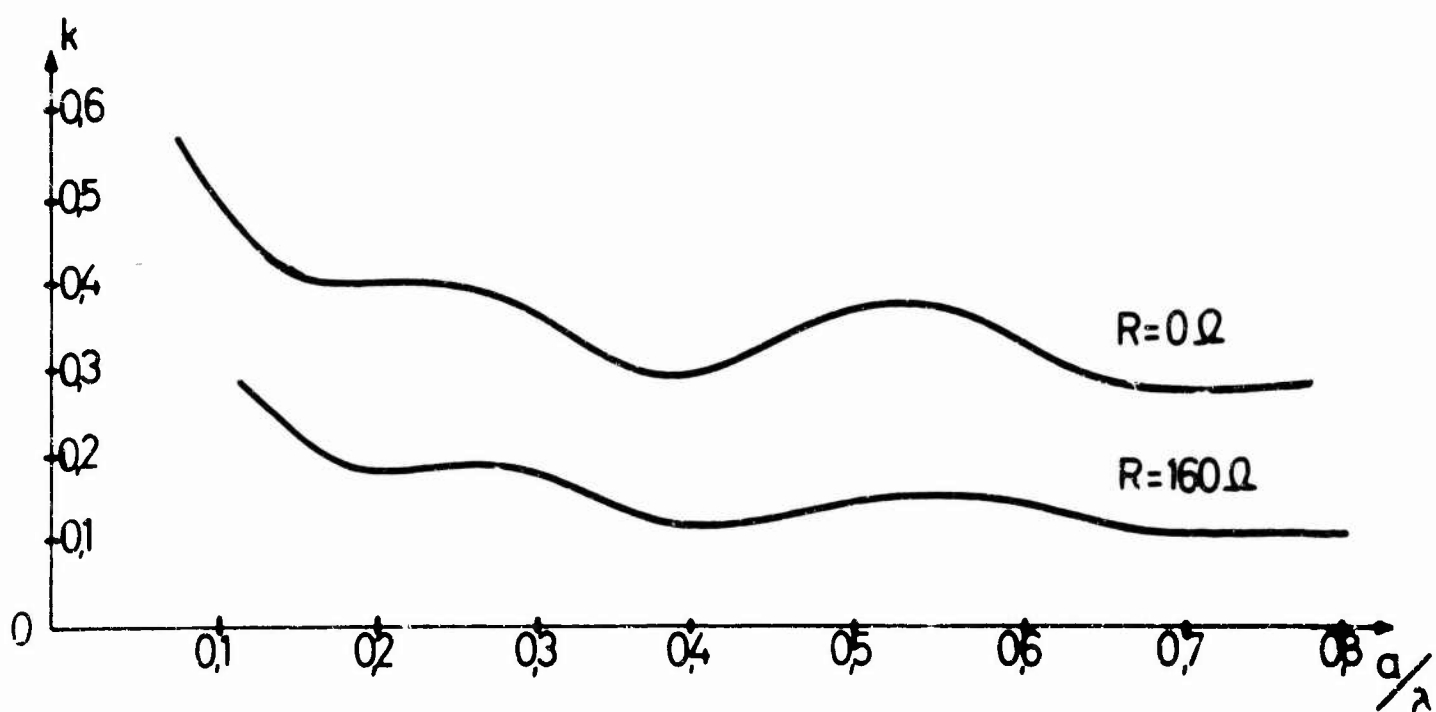
Fig. 44   Coupling factor $k = \dfrac{|Z_{12}|}{|Z_{11}|}$

of the two identical antennas was D = 0,8 cm. The difference
between our measurements and the measurements of Morita may
originate from our relatively small ground plane of 1 m^2 and
from measuring indoors. After this we have insertet into a

$\lambda/2$ dipole various ohmic resistors R in a $\lambda/4$ distance
from the top of the rod (Fig.39) to imitate a varying ohmic
resistance R that could also be realized by a diode by varying
the bias.

Fig.44 shows the coupling factor $k = \dfrac{|Z_{12}|}{|Z_{11}|}$ for two iden-
tical rods with R = 0 Ω (conventional rod) and R = 160 Ω.
If we insert R = 160 Ω there exists a traveling wave between
feeding point and resistor. For this case the coupling factor
is very low (see also [4] and the preceding chapters).

For measuring very small coupling effects the method described
before is not very useful because the circle in the Smith
chart becomes then very small. Therefore we have another method
for the measurement of very small coupling impedances:

If I_{a2} = C (open-circuit) then we get from (61) and (62)

$$\frac{U_2}{U_1} = \frac{Z_{12}}{Z_{11}} \tag{67}$$

From this we get the absolute value of Z_{12}

$$|Z_{12}| = |Z_{11}| \cdot \frac{|U_2|}{|U_1|} \tag{68}$$

For the measurement of $|Z_{11}|$, $|U_1|$ and $|U_2|$
we use the following arrangement:

α) Measurement of Z_{11} and $|U_1|$ (Fig.45).

Z_{11} is measured with well-known methods by the slotted line
connected to antenna 1. The generator feeds the slotted line.
The movable short in the coaxial line connected to antenna 2
must have a distance of $\lambda/4$ from the feeding point to guarantee
I_{a2} = 0. A voltage proportional to U_1 is measured by the capaciti-
ve probe of the slotted line if the probe has a distance of $\lambda/2$
from the feeding point of antenna 1, because at a distance
$\lambda/2$ from the feeding point the voltage in the slotted line
is the same as the voltage at the feeding point.

antenna 1   antenna 2

groundplane

slotted line for
impedance and
voltage measure-
ment (charact.
impedance $60\,\Omega$)

$\frac{\lambda}{2}$

feeding
point

$\frac{\lambda}{4}$

coaxial line
with movable
short

10 dB
attenuator
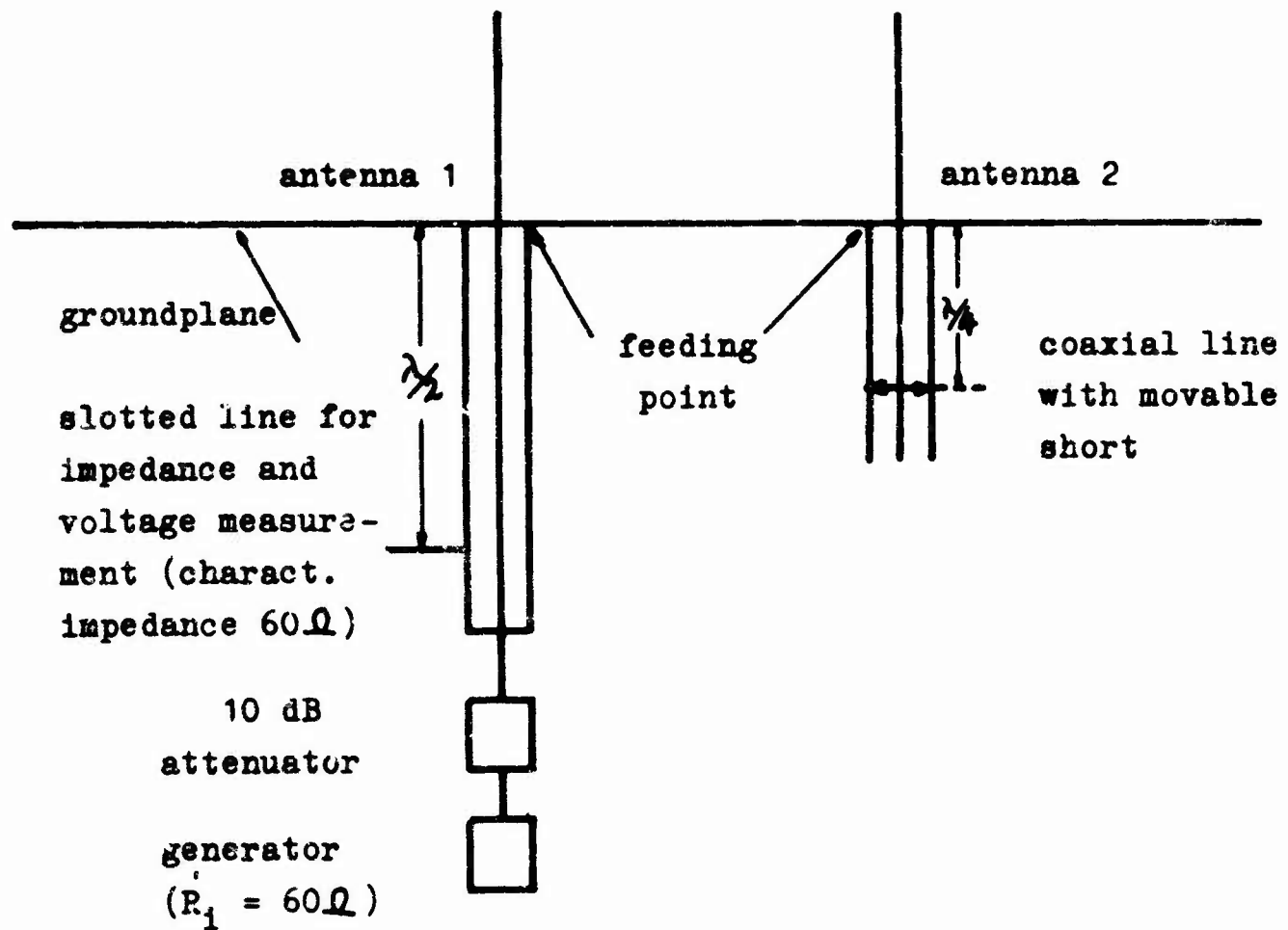
generator
($R_1 = 60\,\Omega$)

Fig. 45

β) Measurement of $|U_2|$ (Fig.46)

The antennas 1 and 2 are interchanged on the ground plane.
The generator and attenuator are now directly connected to
antenna 1. Generator and attenuator must not be varied to
guarantee the same voltage at the feeding point of antenna 1
as in the previous case. Also all internal resistances and
characteristic impedances must be equal. The coaxial line with
movable short is now connected to the slotted line. The movable

antenna 2

antenna 1

slotted line
for voltage
measurement
(charact.
impedance
60 Ω)

$\frac{\lambda}{2}$

feeding
point

$(2n+1) \cdot \frac{\lambda}{4}$

groundplane

attenuator
(10 dB, 60 Ω)

generator
(R_1 = 60 Ω)

coaxial line with
movable short
(char. imp. 60 Ω)
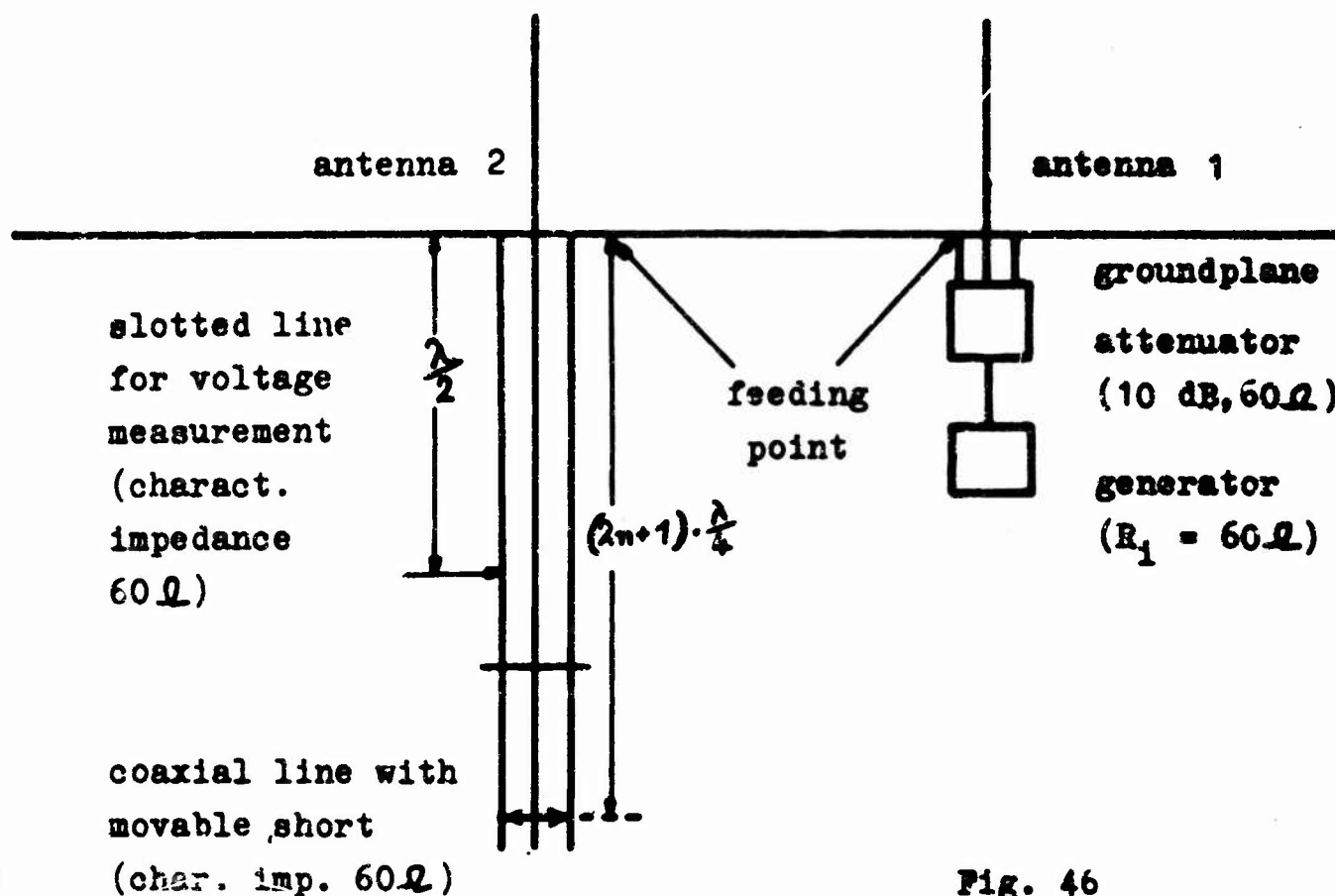
Fig. 46

short must have a distance of $(2n + 1) \cdot \lambda/4$ from the feeding
point of antenna 2. A voltage proportional to $|U_2|$ is then
measured by the capacitive probe of the slotted line at a
distance $\lambda/2$ from the feeding point. As we use the same slotted
line for the measurement of $|U_1|$ and $|U_2|$ we get $|U_2|/|U_1|$
as needed in eq. (68) by dividing the voltage proportional
to $|U_2|$ measured in sec. β by the voltage proportional to
$|U_1|$ measured in sec. α.

Some other possibilities to determine the coupling of two antenna are described in [4].

Measuring the coupling of antennas with integrated TDs we have to fulfil certain stability conditions (see chapter I.3). Therefore all methods where at the input of one of the antennas an open circuit is generated, are of no use. A more practicable way of measuring the coupling is then offerend by the following method:

Like in chapter 11 the antennas are fed symmetrically (case A), respectively anti-symmetrically (case B) through internal resistances, which are chosen according to the stability conditions. Z_{11} and Z_{12} then can be obtained from equ. (48, 49). In a very simple manner case B can be realized:
Mounting a well conducting plane at the distance $a/2$ from a single antenna, the plane being in parallel with the antenna axis, the radiation field of this antenna is about the same as if it was produced by two identical antennas with the distance a, which are driven anti-symmetrically. Since Z_{11} is nearly equal to the input impedance Z_1 of the isolated antenna, the coupling approximately can be determined with only one antenna being at hand. According to equ. (47) the input impedance of the arrangement with the conducting plane is

$$Z_{1B} = Z_{11} - Z_{12}$$

Since $\qquad Z_{11} \approx Z_1,$ consequently:

$$Z_{12} = Z_1 - Z_{1B} \tag{69}$$

respectively

$$k = \frac{|Z_1 - Z_{1B}|}{|Z_1|} \tag{70}$$

Part. II. Scimitar Antennas

Scimitar antennas as shown in Fig.47 have a frequency dependent
radiation diagram and a frequency dependent input impedance,
which tends to values which are too high for matching to
standard values of the characteristic impedance of coaxial
cables. In our research we are studying different possibilities
to improve the quality of scimitar antennas. At first we had
to study the conventional form for better understanling the
behaviour of the scimitar and to find out, why this antenna
shows some unwanted effects. In a second step we studied new
forms of scimitars to see whether we can improve some effects.

The basis of our research are measurements in the near field,
especially current distribution, electric field and magnetic
field on or near the surface of the soimitar it self and on the
ground plane near the radiator. By this we learned to under-
stand the form of radiation pattern at different frequencies
and, by help of our basic knowledge on broadband radiators,
learned to understand the input impedance. We tried different
variations of the radiator form and could develop a better broad-
band input impedance, which is matched to standard coaxial cable.
We could develop some change in the radiation diagram, but
this is only a beginning and may be continued. We hope that
some slots in the scimitar may change the current distribution
in a favourable manner.

1. Conventional Scimitar Antenna

a) Input impedance of Conventional Scimitar Antenna

The conventional scimitar antenna has been invented by
E.M.Turner and W.P.Turner [10]. It has physical properties
such as ruggedness, simplicity, ease of mounting and low
drag that make it particularly suited for use on aircraft.
The general configuration is that of a soimitar blade having
its broad end electrically and mechanically attached to the
ground plane which may be the surface of the aircraft. The
point F of the blade is coupled to the coaxial feed line.
Fig.47 shows the general configuration of the antenna element.
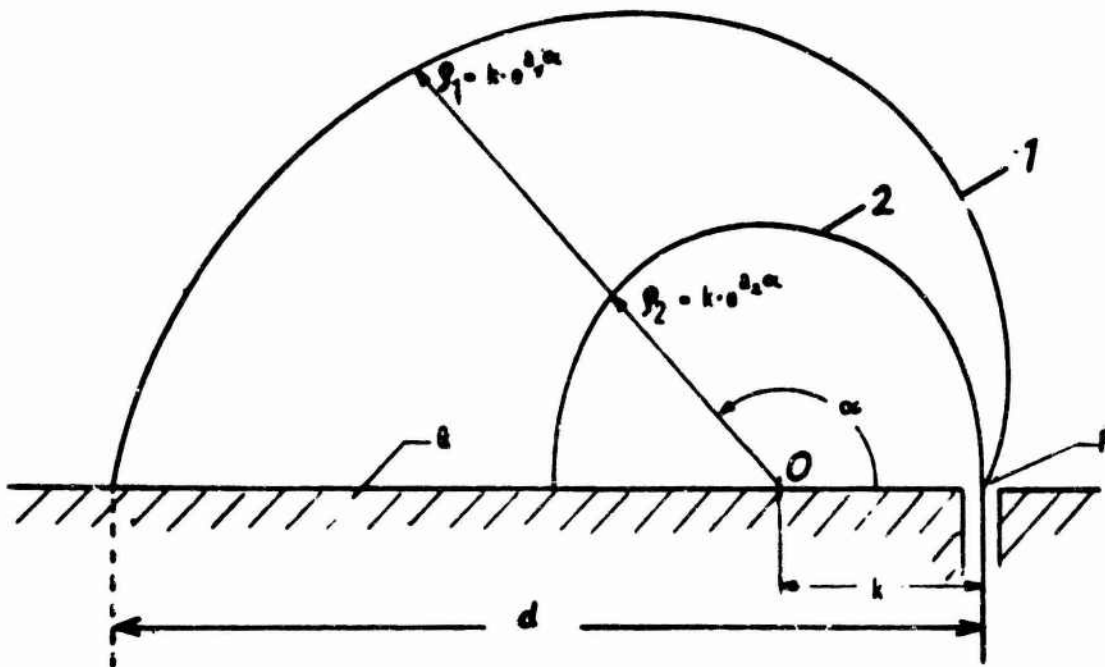
Fig. 47 Conventional Scimitar Antenna

The outer and inner boundaries of the blade which may be cut
from a sheet of conductive material, follow diverging spiral
paths 1 and 2. These start at feed point F and end at a conduc-
tive ground plane G to which the broad end of the element is
electrically connected. The curves 1 and 2 are logarithmic
spirals having their origin at O which, in this case, lies
in the ground plane G.

The general equation of these curves is

$$\rho = k e^{a\alpha}$$

where ρ is the distance from origin to curve, α is the direc-
tion of ρ measured from the starting point, in this case the
feed point F; e is the natural logarithm base, and k and a
are constants which provide the parameters through which various
forms of the antenna element may be derived. The constant k
is the same for both inner and outer boundaries and determines
the overall size of the antenna element. The constant a
determines the rate at which the spiral moves outward from the
origin O. As a approaches zero, the spiral approaches a circle.

In Fig.47 the values of a for the outer boundary, called a_1, is 0.35 while that for the inner boundary, called a_2 is 0.02. The difference between a_1 and a_2 determines the rate of divergence of the outer and inner boundaries of the antenna element. The antenna is fed by a coaxial transmission line having its outer conductor connected to the ground plane and its inner conductor extending through a hole in this surface to the feed point F. Fig.48 shows a scimitar antenna on the measuring plane.

The impedance of the scimitar antenna at the feeding point is measured by an electrical probe in the slotted feeding line. Fig.49 shows the antenna on a rectangular ground plane of 1x1 m^2. Below the ground plane the 60 Ω slotted feeding line, two generators and a receiver is to be seen. For lower frequences from 30 to 300 Mc/s we used a direct indicating Z-G-Diagraph from Rhode a. Schwarz- Company for impedance measurements.

First we had to decide how large the ground plane should be to get no considerable impedance error compared to an infinitely large ground plane. So we measured several antennas of different size but identical shape over a rectangular ground plane of 1x1 m^2 and over a rectangular ground plane of 4x4 m^2. The experiments showed that for a scimitar antenna with d = 30 cm (see Fig.47), or smaller the impedance on the small ground plane (1x1 m^2) was nearly identical with the impedance on the large ground plane with deviations of maximal 3% if measured from 30 to 1000 Mc/s. So for our further impedance measurements we decided to use the more practical ground plane of 1x1 m^2 and an antenna size of d = 15 cm.

Fig.50 shows the measured impedance of the antenna of Fig.47 with d = 15 cm on this ground plane from 30 to 1000 Mc/s in a Smith Chart, for a characteristic impedance of 60 Ω for the slotted line.

For very low frequencies the impedance goes to zero because at very low frequencies the antenna is an electrically short loop together with its mirror image below the ground plane.
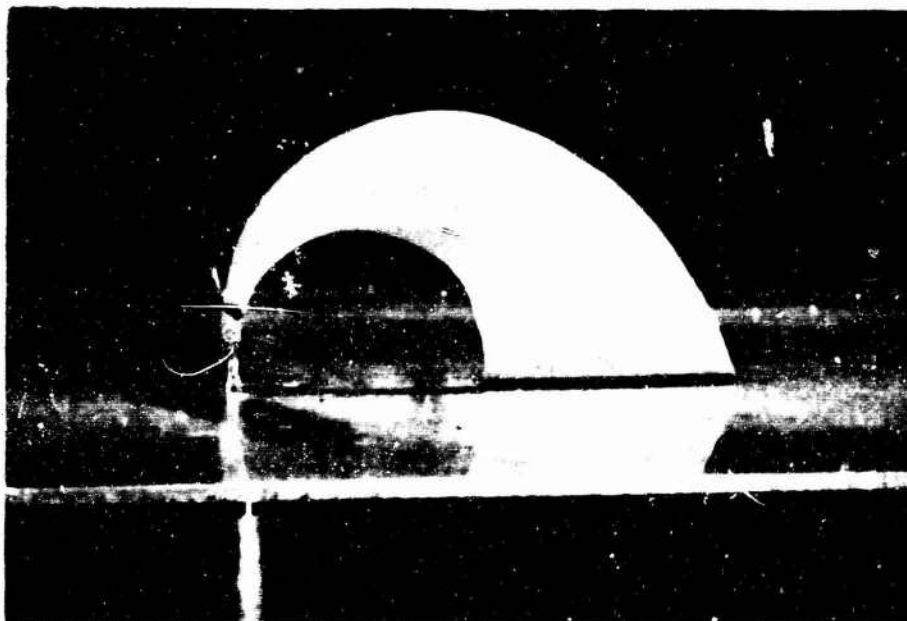
Fig.48: Scimitar Antenna on ground plane
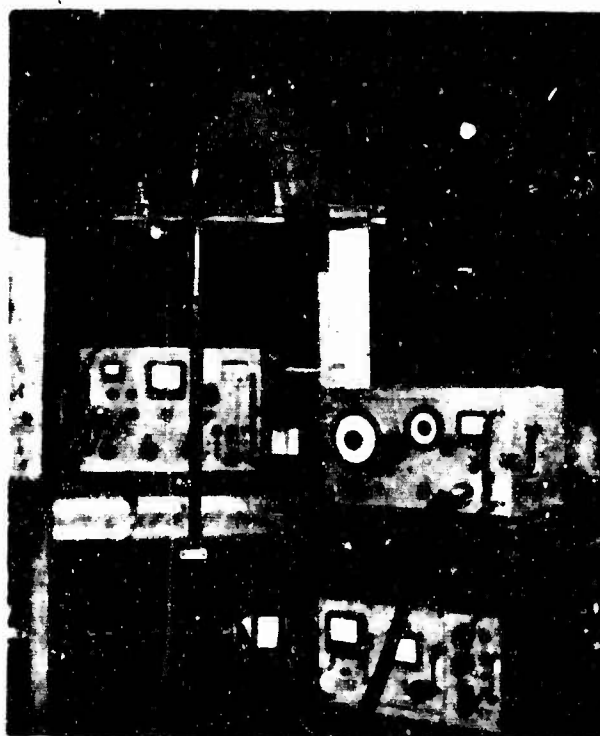
Fig. 49: Impedance measuring equipment
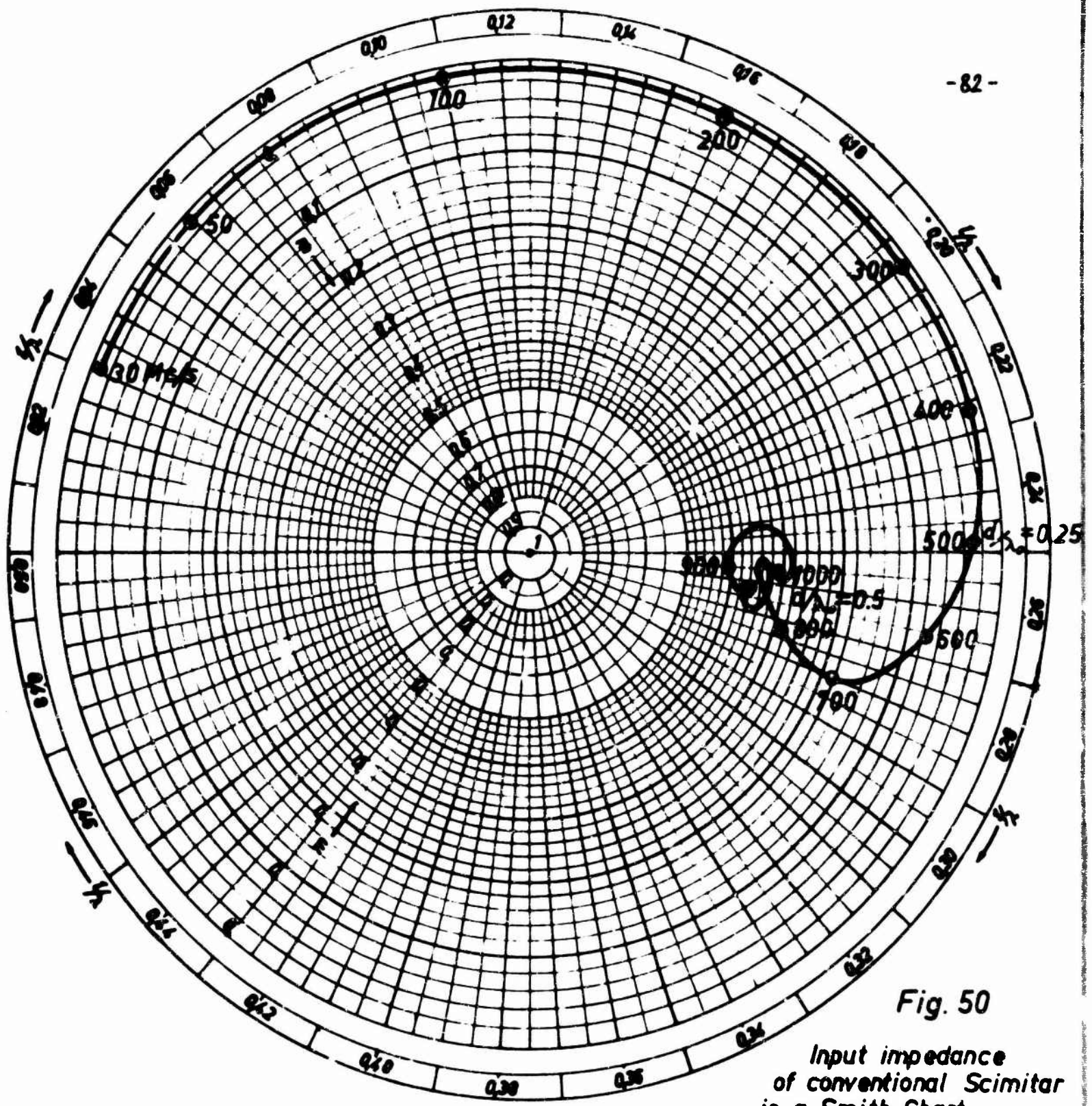
Fig. 50

Input impedance
of conventional Scimitar
in a Smith Chart

At a frequency of about 500 Mc/s the impedance-curve intersects first the real axis at a very high value of resistance. At this frequency the length of the inner spiral of the scimitar is $\lambda/4$ (λ_o= wavelength in free space) measured from the point where it is connected to the ground plane to the feeding point. This loop then behaves together with the mirror image (below the ground plane) like a $\lambda_o/4$, line short circuited at its end.

Above of 800 Mc/s, i.e. for $d/\lambda_o > 0.4$ the impedance of this scimitar antenna is broadbanded and stays inside the relatively small dotted circle. There it has a nearly constant value of about 180 Ω. The reason for this is that at relatively high frequencies almost the total energy is radiated near the feeding zone where the scimitar antenna is very simlar to a flat cone (plane structure, Fig.51) which according to [11] is frequency independent if the frequency goes to infinity. The high impedance of 180 Ω originates from the small angle of the cone at the feeding point, which produces a high characteristic impedance near the feeding point.
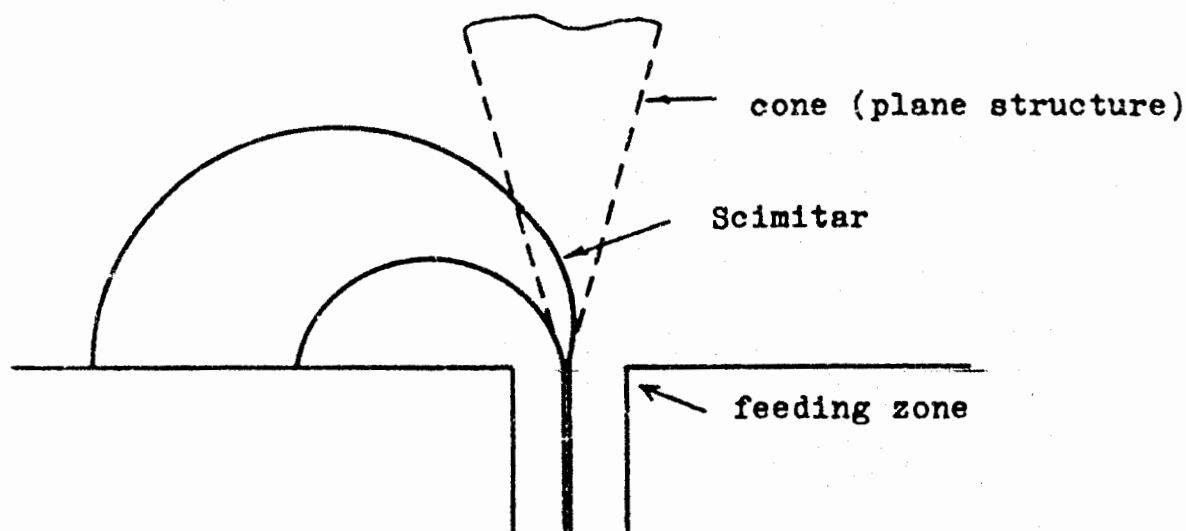
Fig. 51: Analogy of cone and spiral shape at feeding zone

Fig. 52:   Interior of hollow Scimitar
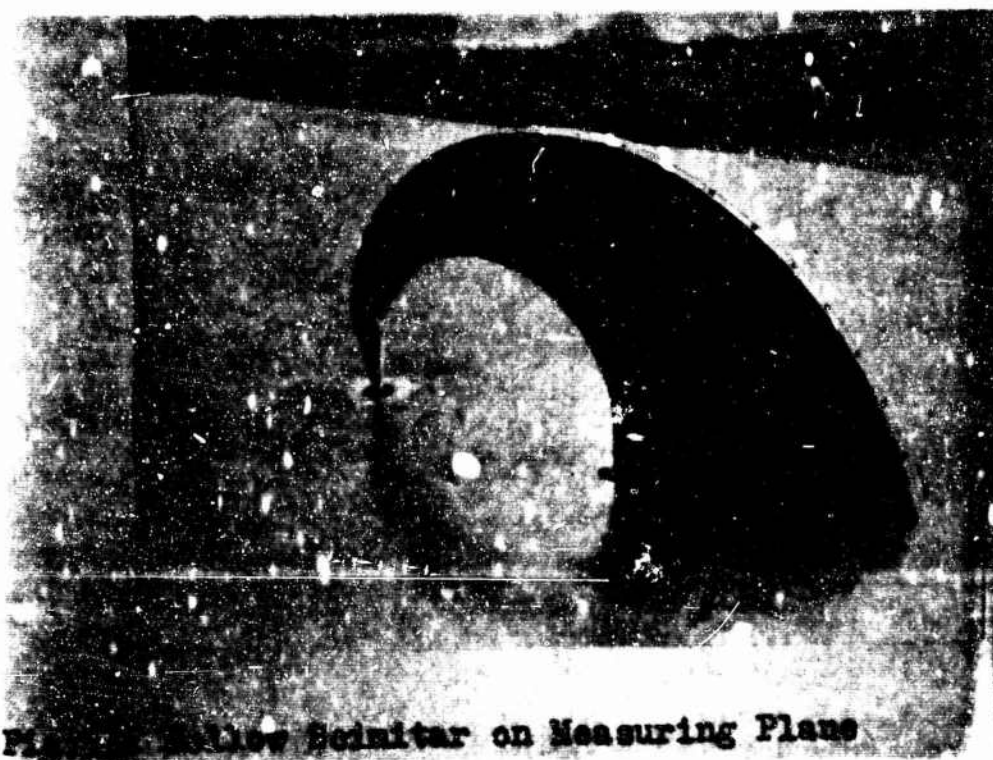
Fig. 53: Hollow Scimitar on Measuring Plane

b) <u>Near Field Measurements of the Conventional Scimitar Antenna</u>

We measured the electric and magnetic field vector of the
near field of the scimitar antenna directly on the metallic
surface of the antenna and of the ground plane. For field
measurements on the surface of the antenna we used a hollow
scimitar according to Fig.52 and 53. The scimitar has a maximum
dimension of $d = 33$ cm. It was mounted on a ground plane of
1×1.30 m^2. The field distribution near the antenna will not
differ considerably from the field distribution of an antenna
on an infinitely large ground plane since it was shown in
sect. II.1a that the feeding point impedance is nearly iden-
tical in both cases. A cable goes through the ground plane into
the interior of the hollow scimitar and ends at a probe, which
is put through one of the holes of the scimitar walls. One
side plate of the scimitar can be removed for putting the
probe into different holes. For finding the direction of
the magnetic field vector which is parallel to the metallic
surface of the antenna the magnetic probe was turned around
its axis using a polystyrol screw driver until maximum indi-
cation was obtained. Fig. 54 shows the antenna mounted on a
ground plane of 1×1.30 m^2 with holes for probing the field
at the ground plane.

Fig.54 Ground Plane with Measuring Holes

All holes have a diameter of 4 mm. It can be assumed that the electric and magnetic field distribution is not disturbed essentially by the holes.

Fig.55 shows the construction of the capacitive and inductive probes. The capacitive probe consists of the inner conductor of a coaxial line. The inductive probe is a loop which is shielded against disturbing electrical fields by coating the wire of the loop with an insulating layer and then coating a part of the insulation with silver. This silver is connected to the outer conductor of the coaxial cable. The area of the loop is about 4 mn^2. The correct shielding of the loop was tested at various points of the metallic surface of the antenna and of the ground plane by comparison of the measured amplitude and phase if the loop was turned by 180° out of its original direction. The amplitude then must be equal in both positions and the phase must have changed exactly by 180° if the shielding is perfect.

For the measurement of amplitude and phase we used the following principal arrangement, (Fig. 56 and 57). The generator feeds two lines a and b in parallel. Line a is the feeding line of the the antenna. A part of this energy is taken up by the probe and comes to the receiver. Line b is needed for the comparison of amplitude and phase. The amplitude of line b can be adjusted by the calibrated variable attenuator; the phase can be adjusted by shifting a measuring probe on the slotted line which is terminated by its characteristic impedance Z_L. In this case the phase changes linear with the shifting of the probe along the line. For exact measurements also the phase delay that originates from the attenuator and which is dependent of the degree of attenuation must be taken into consideration. This line b also comes to the receiver in parallel with line a. Amplitude and phase appearing at the antenna probe can now be measured by adjusting the calibrated attenuator in such a manner that the amplitude arriving at the receiver is equal in arm a and b. The phase is then changed by shifting the probe of the slotted line so that the phase arriving from arm b is opposite to the phase arriving from arm a. If both conditions are fulfilled the receiver shows a zero of indication. By this method relative amplitudes and
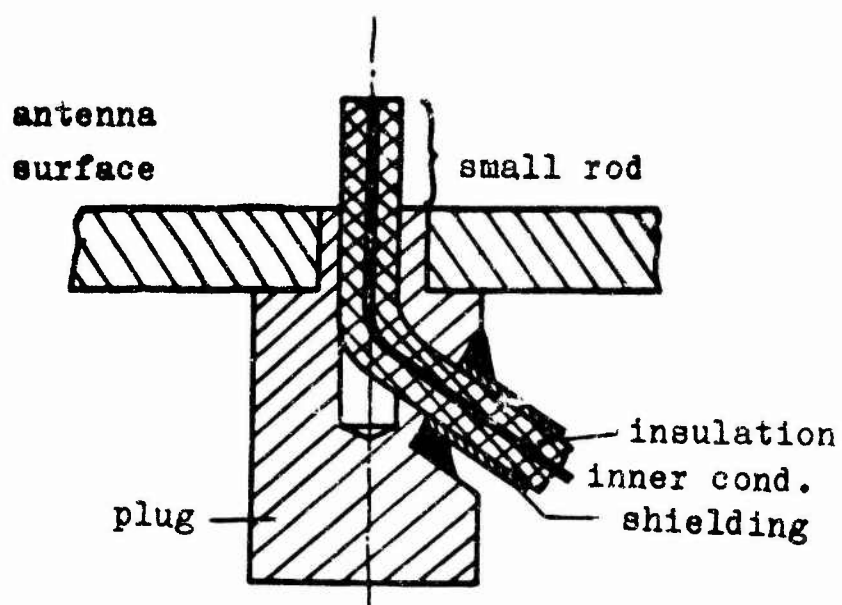
Fig. 55a: Electrical rod Probe
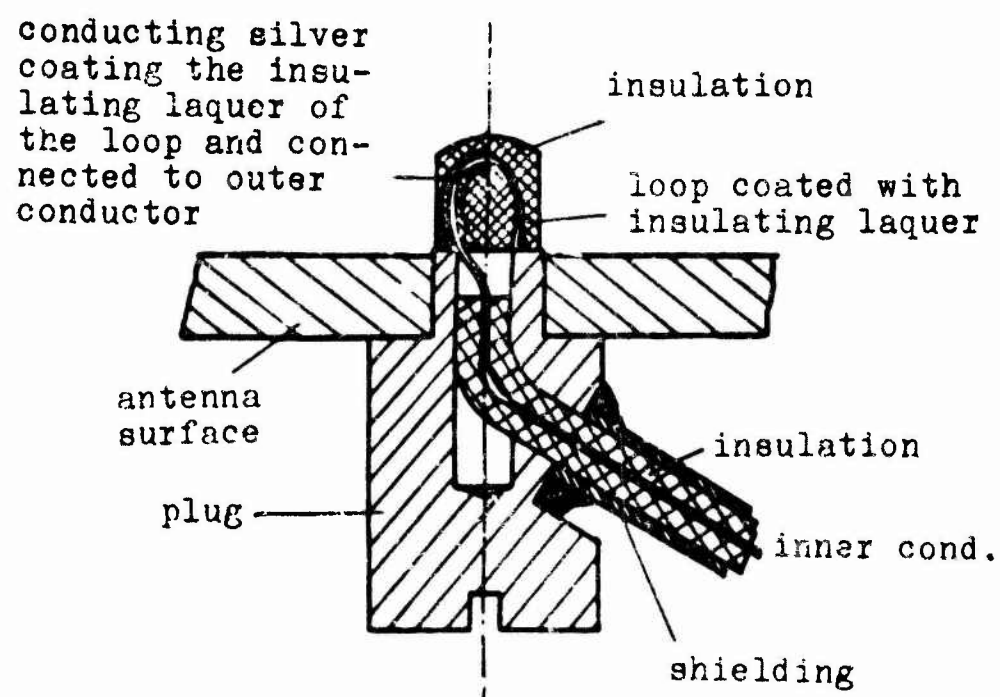
Fig. 55b: Magnetic loop Probe
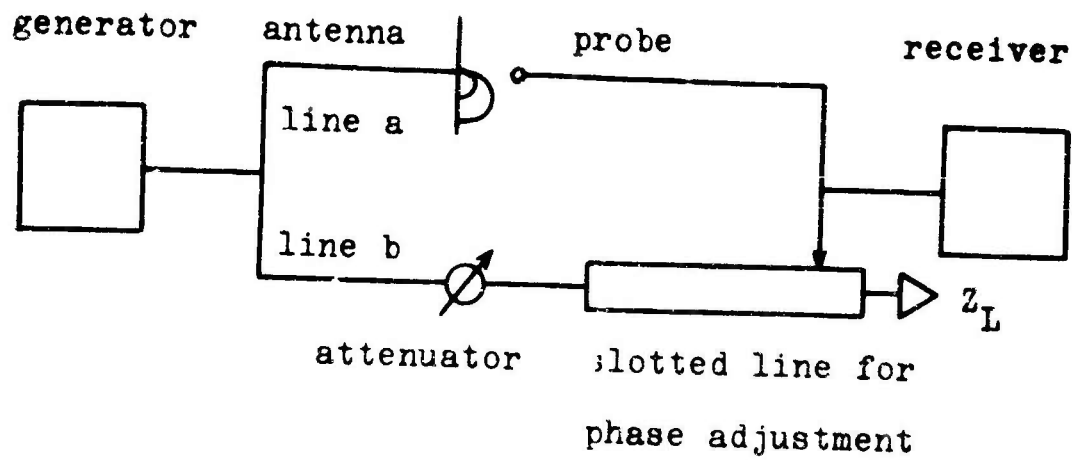
Fig. 56: Schema of measuring equipment
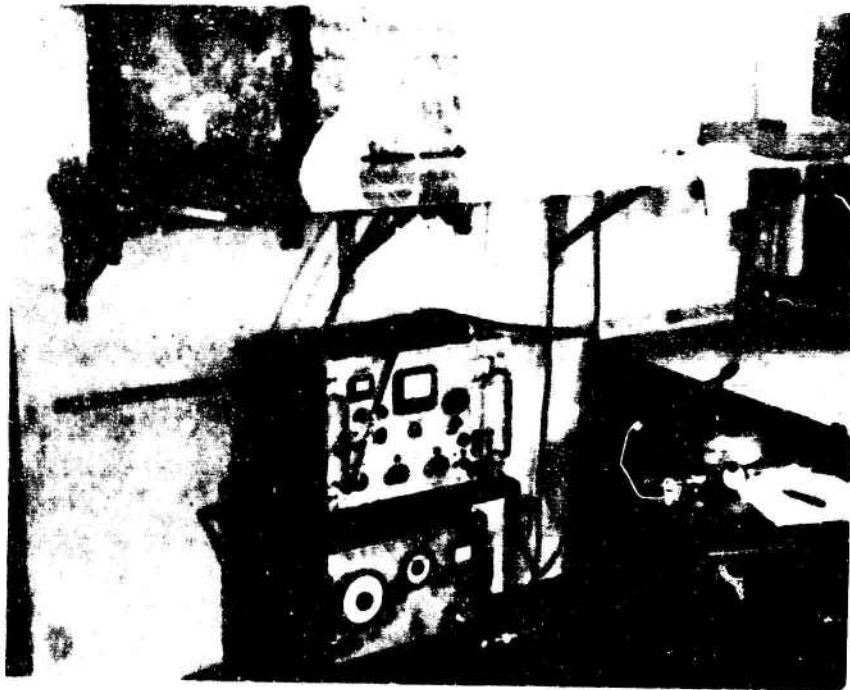
Fig. 57: Measuring equipment

phases of different points on the antenna surface can be measured. We used a scimitar antenna with d = 33 cm. All field distributions have been measured at many various frequencies. Only a few results can be presented here our complete results contain more than 100 pages. Since the electric field is always perpendicular to the metallic surface it is sufficient to measure its amplitude and phase.

Fig.58 shows lines of constant amplitude of the electrical field on the surface of the antenna at a frequency f = 1000 Mc/s $(d/\lambda_0 = 1.1)$. Since only relative values of the amplitude are interesting the curve that lies next to the feeding point is marked with 0 dB.

Fig. 59 shows the E-field amplitude for f = 1500 Mc/s $(d/\lambda_0 = 1.6)$ It can be seen from these pictures that with increasing distance from the feeding point the E-field amplitude is decreasing. At f = 1500 Mc/s the curve with -30 dB forms an island; this indicates energy reflected from the ground plane (standing wave).

Fig.60 and 61 shows lines of constant phase at the same frequencies. Since only relative values are interesting the first line is near the feeding point[1] marked with a phase of 0°. With increasing distance from the feeding point the phase delay is increasing. In such regions of the antenna surface where the amplitude is very low no lines of constant phase have been drawn since in such regions the phase is of no interest. We find that there is a traveling wave along the antenna coming from the feeding zone. In that region of the antenna where it is connected to the ground plane standing waves are dominant. This can be seen from the rapid variation of amplitude and phase in this region. As we know from standing waves the amplitude is very small when the phase changes rapidly.

Fig.62 shows the measured lines of constant amplitude of the E-field on the ground plane for f = 1000 Mc/s.

Fig.63 shows the corresponding lines of constant phase.

The magnetic field is always parallel to the metallic surface of the antenna and ground plane. The direction of the H-field

E-field amplitude in db

f=1000 Mc/s
d/λ₀=1.1

d=33cm

Fig. 58

E-field
amplitude
in db

f = 1500 Mc/s
d/λ₀ = 1.6

d = 33 cm

Fig. 59

E-field
phase
f = 1000 Mc/s
d/λ₀ = 1.1

0°

-90°

-180°

-270°

-360°

Fig. 60

E-field
phase
f=1500 Mc/s
d/λ₌1.6

0°

-90°

-180°

-270°

-360°
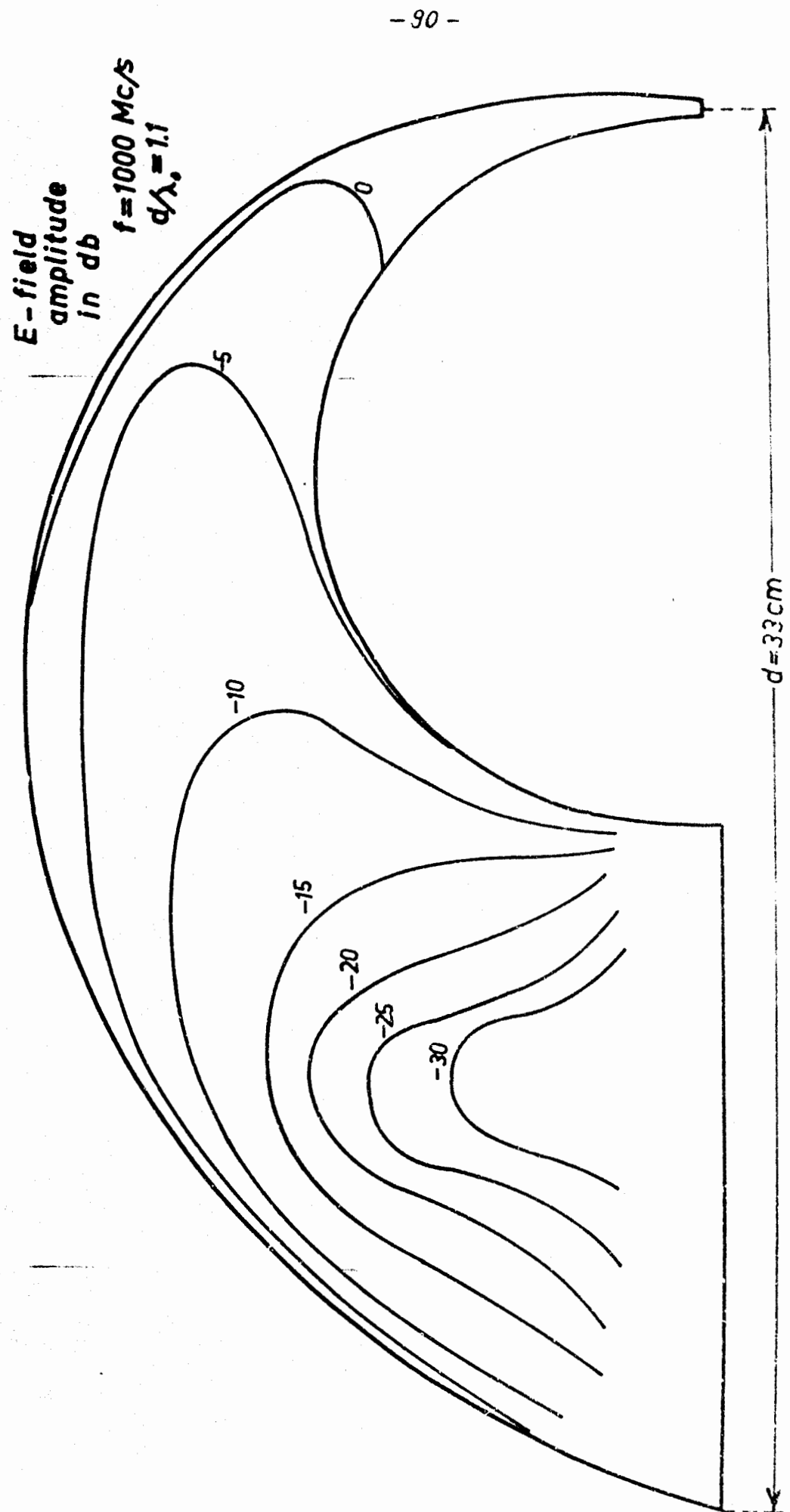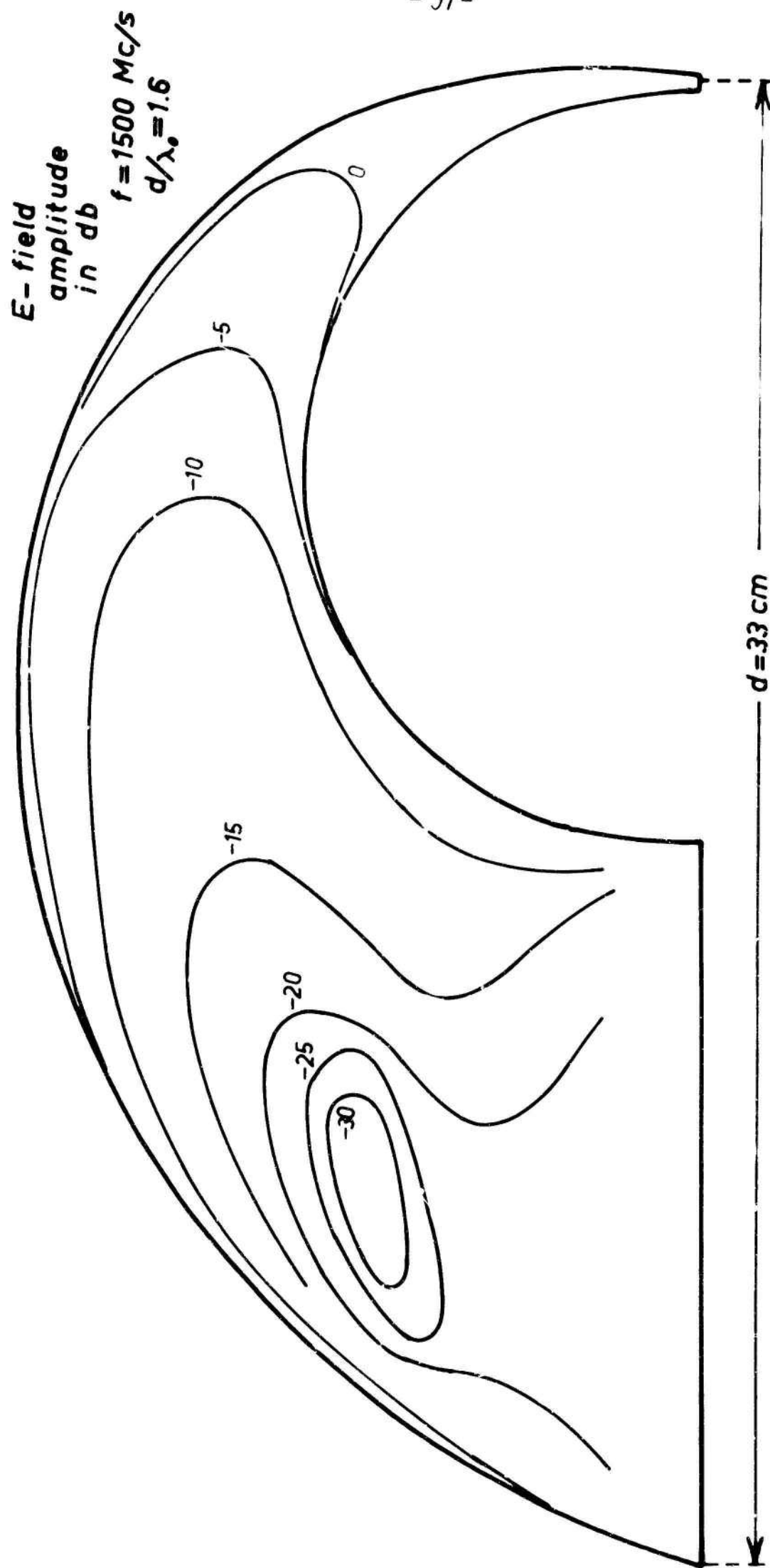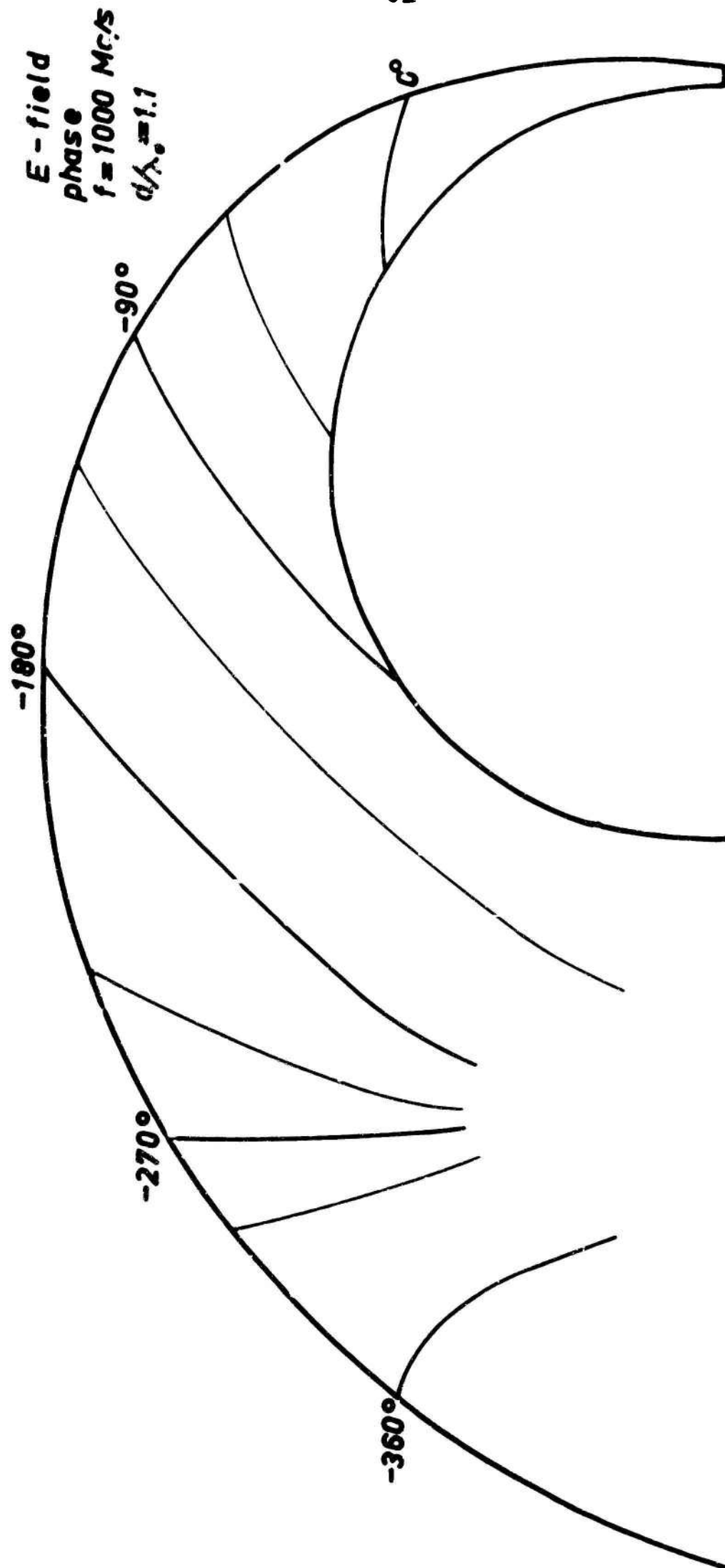
-450°
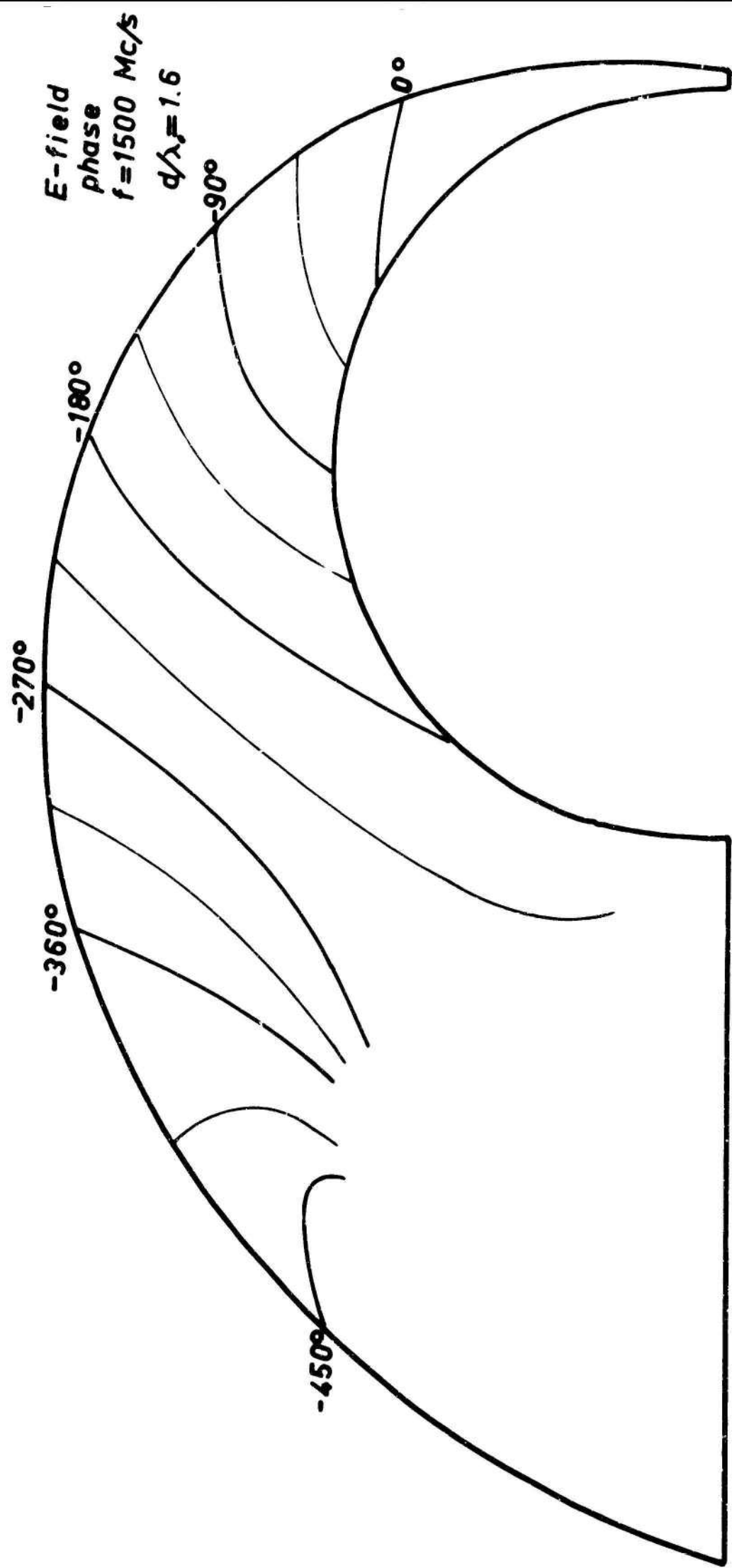
Fig. 61

Fig. 62 E-field, amplitude
on ground plane
f = 1000 Mc/s (d/λ_0 = 1.1)
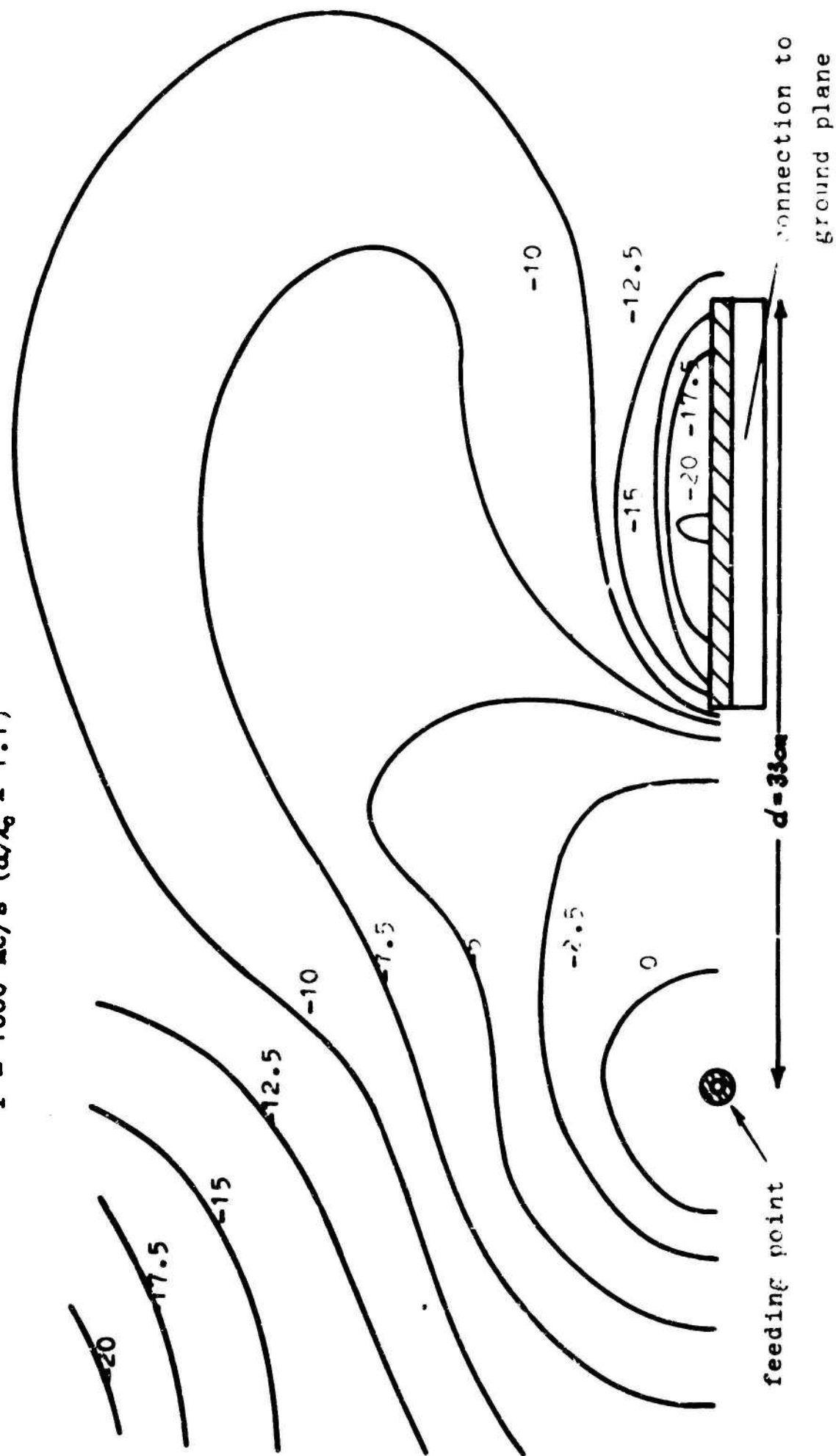
Phase of

Fig. 63 E-field on ground plane
f = 1000 Mc/s ($d/\lambda_0 = 1.1$)
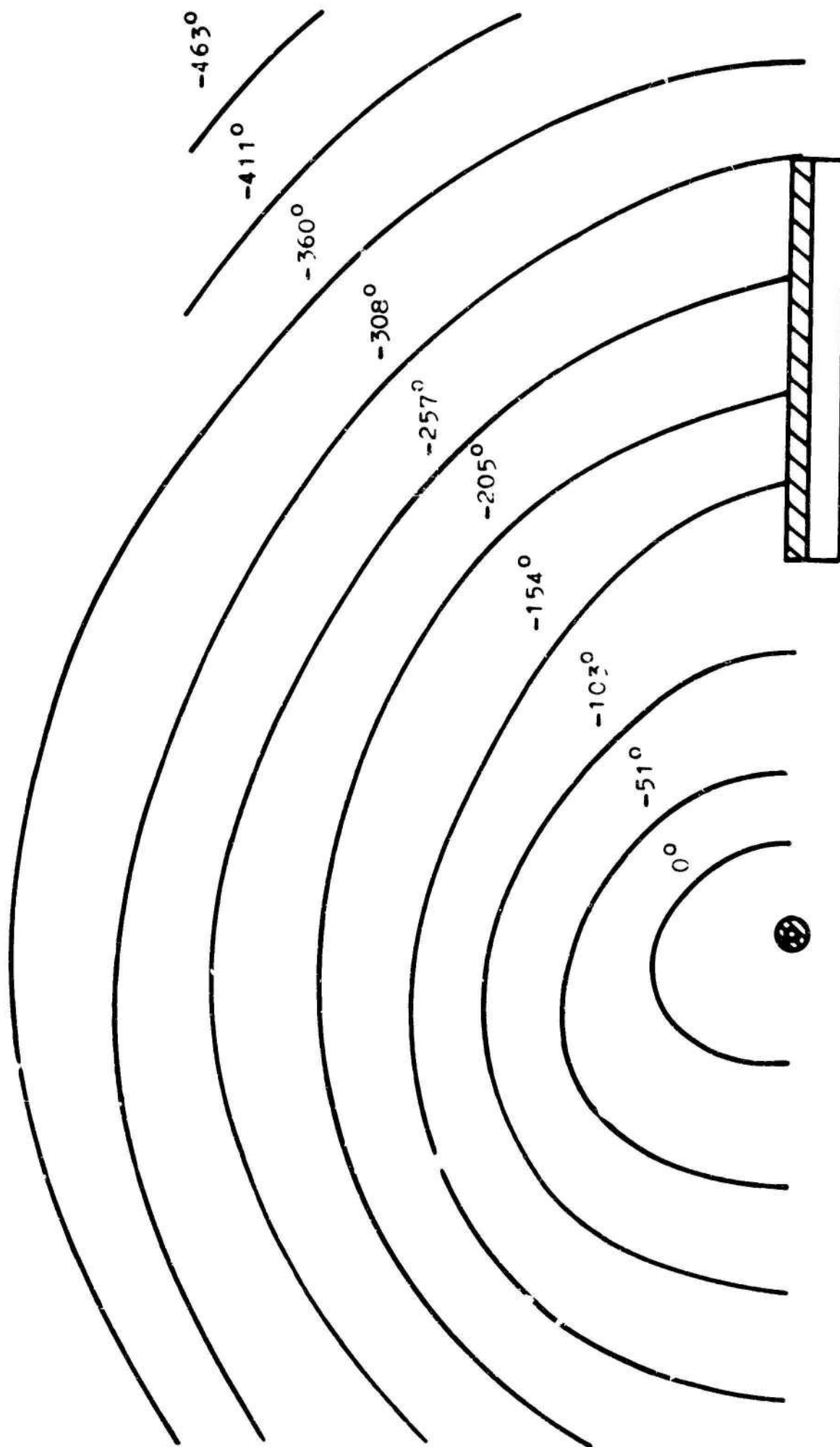
can be found by turning the loop probe around its axis until it shows an output maximum. In most regions of the antenna a zero of the H-field can not be found when turning the loop probe. This indicates that there exists elliptical polarization. This elliptical polarization probably originates from oblique reflection of waves on the antenna plane.

The current distribution on the metallic surface is perpendicular to the direction of the H-field. Therfore also the ellipses of current can be drawn if the amplitude of H is measured at the major and minor axis of every ellipse. With increasing time the vector of current is turning clockwise or counterclockwise in every ellipse.

Fig.64 shows the major und minor axis of ellipses of current on the antenna at a frequency f = 1000 Mc/s (d/λ_o = 1,1). For this frequency the current vector is turning counterclockwise with increasing time in all ellipses. The length of the major and minor axis is drawn proportional to the amplitude of current.

If the phase of current is also measured at the major axis of every ellipse it is possible to construct momentaneous pictures of the current distribution. At every moment of time the vector of current rotating in every ellipse thas a definite direction.

Fig.65a-f shows these directions for every ellipse of Fig.64 for various moments of time in six steps from t = 0 to t = T/2 if T is the time for one period. For t = T/2 we get the same picture as for t = 0 with the only difference that every arrow has opposite direction. All arrows are drawn with equal length. Looking at the same point of the surface at various times we see that for this frequency of 1000 Mc/s every vector is turning counterclockwise with increasing time.

The current distribution on the surface of the scimitar antenna resembles the current distribution on the walls of common waveguides where elliptical polarization of the H-field is a well known fact. A wavelength λ_A on the antenna can be found which is shown in Fig.65a and which varies of course dependent on the antenna region since the scimitar antenna is no homogeneous structure. The waves on the antenna surface are traveling away

Ellipses of current
f=1000 Mc/s
d/λ$_e$=1.1

Fig. 64

Momentaneous picture
of current

f=1000 Mc/s
t=0

Fig. 65a

f=1000 Mc/s
t=T/10

Fig. 65b

f=1000 Mc/s
t=2T/10

Fig. 65c

f=1000 Mc/s
t=3T/10

Fig. 65d

f=1000 Mc/s
t=4T/10

Fig. 65 e

f=1000 Mc/s
t=T/2

Fig. 65 f

Momentaneous picture
of H-fieldlines

f=1000 Mc/s
t=0

Fig. 66a

f=1000 Mc/s
t=T/10
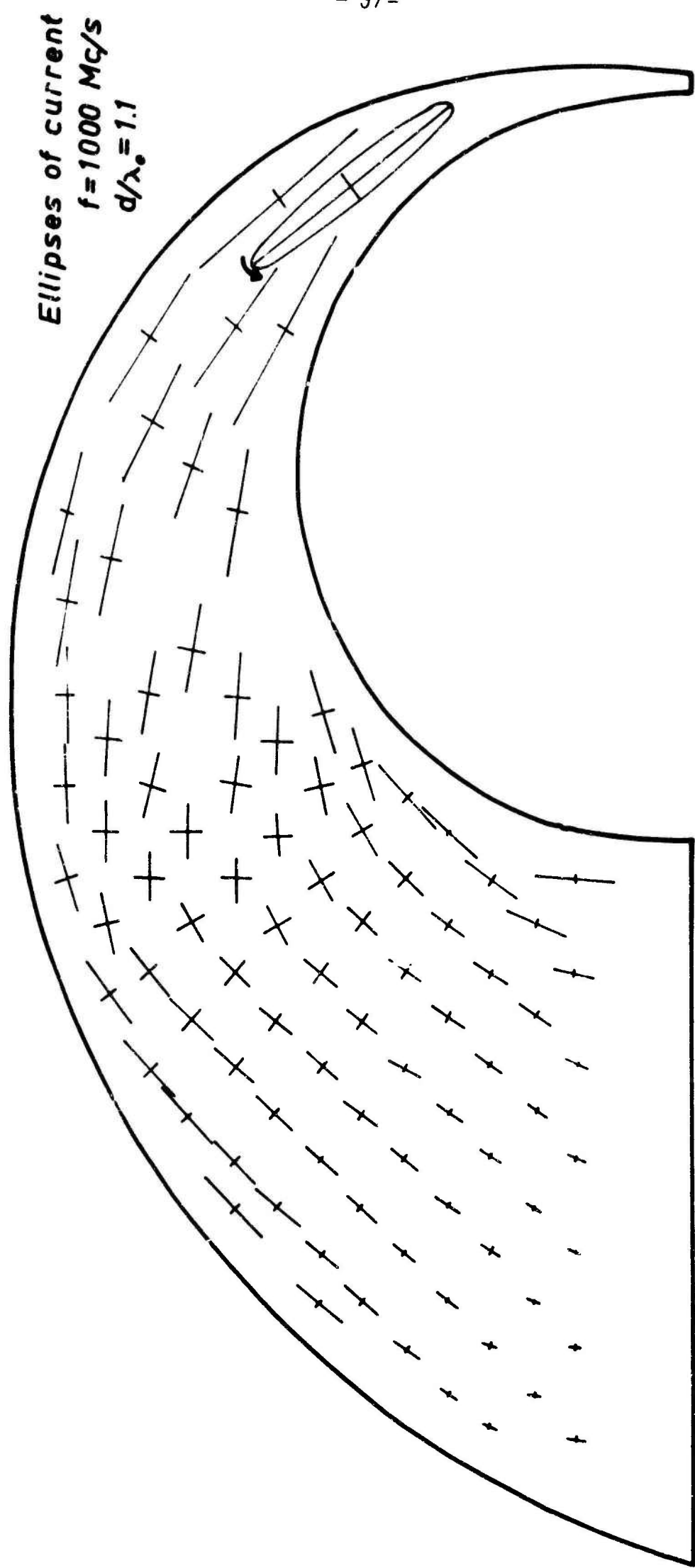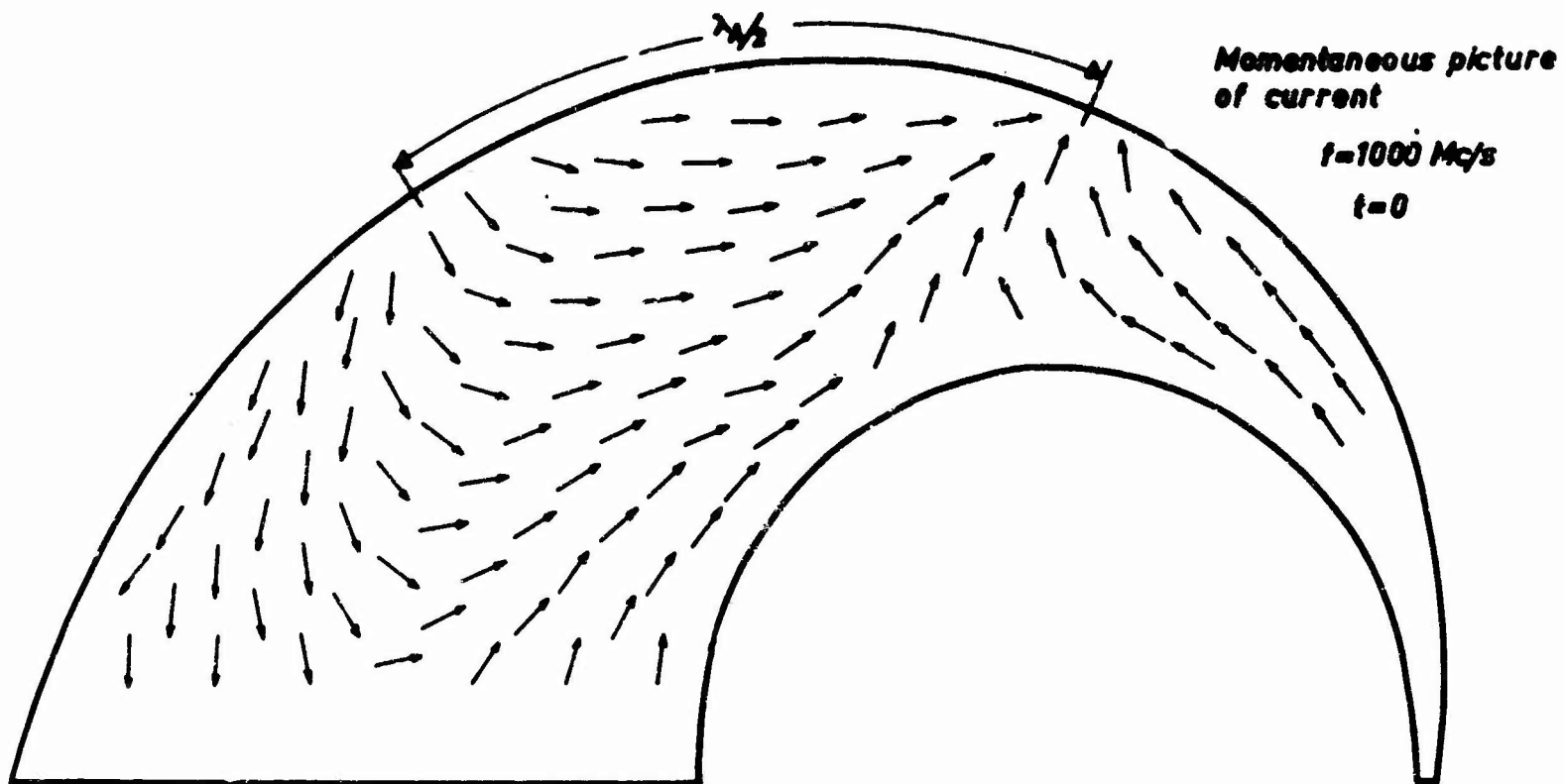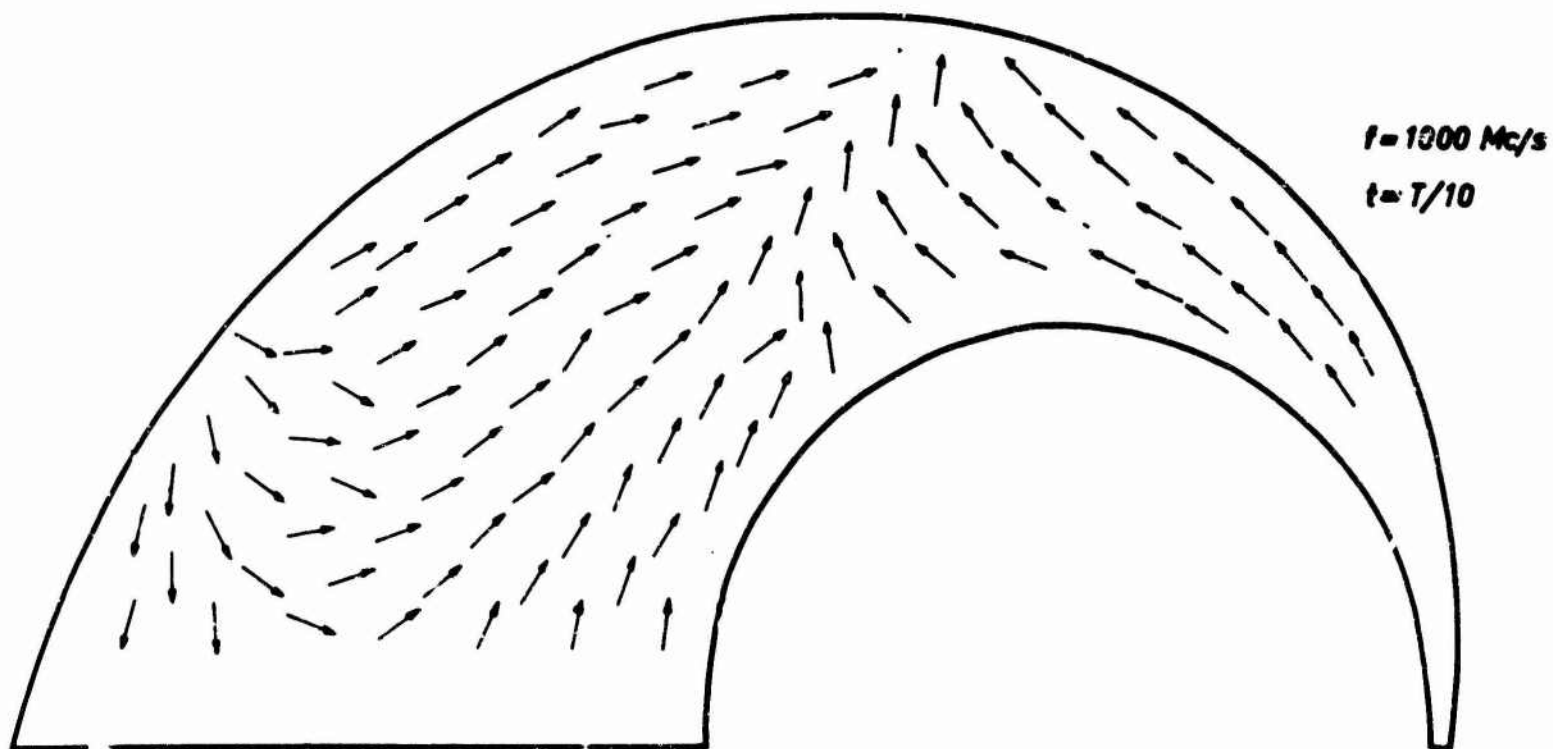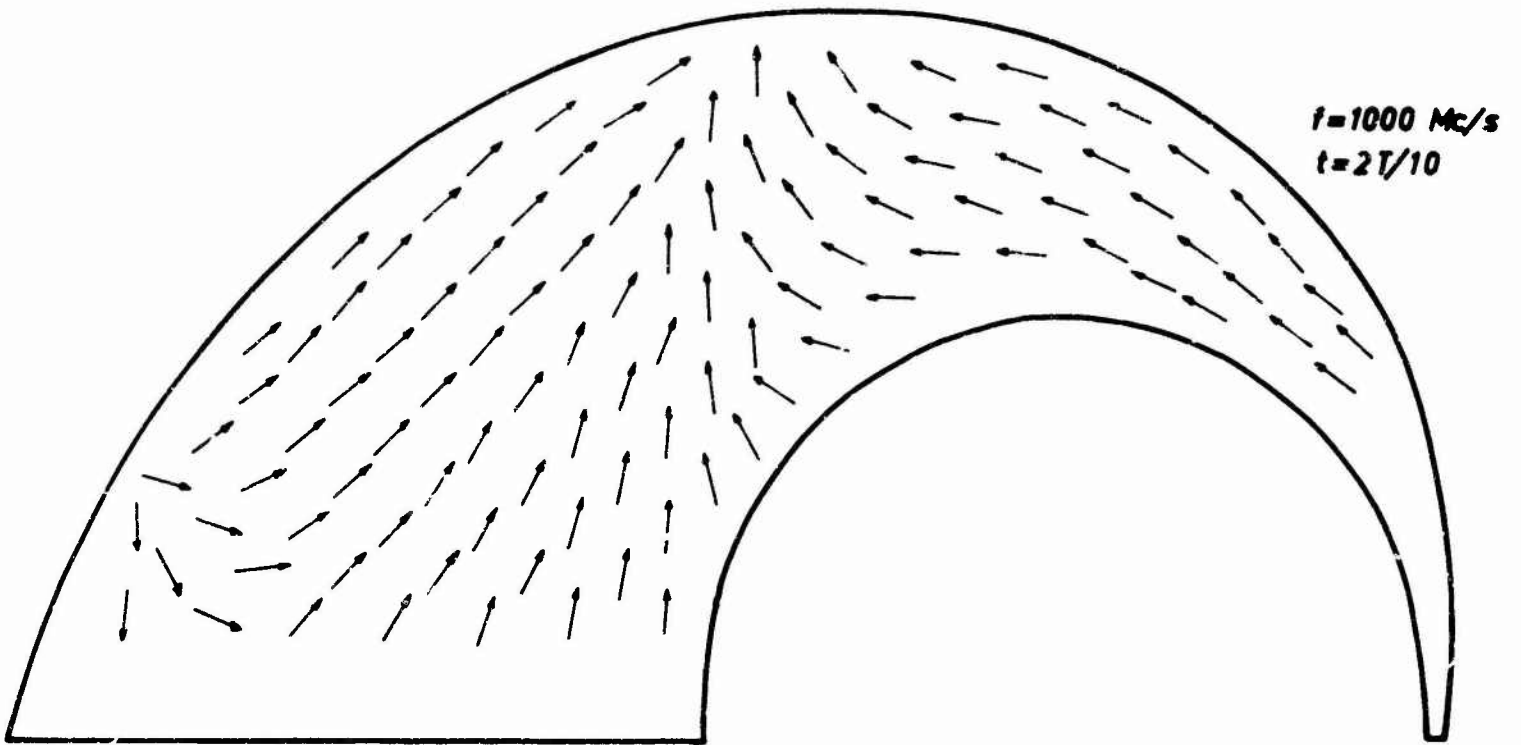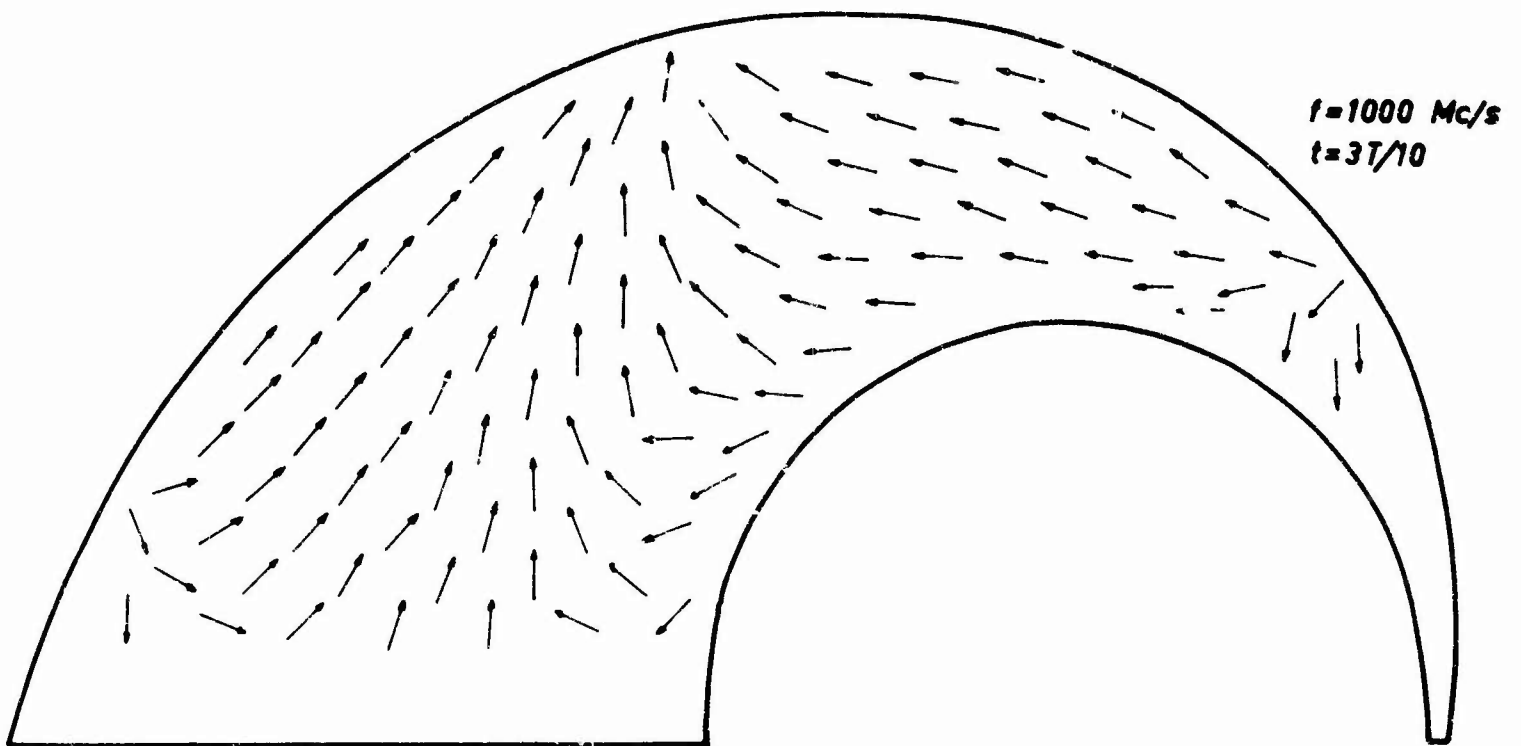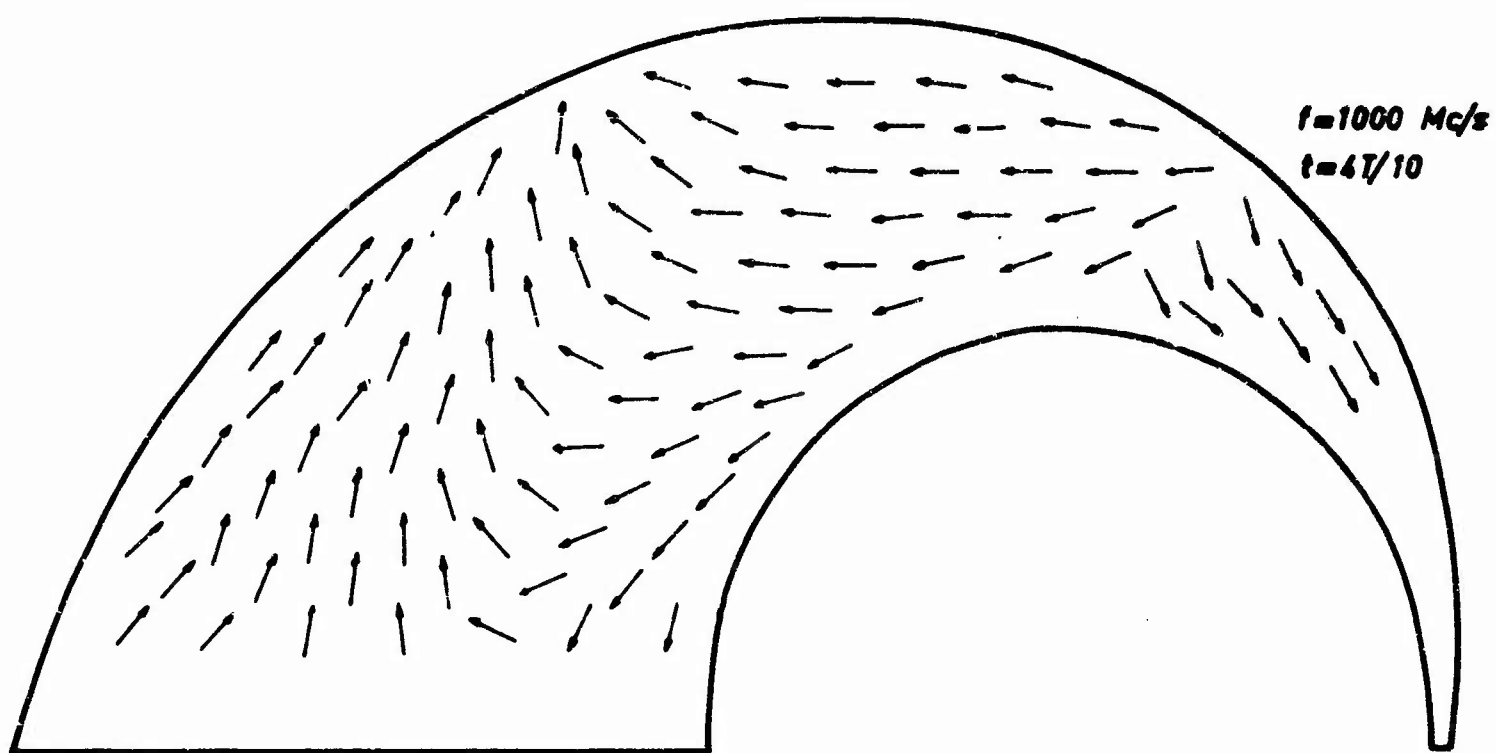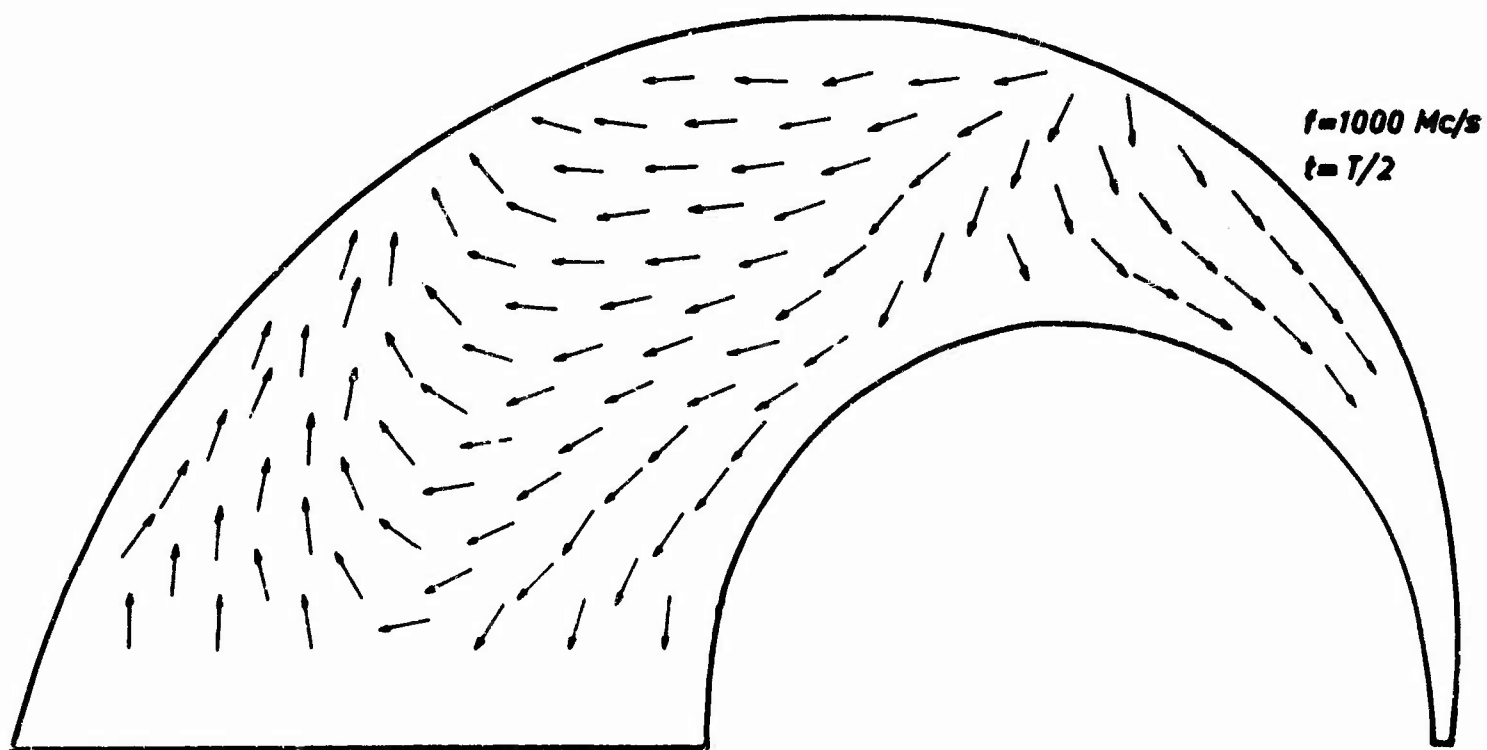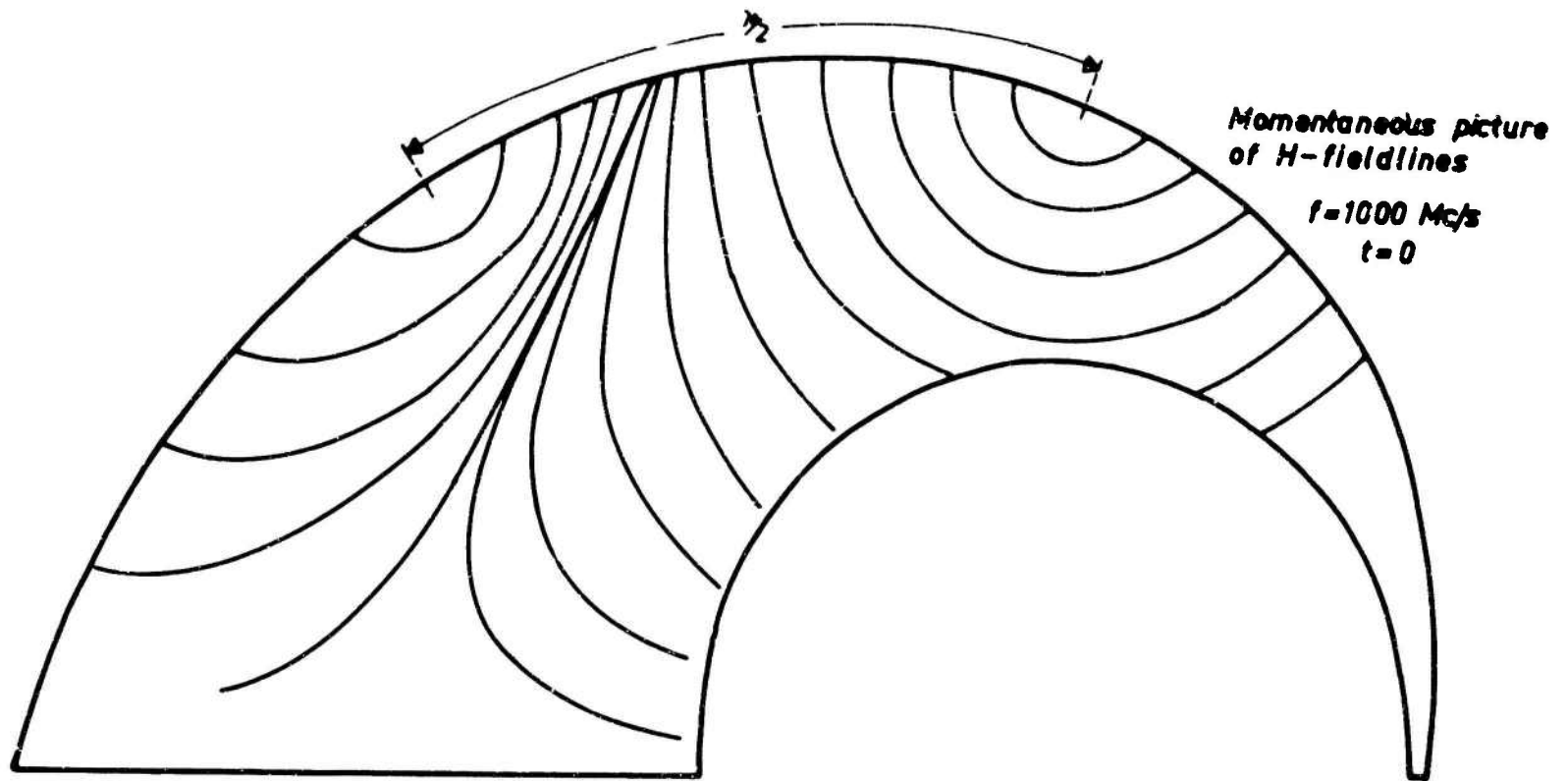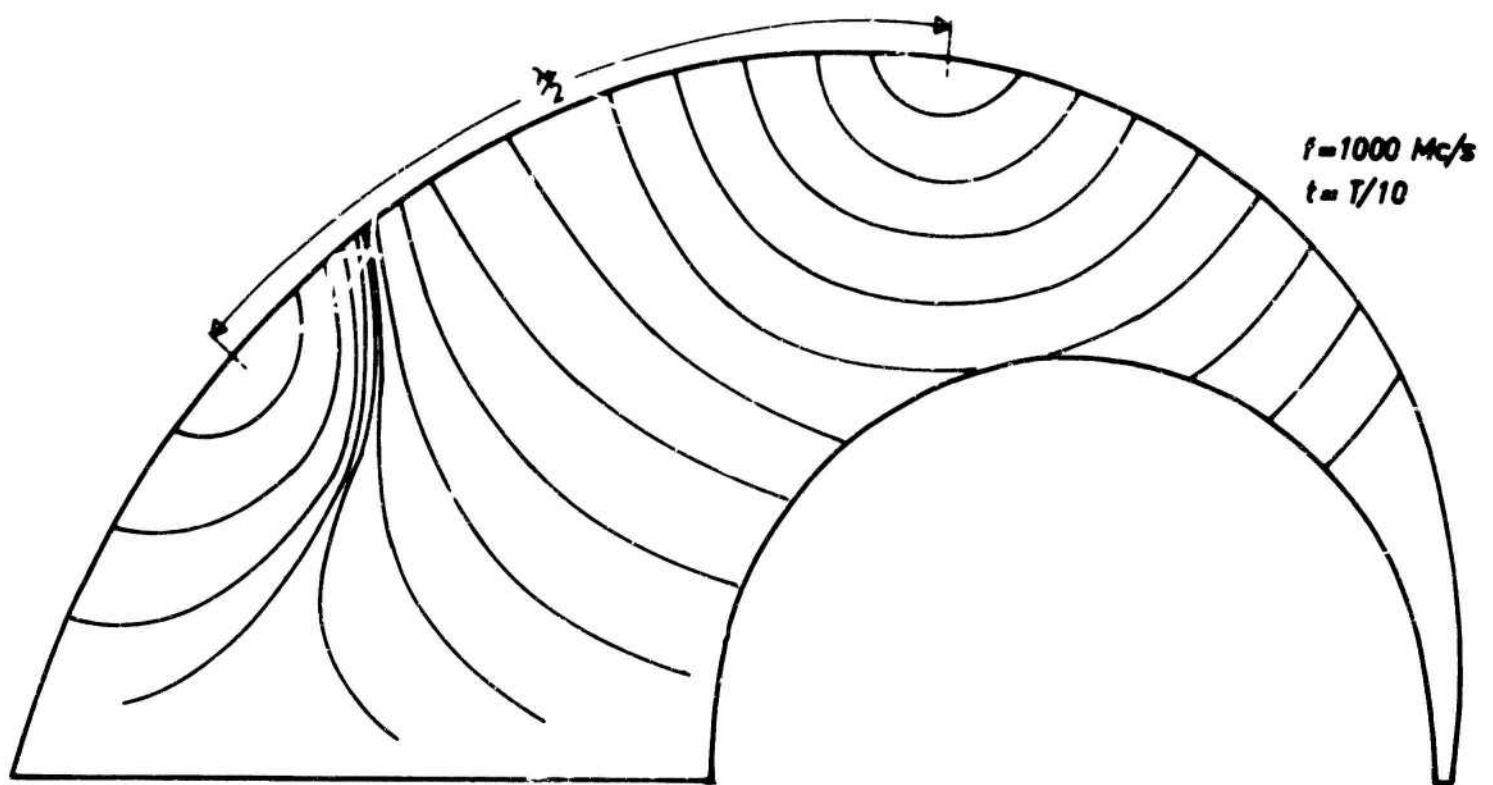
Fig. 66 b

from the feeding point with increasing time. The similarity
of the wavefields on the antenna with those in a common wave-
guide can be shown more easily if the H-field distribution is
drawn instead of the current distribution.

Fig.66 shows at a frequency of 1000 Mc/s $(d/\lambda_0 = 1,1)$ magnetic
field lines on the antenna for a moment of time called $t = 0$
and for $t = T/10$ respectively. Comparing this to a TE_{10} wave
in a curved waveguide we find nearly analogous magnetic field
lines (Fig.67)
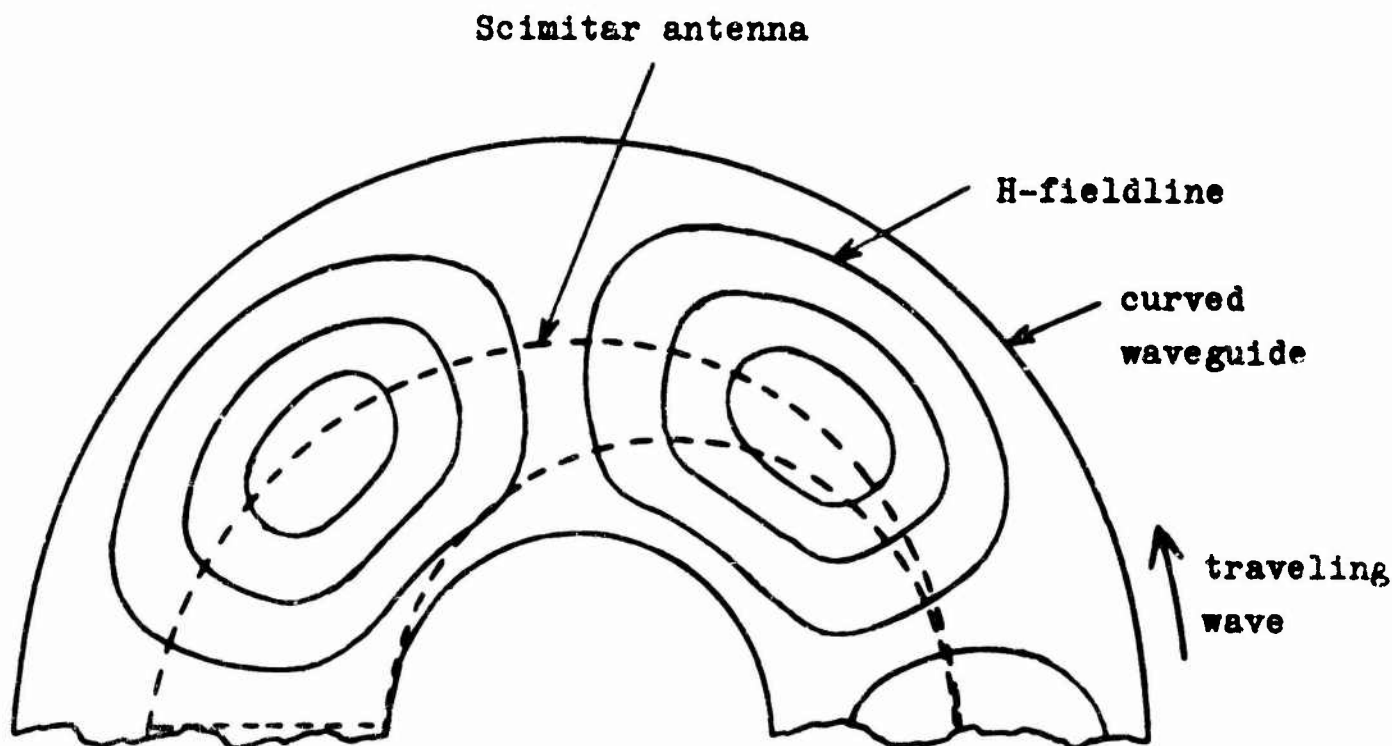
Fig. 67: TE_{10} wave in a curved waveguide

Fig.68 shows the ellipses of current on the antenna for f = 1500 Mc/s (d/λ_o = 1,6). At this higher frequency we find also a region where the current vectors are turning clockwise (region encircled with dotted line). This effect can also be found in waveguides where higher modes exist at higher frequencies.

Fig.69 shows the ellipses of current on the ground plane for f = 1000 Mc/s. All current vectors have the same direction of rotation at this frequency. At higher frequencies this direction of rotation varies on the area of the ground plane.

c) <u>Radiation Patterns of the Conventional Scimitar Antenna</u>

The radiation patterns were measured from 300 to 4000 Mc/s on a ground plane of 4x4 m^2 (Fig.70). Fig. 71 shows the used spherical coordinate system. The electrical size of the antenna is defined by d/λ_o (d = maximal dimension of the antenna).

Fig. 72a - e shows the various measured radiation patterns. Because of the complicated form of the antenna we have both vertical and horizontal polarization that means characteristics of rod and loop together. The vertical polarization (Fig.72a, b) shows many lobes and is not very constant with frequency. The horizontal polarization (Fig.72c) is a bit more constant but its average amplitude only 80 % of the average amplitude of the vertical polarization.

2. <u>Improved Forms of Scimitar Antennas</u>

a) <u>Input Impedance of Improved Scimitar Antenna</u>

We have seen in sect. II.1a that the impedance of the conventional scimitar form approaches a constant but relatively high value of about 180 Ω for higher frequencies. This results from the fact that the cone angle of the antenna blade near the feeding point (plane structure) is rather small. For broadband adapting of this relatively high impedance to a feeding cable of 50 or 60 Ω a tapered line must be used. The length of this line must be at least one half wavelength of the lowest frequency.

To come out of this trouble we developed an improved shape of scimitar antenna which shows a nearly constant impedance of 60 Ω

Ellipses of current
f=1500 Mc/s
d/λ₀=1.6

d=33cm
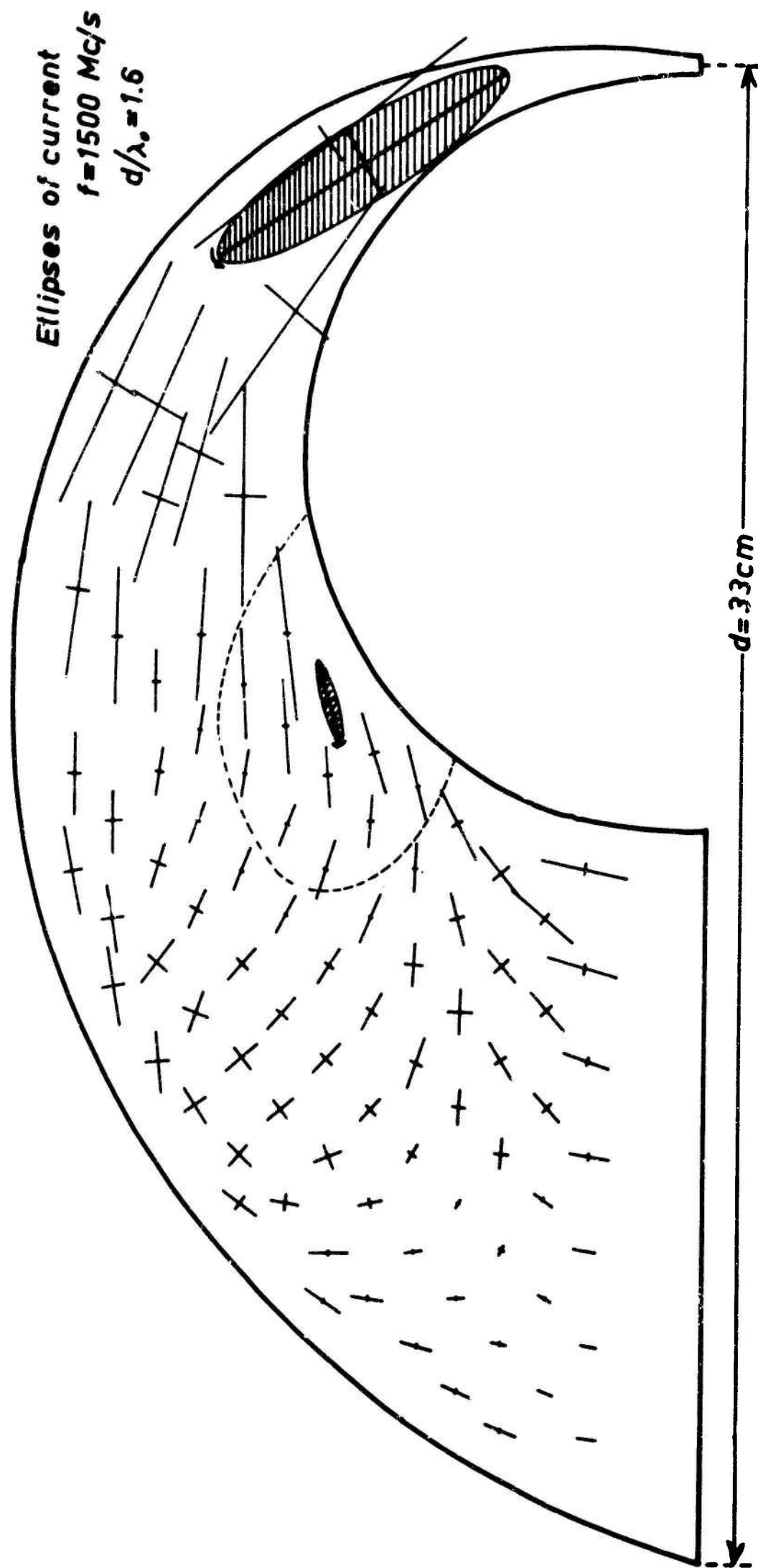
Fig. 68

Ellipses of current on ground plane   f = 1000 Mc/s   Fig. 69

$$\frac{d}{\lambda_o} = 1.1$$
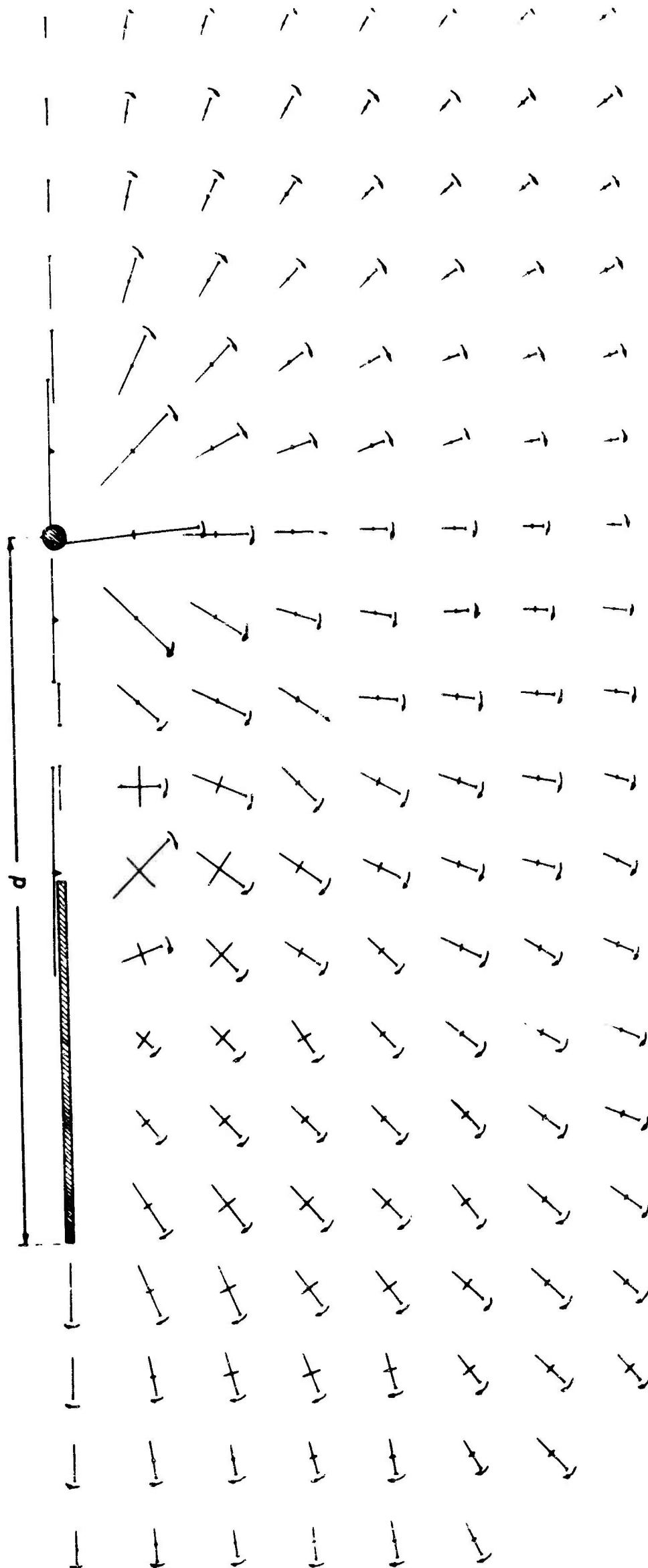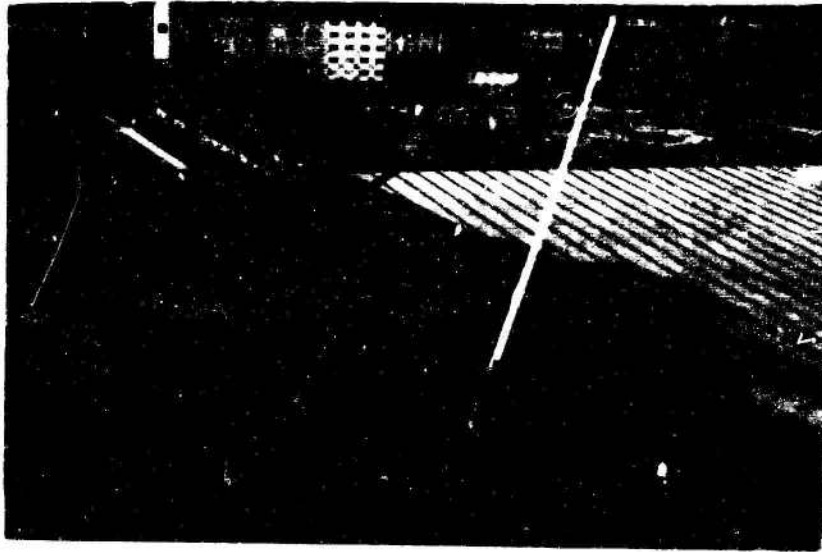
Fig. 70: Measuring plane
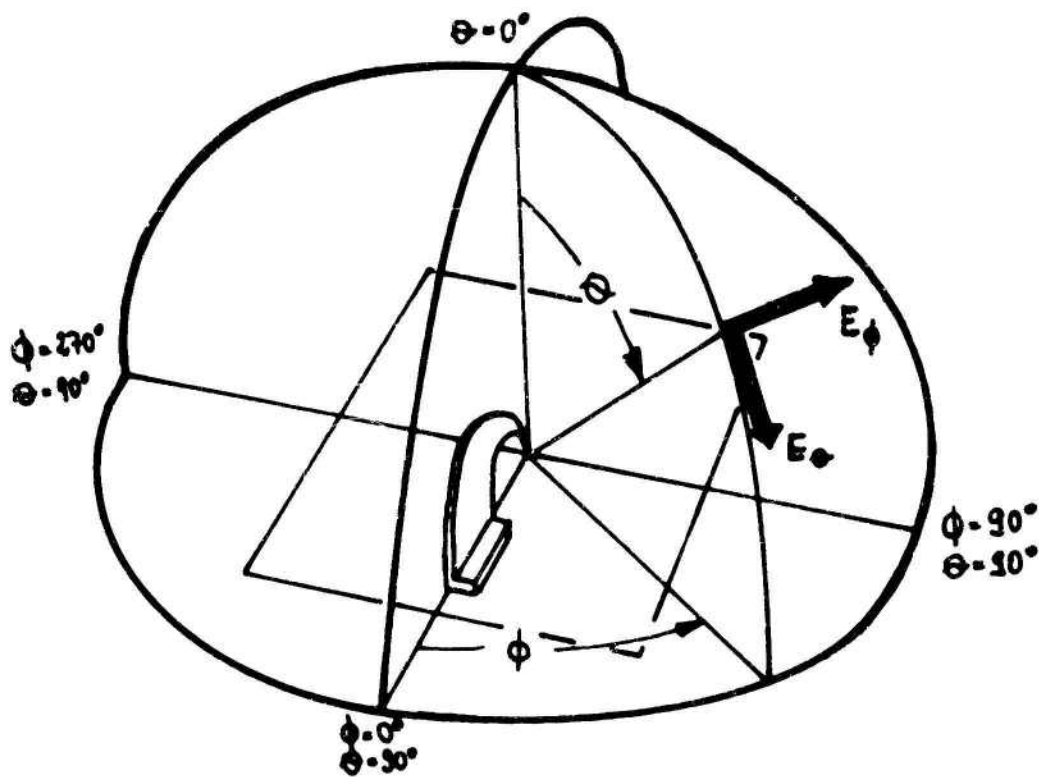
Fig. 71: Antenna in spherical coordinate system

Fig. 71 b

Fig. 72 a

VERTICAL DIAGRAM
$\phi = 0°$ θ var.
POLARIZATION E_ϕ

VERTICALDIAGRAM
ϕ = 90° Θ var.
POLARIZATION E$_\phi$

Fig. 72 b

Fig. 72 d

Fig. 72 c

VERTICAL DIAGRAM
$\phi = 90°$ θ var.
POLARIZATION E_ϕ

0,728

1,82

0,546

1,45

0,364

1,09

3,055

d/λ_0
0.182

0,908

2,62

0,728

1,82

0,546

1,45

0,364

1,09

3,055

d/λ₀
0,182

0,908

2,62

HORIZONTALDIAGRAM
θ=86°   φ var.
POLARIZATION E_θ

Fig. 72 d

Fig. 72 e

HORIZONTALDIAGRAM
Θ = 0° φ var.
POLARIZATION E φ
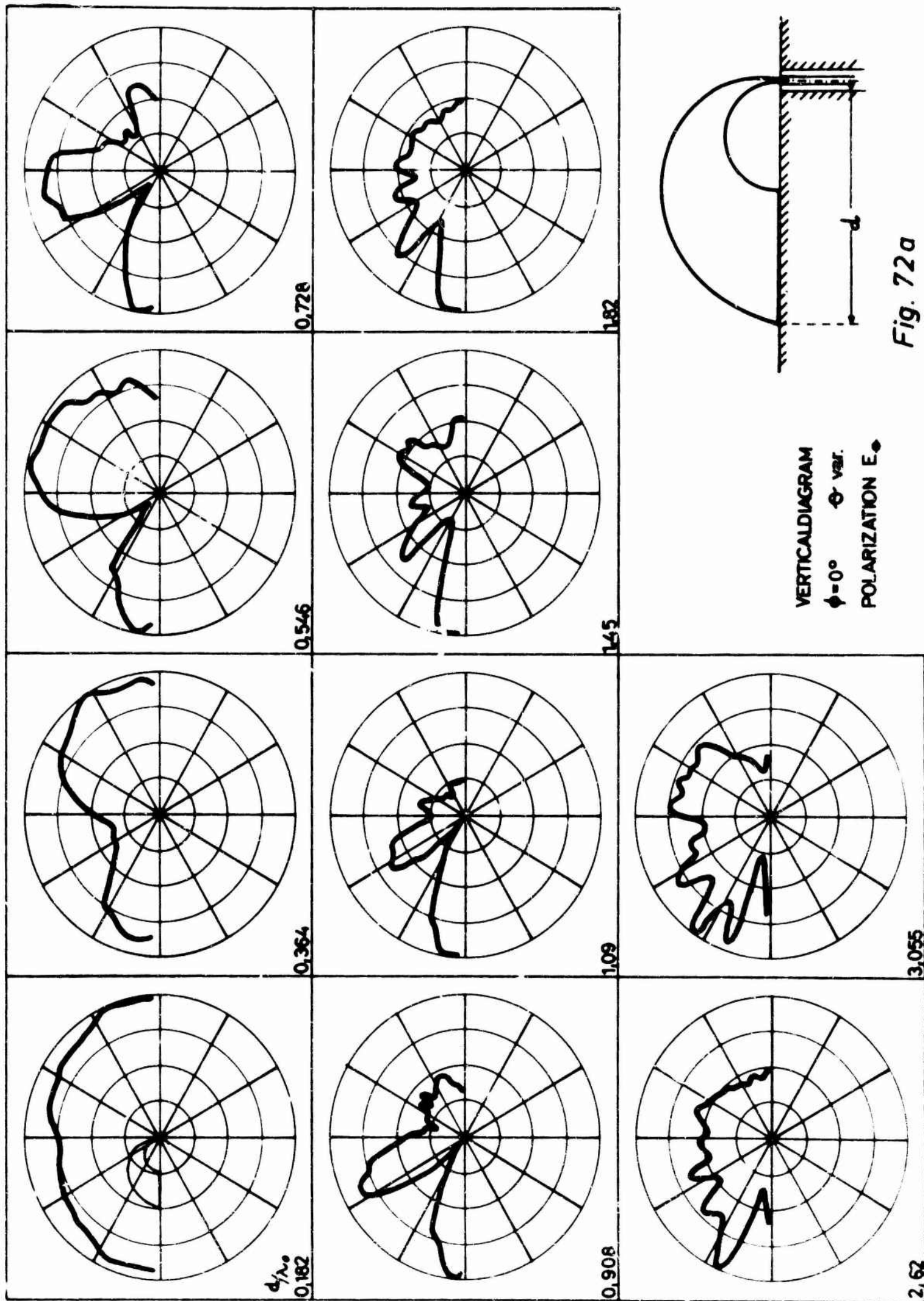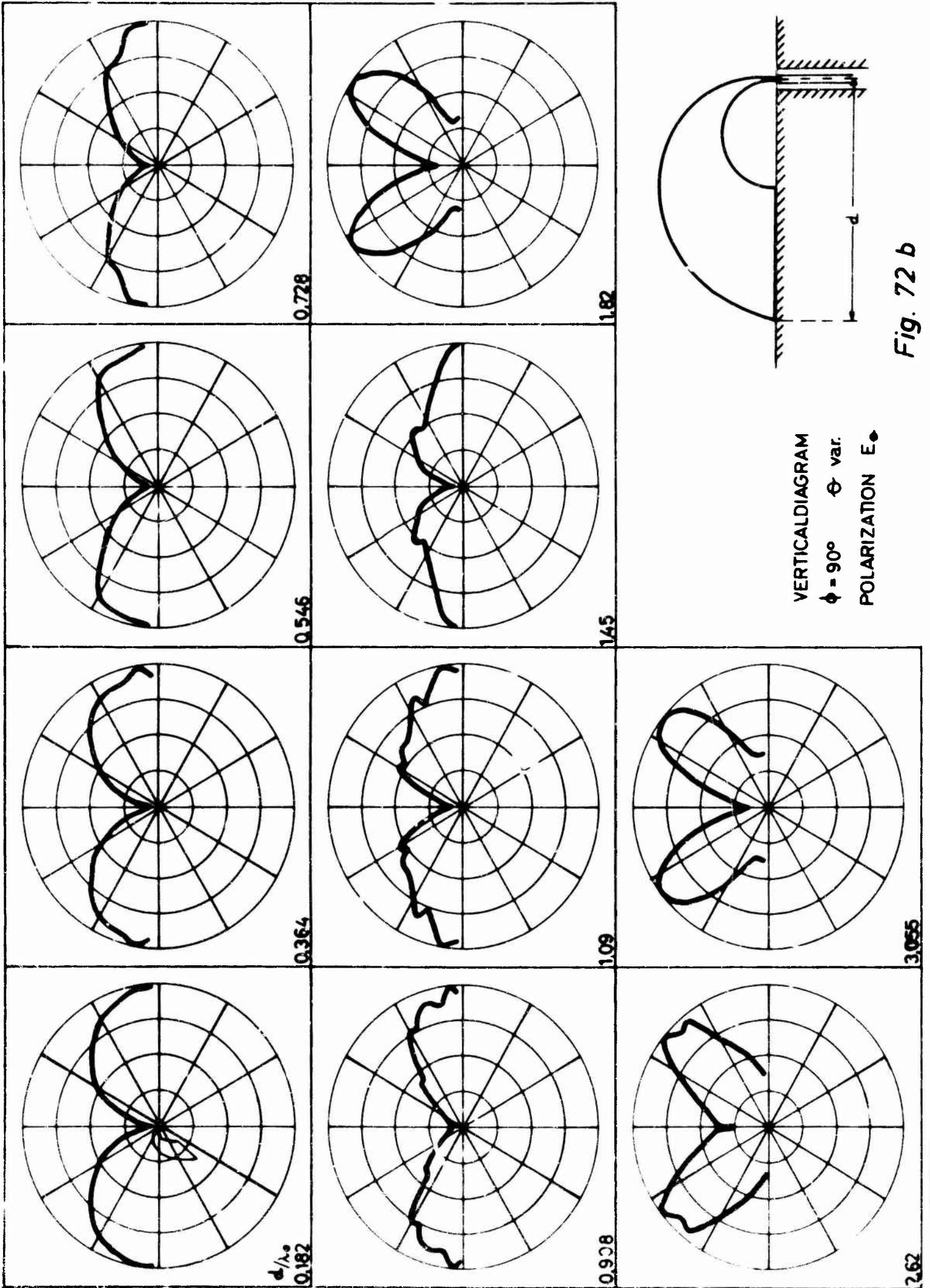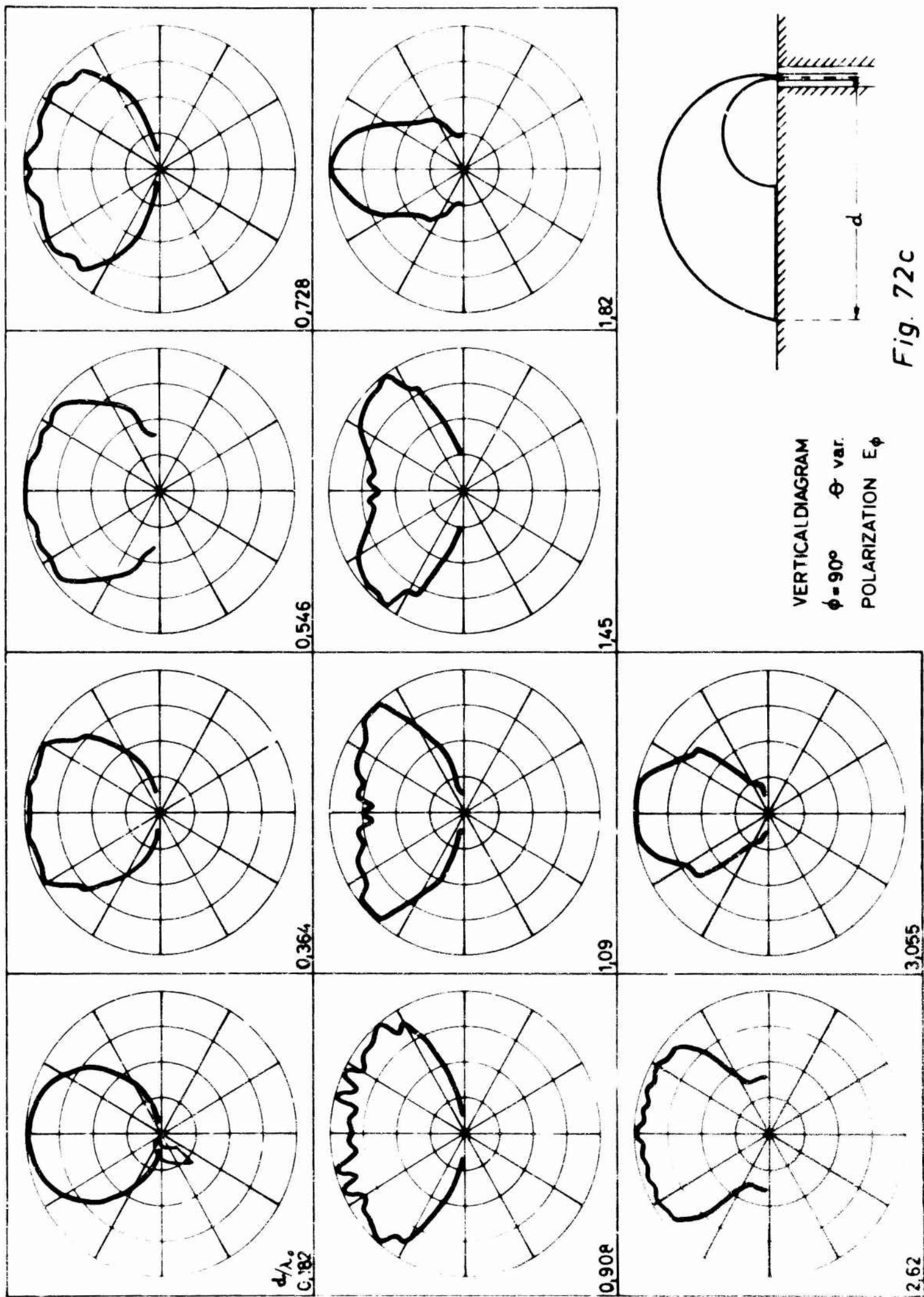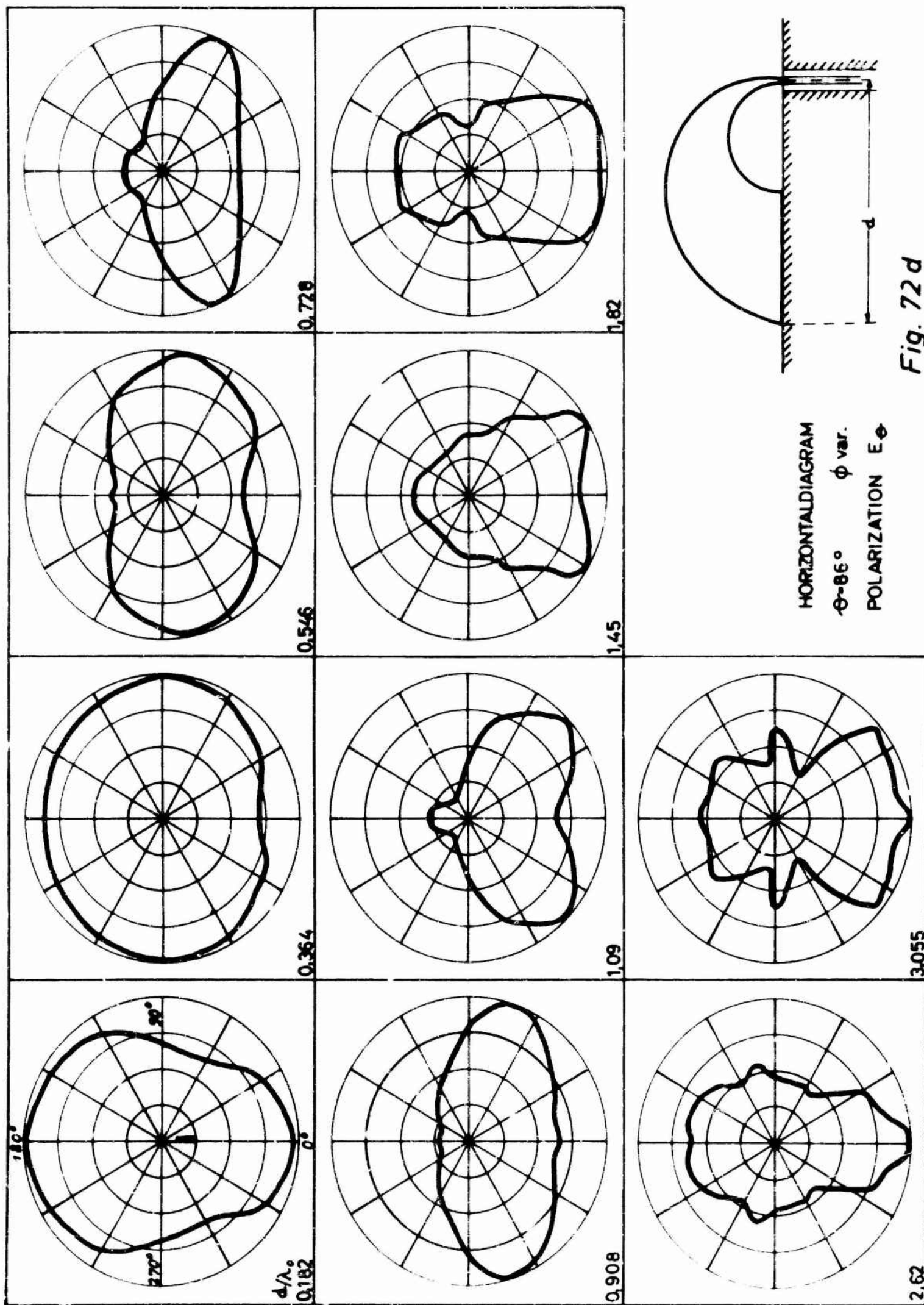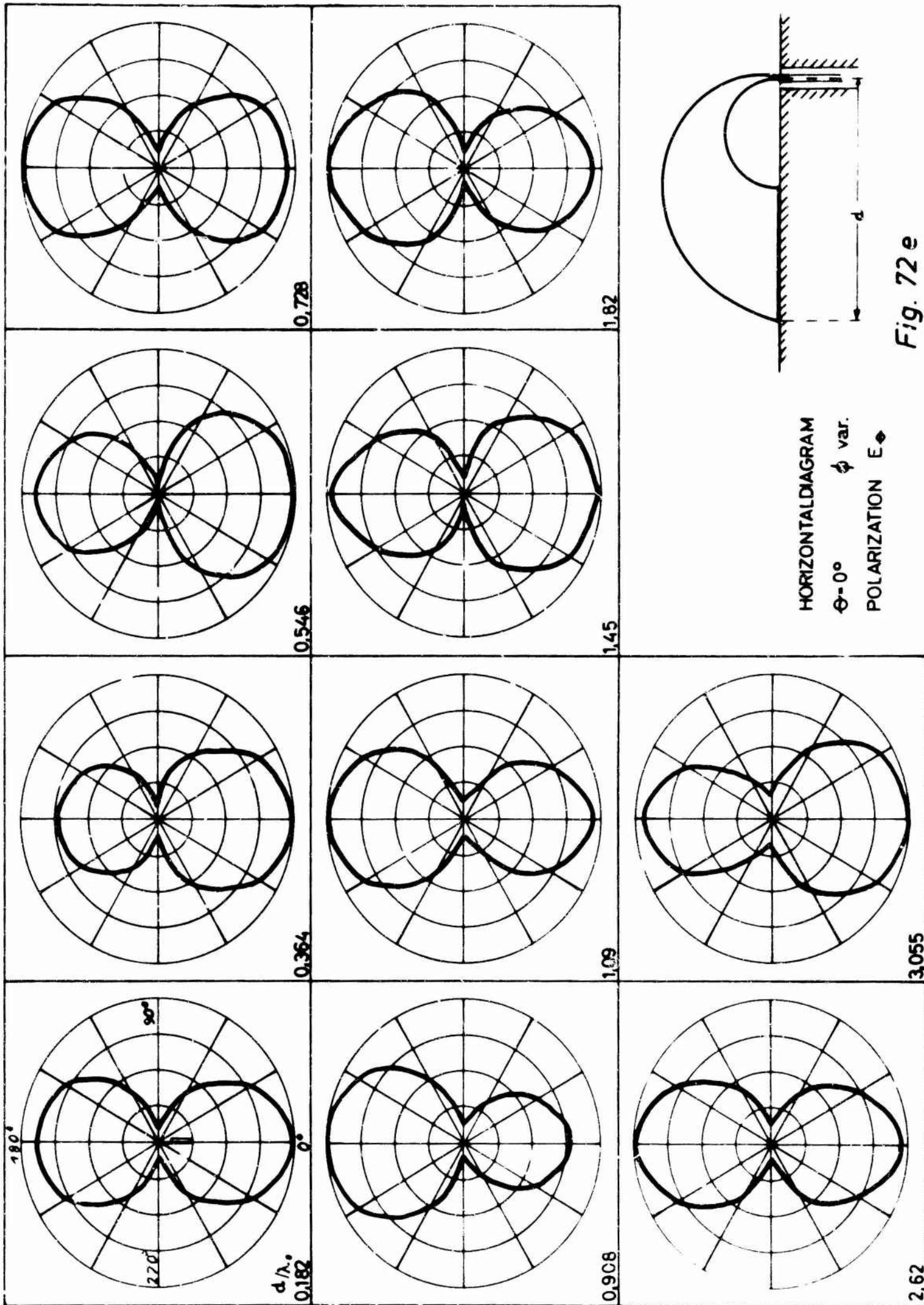
at its feeding point for high frequencies. We used a broader cone
angle to have a lower characteristic impedance against the ground
plane. Since the logarithmic spiral form is not essential for
the function of the antenna (this form is no more a frequency
independent structure because of its mirror image below the
ground plane) we could deviate from this conventional form.
Fig. 73a-l shows several forms that have been studied by us.
The first idea was to get half of the original impedance by
doubling the structure symmetrically (Fig.73a-d). But this has
no good impedance since the loop turning left compensates the
loop turning right and cancels a part of the radiation.

Finally we came to the form of Fig.73l. Fig.74 shows this antenna
in detail. The length d is defined in analogy to sect. II.1a
as the distance from the feeding point to the end of the antenna.
The cone angle of 140° near the feeding point is the important
feature. This cone angle generates the characteristic impedance
of 60 Ω near the feeding point and a good match to the coaxial
feeding cable for high frequencies since for high frequencies
almost the total energy is radiated in the region of this cone.
For a characteristic impedance of 50 Ω we found a cone angle
of 160° by measurements.

The solid line in Fig.75 shows the impedance of the antenna of
Fig.74 in a Smith chart related to 60 Ω measured from 30 to
4600 Mc/s. The real axis is intersected first at about 300 Mc/s.
At this frequency the length of the inner edge of the antenna
is about $\lambda_0/4$. From 1000 Mc/s ($d/\lambda_0 = 0.5$) to 4600 Mc/s
($d/\lambda_0 = 2.3$) and probably for still higher frequencies the
impedance stays inside the relatively small dashed circle around
60 Ω (VSWR = 1,17).

At frequencies above 1000 Mc/s almost the total energy is ra-
diated in the conical feeding zone and therefore that part of
the antenna that leads to the ground plane and is connected
mechanically to it is electrically of no interest. This arm is
necessary for mechanical stability on high speed aircraft only.
Shortening the inner edge of the antenna and broadening the
arm (Fig. 76) does not change the high frequency behavior. The
only change is the first intersection of the impedance curve
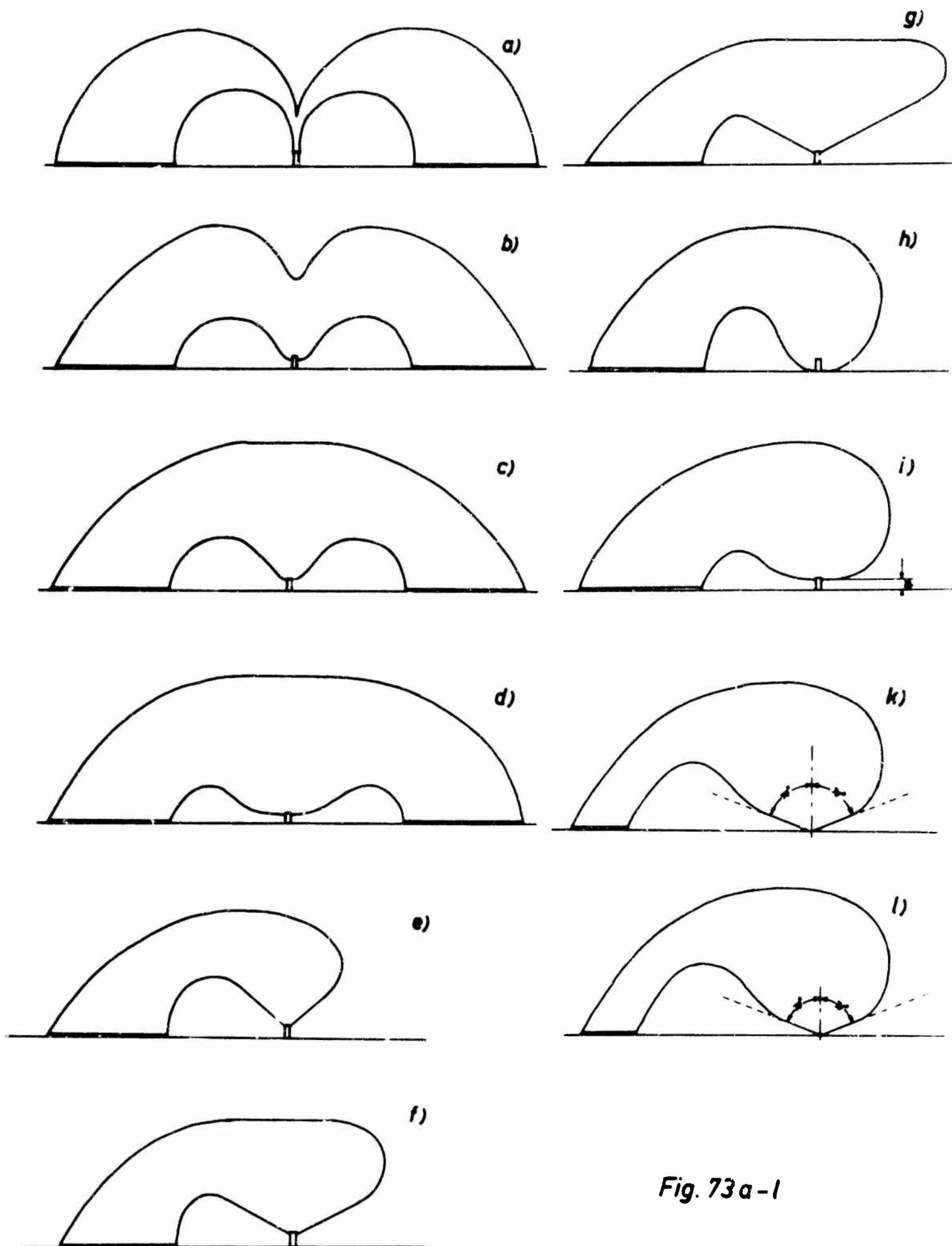
Fig. 73 a - l
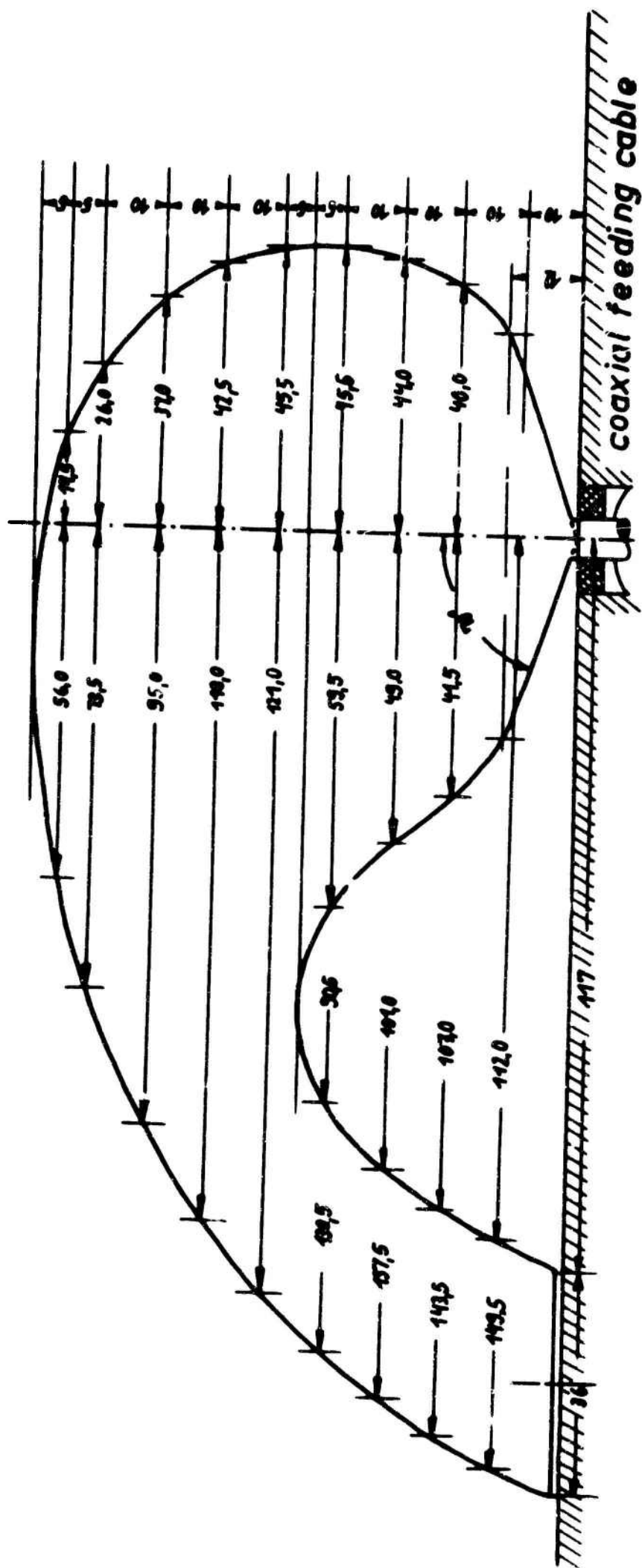
Fig 74   Improved form of Scimitar antenna
(length in mm)

Fig. 75

Input impedance of
improved Scimitar in
a Smith chart

f = 30 .... 4600 Mc/s

with the real axis since the length of the inner edge of the
antenna always must be about $\lambda_0/4$ at this intersection point.
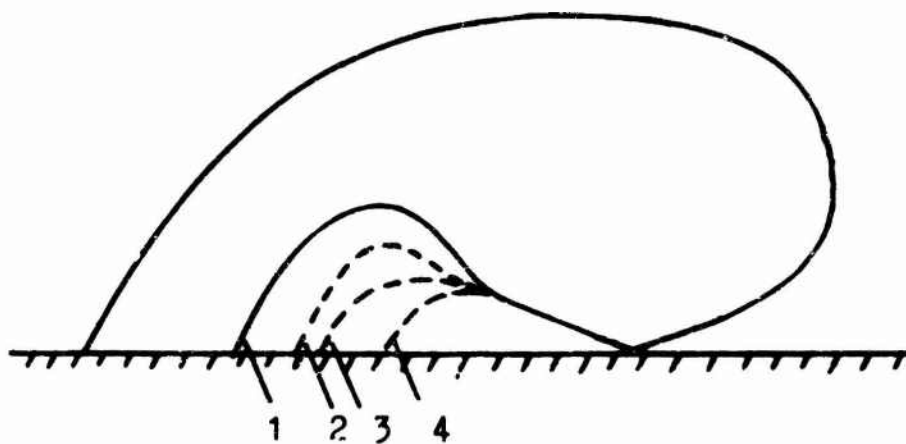
Fig. 76: Size variation of inner edge

Instead of directly connecting the arm of the scimitar to the
ground plane it may be connected by a Ohmic resistor R parallel
to a capacitance C. This C consists of the capacity of the an-
tenna plate. If R is chosen 60 Ω the impedance of the antenna
at very low frequencies is 60 Ω since the resistor is the ter-
mination of the feeding line at very low frequencies. The
efficiency of this antenna goes to zero at very low frequencies
since almost the total energy is then lost in the resistance.
At high frequencies the resistance does not disturb in any way
since almost the total energy is radiated near the feeding zone
of the antenna and the current in that arm goes to zero. Also
the resistor is short circuited by the capacitance at high fre-
quencies. The capacitance C against the ground plane must be
so small that the resistance is not shorted by C at low fre-
quencies. The critical frequency of the RC-combination is cho-
sen at 900 Mc/s or higher. Fig. 77 shows this antenna. The Ohmic
resistor is to be seen in parallel to the insulating polystyrol
plate. The RC-combination could also be designed in form of a
resistive plate between scimitar arm and ground plane. The dotted
curve in Fig.75 shows the impedance of the antenna for R = 60 Ω;

Fig.77: New Scimitar Antenna with Ohmic Resistor
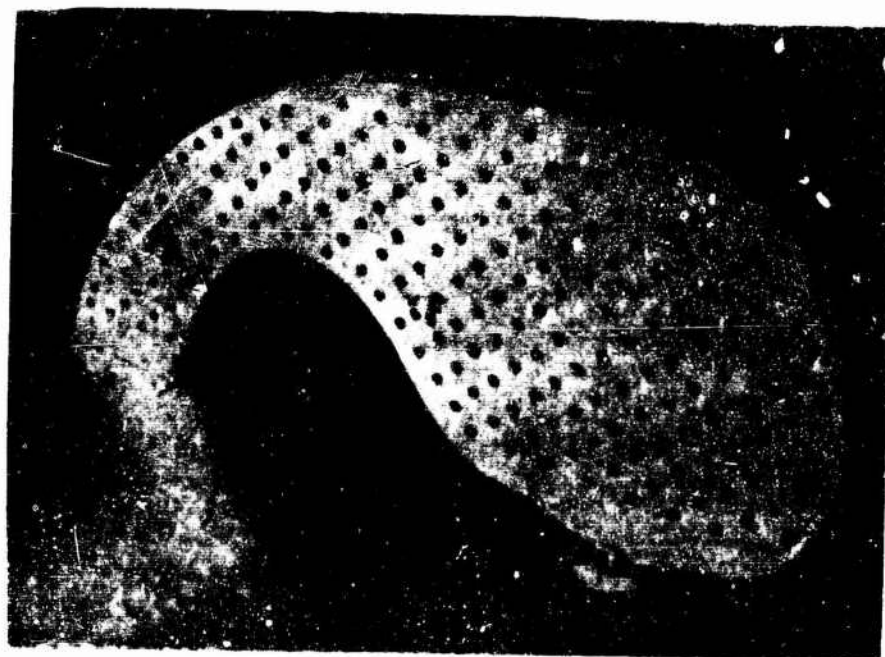
Fig.78: Improved Scimitar form for near Field Measurements

the dash-dotted curve for R = 90 Ω. These curves start at 60
or 90 Ω for very low frequencies. With increasing frequency they
leave this point. At 1000 Mc/s $(d/\lambda_o = 0.5)$ and higher the
curves come to 60 Ω and are then identical with the impedance
curve of the antenna connected directly to the ground plane
(solid curve in Fig.75).

b) **Near Field Measurements of the Improved Scimitar Antenna**

The improved form of scimitar antenna has been constructed with
a hollow interior and with one movable side plate like the
conventional scimitar antenna discribed in sect. 1b. The dis-
tance from the feeding point to the end of the arm connected
to the ground plane was 33 cm as before. The ground plane had
a size of 1x1.30 m^2 as before. Fig. 78 shows this antenna on the
measuring plane. The measuring equipment used was the same as
in sect. 1b.

Fig.79 shows the measured lines of constant amplitude for the
E-field on the antenna at f = 1000 Mc/s $(d/\lambda_o = 1.1)$. The
strongest E-field is at the edges of the antenna. This shows
that for this improved antenna form the energy is divided in
2 parts. One part is traveling near the outer edge. At the
center of the blade above the feeding point we find a amplitude
minimum of -24dB. Also at that region where the arm is connected
to the ground plane we find closed lines of constant amplitude
encircling a minimum of -28 dB. This indicates standing waves
in this zone, i.e. a part of the energy travels in the arm in
direction to the ground plane and is reflected at the ground
plane.

Fig. 80 shows the measured amplitudes of the E-field for
f = 1700 Mc/s $(d/\lambda_o = 1.8)$. Here we find again a minimum at the
center of the blade above the feeding point and varying amplitu-
des in the arm leading to the ground plane indicating standing
waves.

Fig.81 shows the measured lines of constant phase for the E-field
at f = 1000 Mc/s. The adjacent lines have a phase difference of
25°. The phase delay is increasing with increasing distance
from the feeding point.

Fig.82 shows the measured E-field phase for f = 1700 Mc/s.
The adjacent lines have a phase difference of 45°. The lines of

E-field amplitudes in db

f=1000 Mc/s   d/λ₀=1.1

d=33 cm
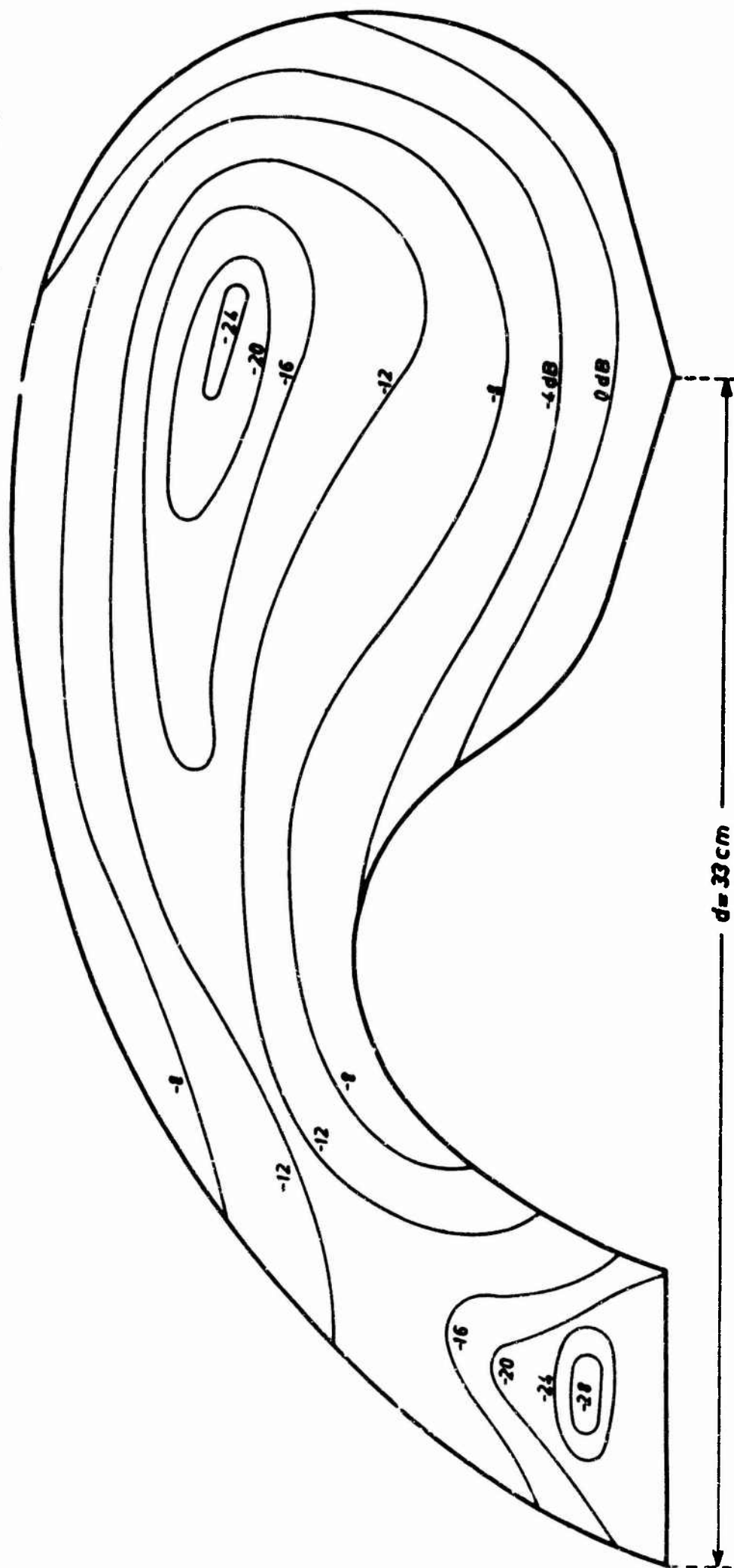
Fig. 79

E-field amplitudes in db

f-1,00 Mc/s   d/λ.=1.8
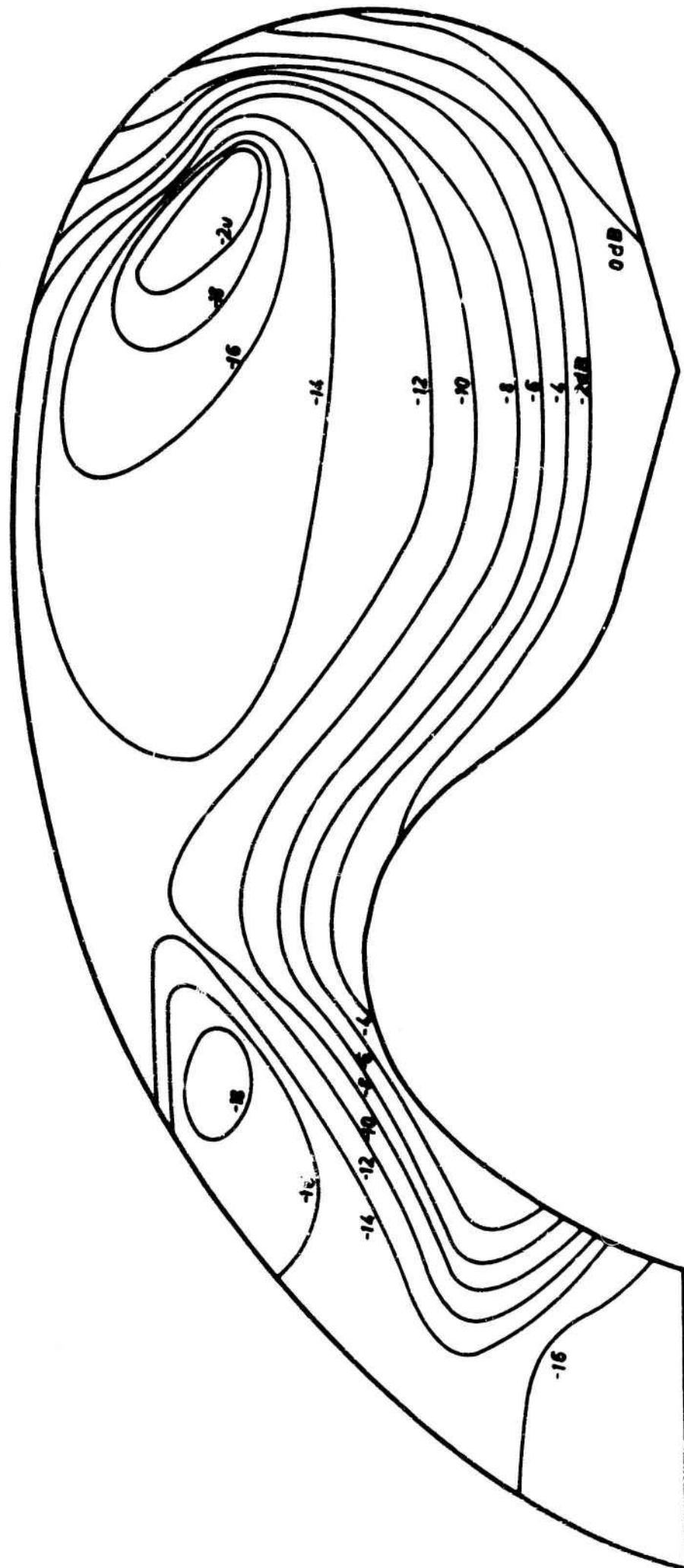
Fig. 80

E-field phase
f-1000 Mc/s d/λ₀=1.1
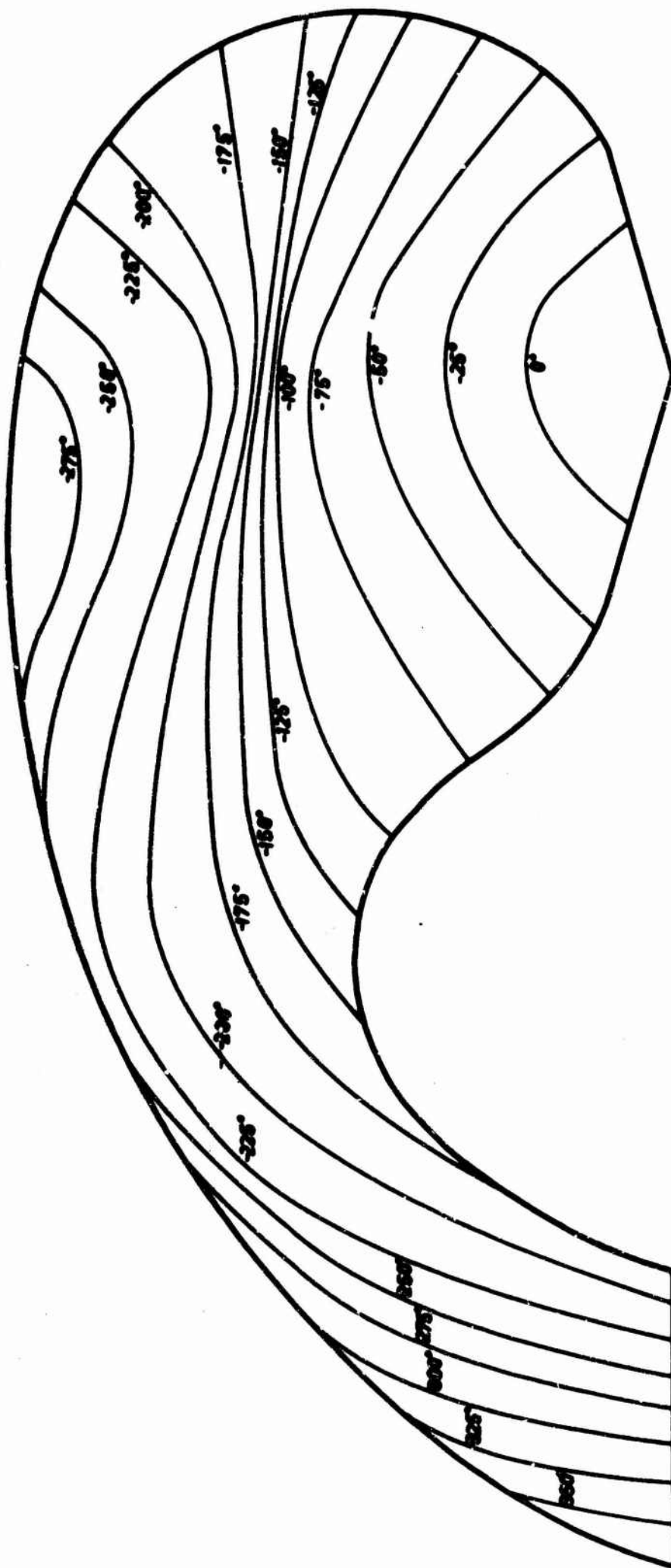
Fig. 81

E-field phase
f = 1700 Mc/s   d/λ₀ = 1.8
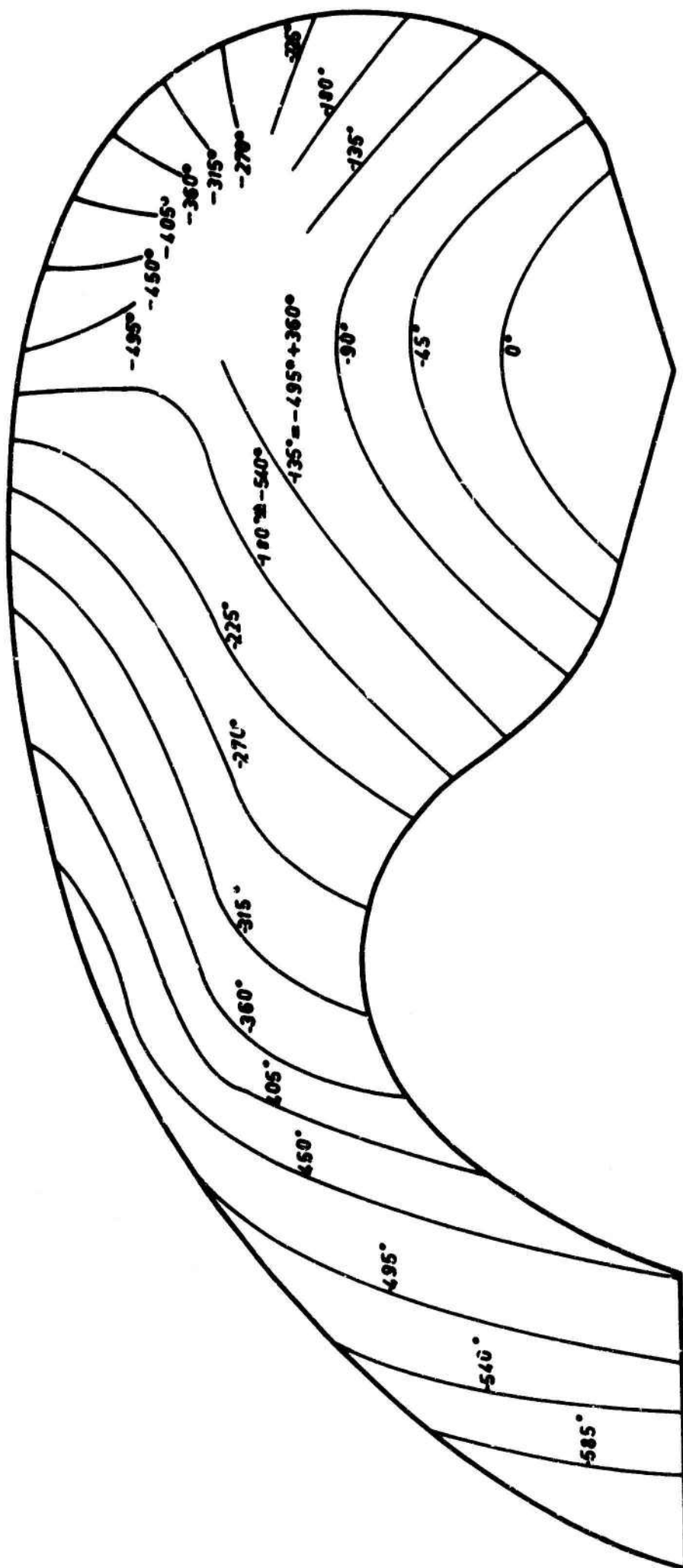
Fig. 82

amplitude on ground plane in db

1000Mc/s, $\frac{d}{\lambda} = 1.1$
E-field

0 db

-4

-8

-12

-16

d = 33cm

connection to
groundplane

feeding point

Fig. 83
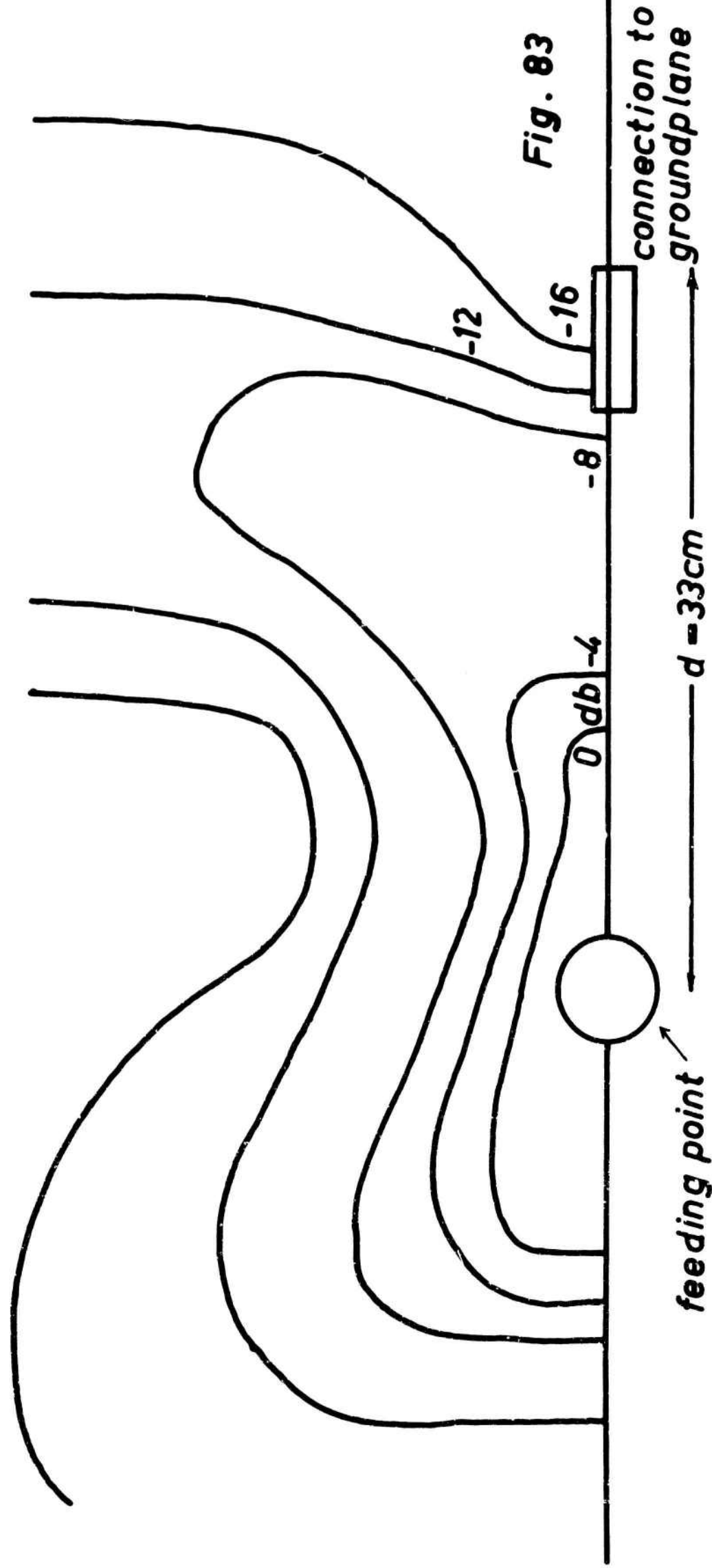
1000 Mc/s; $\frac{d}{\lambda_o} = 1.1$

E-field
phase on
ground plane

d = 33 cm

0   -51°   -102°   -153°   -204°   -266°   -306°
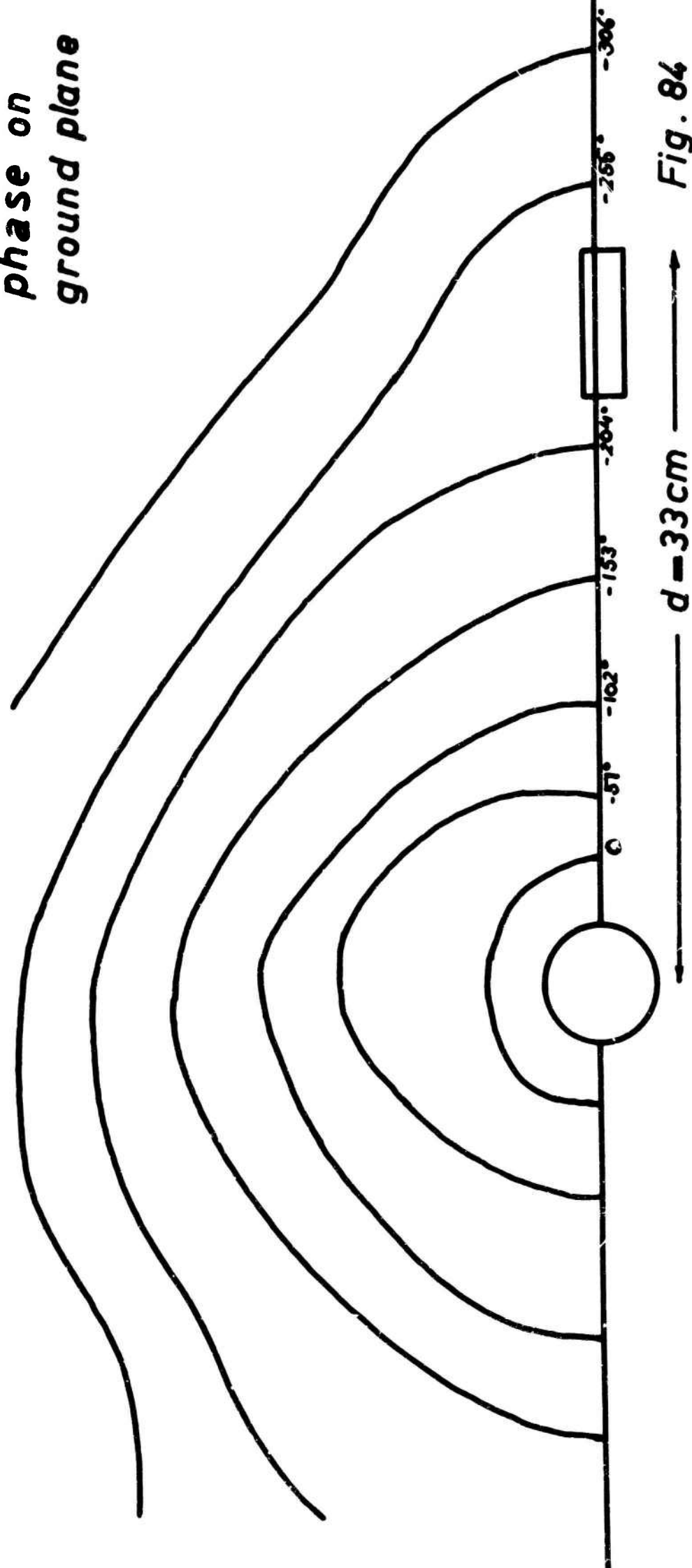
Fig. 84

constant phase have not been drawn in that region above the
feeding point where the amplitude is very low. That wave which
is traveling near the outer edge of the antenna blade has a
longer way than that wave which is traveling near the inner edge.
Both waves meet again at the arm leading to the ground plane.
For the frequency of 1700 Mc/s both waves fit together because
the wave traveling on the outer edge has a phase delay that is
by 360° greater than the phase delay of the wave traveling at
the inner edge of the blade. That effect explains also why there
must be a zero of amplitude in the center of the blade above the
feeding point; the two waves do not fit together in this region.
Then two waves sometimes fit together and sometimes do not de-
pendent on frequency. Therefore the near field and consequently
the radiation pattern is varying considerably if the frequency
is varied.

Fig. 83 and 84 show the measured amplitude and phase of the
E-field on the ground plane.

Fig. 85 shows measurements of the amplitude of current or H-field
on the antenna for $f = 1000$ Mc/s $(d/\lambda_0 = 1.1)$. The amplitude
in this case is the maximum amplitude of the field vector
rotating in the ellipse, i.e. the amplitude of the major axis
of the ellipse. The amplitude of current or H-field has its
maximum at the edges of the antenna like the electric field.
This indicates again two waves, one traveling at the inner edge
of the antenna blade, the other traveling at the outer edge.

Fig. 86 shows the measured major and minor axis of the ellipses
of current at $f = 1000$ Mc/s. The vector of current is not rota-
ting in the same sense in every ellipse as this was the case for
the conventional scimitar at 1000 Mc/s. The sense of rotation
is marked by an arrow at every ellipse.

Fig. 87a-e shows momentaneous pictures of current for $f = 1000$ Mc/s
constructed from the ellipses of current (Fig.86) together with
the knowledge of phase. All arrows that indicate the direction of
current on the antenna surface are drawn with equal length. The
time varies from a time called $t = 0$ to $t = 4/10T$ if T is the time
for one period. For $t = 5/10$ T we get the same picture as for
$t = 0$ with the only difference that every arrow must have opposite

direction. Looking at Fig.87 a-e it can be perceived very well how the waves come out of the feeding point and travel into the antenna blade.

Fig. 88 shows the measured amplitude of current or H-field for $f = 1700$ Mc/s ($d/\lambda_0 = 1.8$). We find again a minimum on the center of the blade above the feeding point. Fig. 89 shows the measured major and minor axis of the ellipses of current at $f = 1700$ Mc/s ($d/\lambda_0 = 1.8$). Fig. 90 shows one momentaneous picture of current for this frequency.

Fig. 91 shows the amplitude of current on the ground plane for $f = 1000$ Mc/s ($d/\lambda_0 = 1.1$). Fig. 92 shows the respective ellipses of current. The sense of rotation of the current vector is changing very often for different ellipses.

c) Radiation Patterns of the Improved Scimitar Antenna

The measurement apparatus was the same as for the conventional scimitar antenna (Fig.70). Fig.71 showed the used spherical coordinate system. The electrical size of the antenna is again defined by d/λ_0 (d = linear dimension of the antenna from feeding point to distant end). Fig. 93 a-e shows the various measured radiation patterns. The measured patterns of the improved scimitar form are not essentially different from the patterns of the conventional scimitar.

current or H-field amplitudes in db

f = 1000 Mc/s   d/λ₀ = 1.1

d = 33 cm
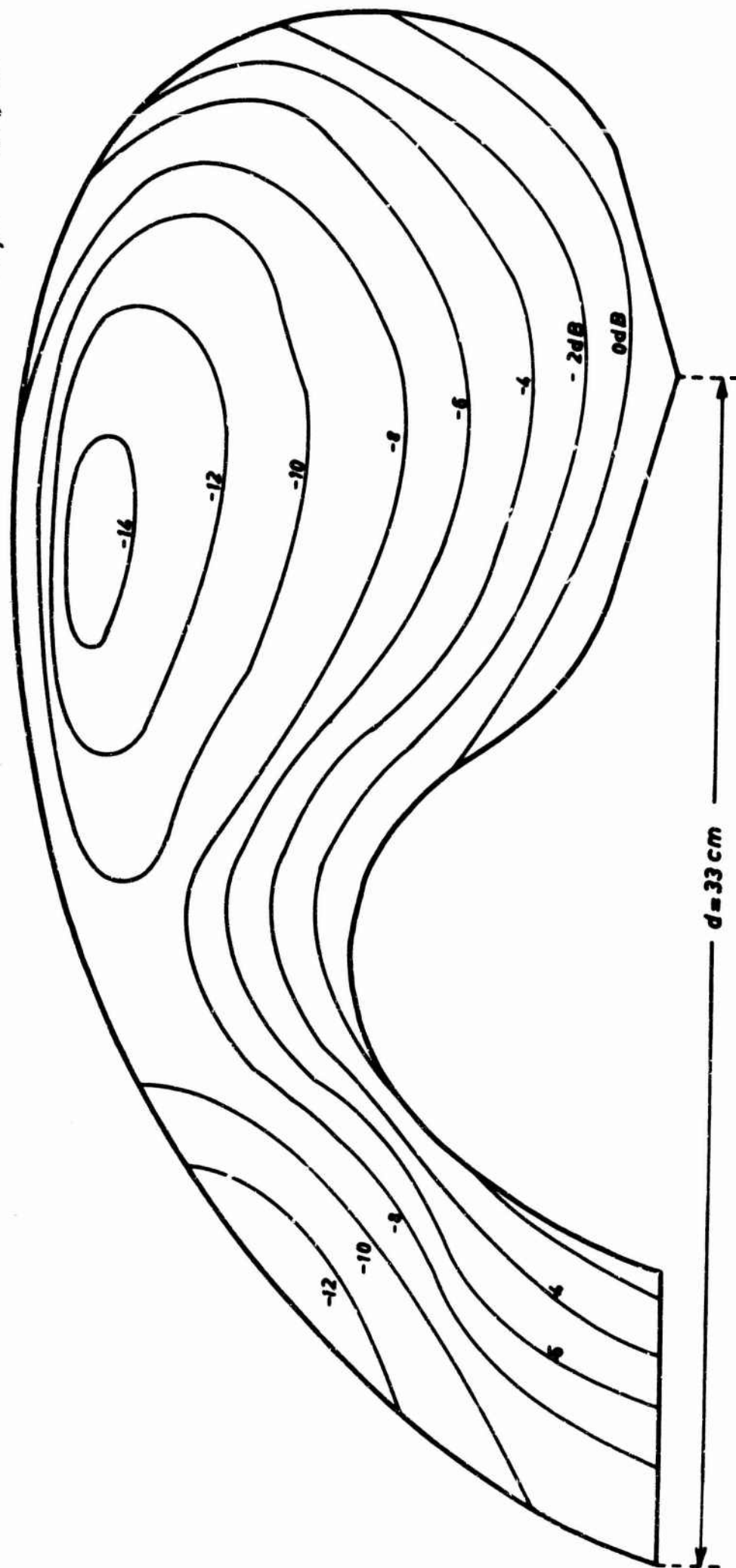
Fig. 85

Ellipses of current
f = 1000 Mc/s   d/λₒ=11
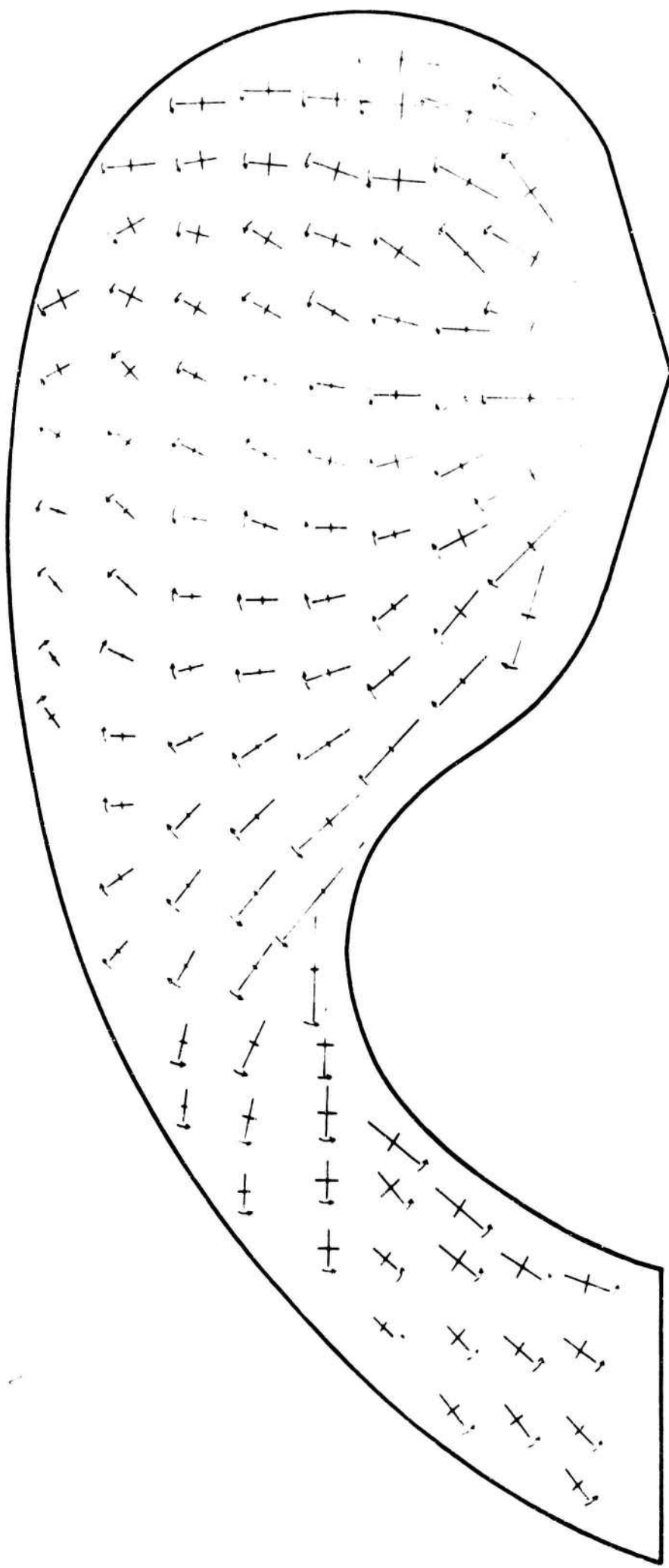
Fig. 86

Momentaneous picture of current
f~1000 Mc/s
t~0
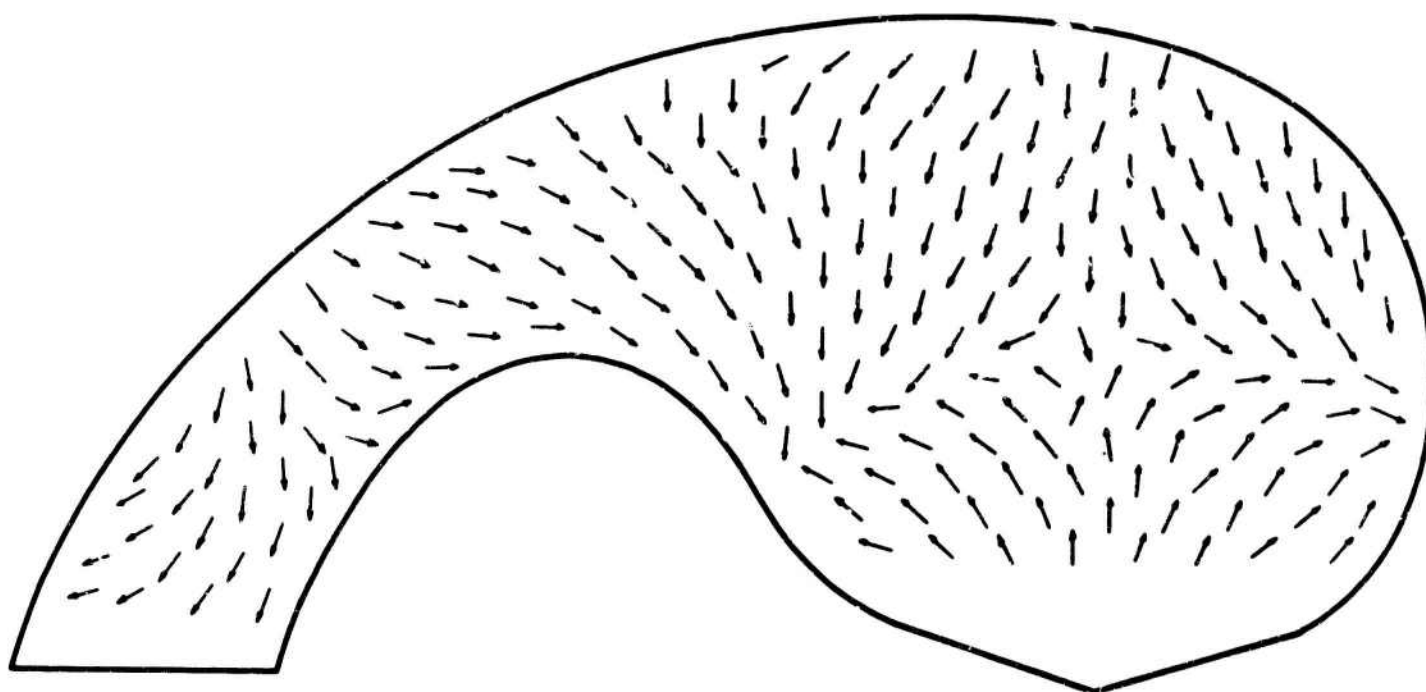
Fig. 87a

f~1000 Mc/s
t~1/10 T
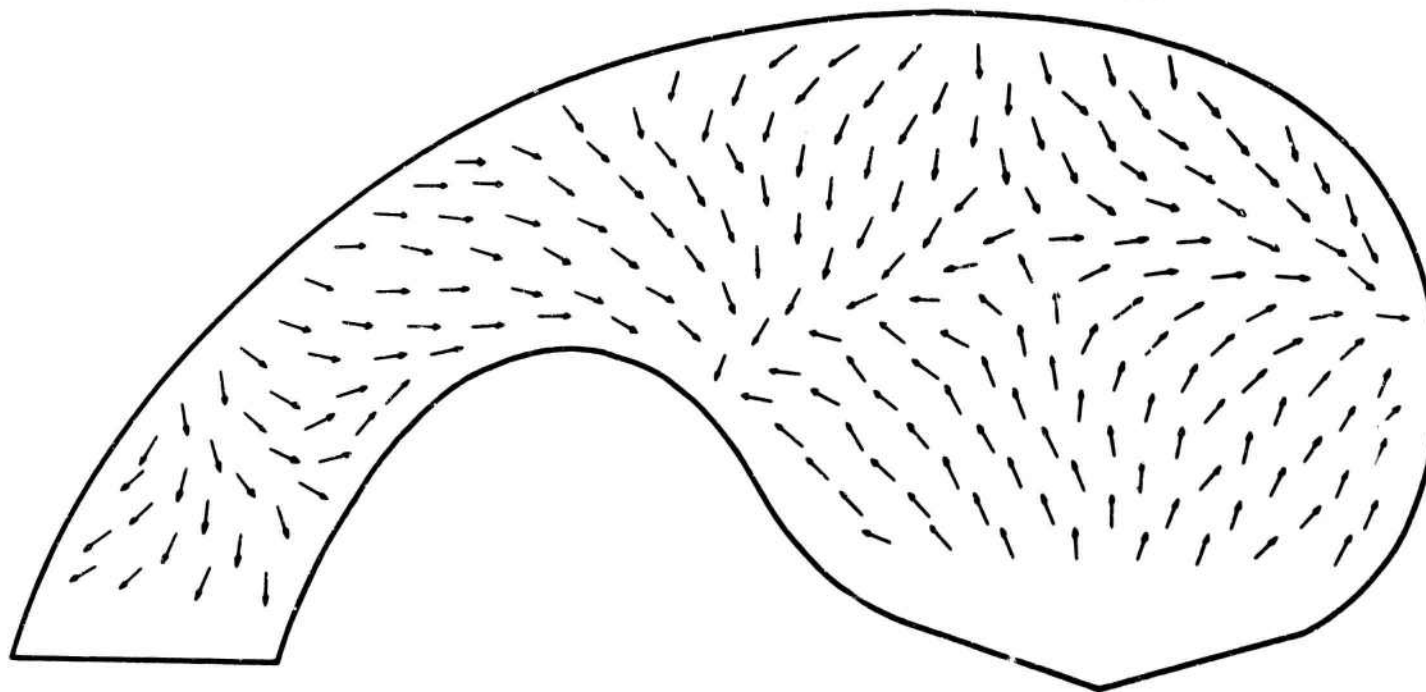
f - 1000 Mc/s

t = 2/10 T
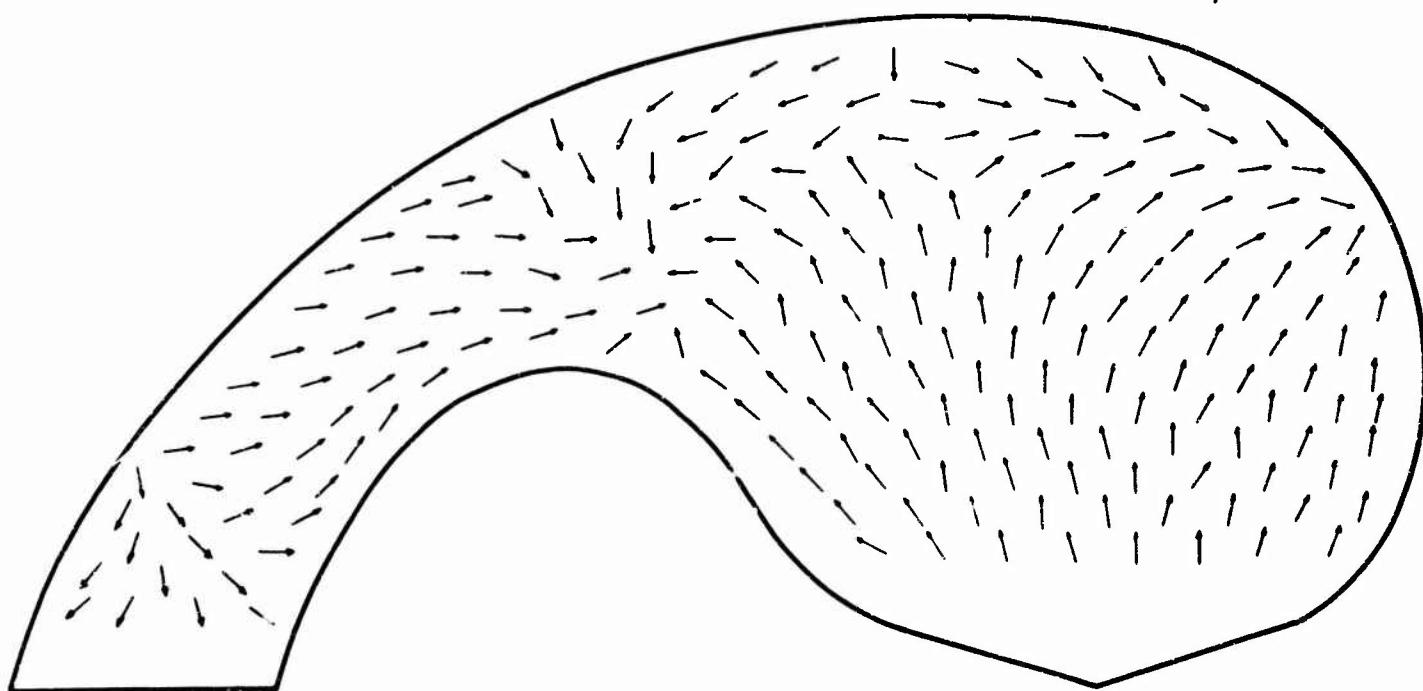
Fig 87c

f - 1000 Mc/s

t - 3/10 T
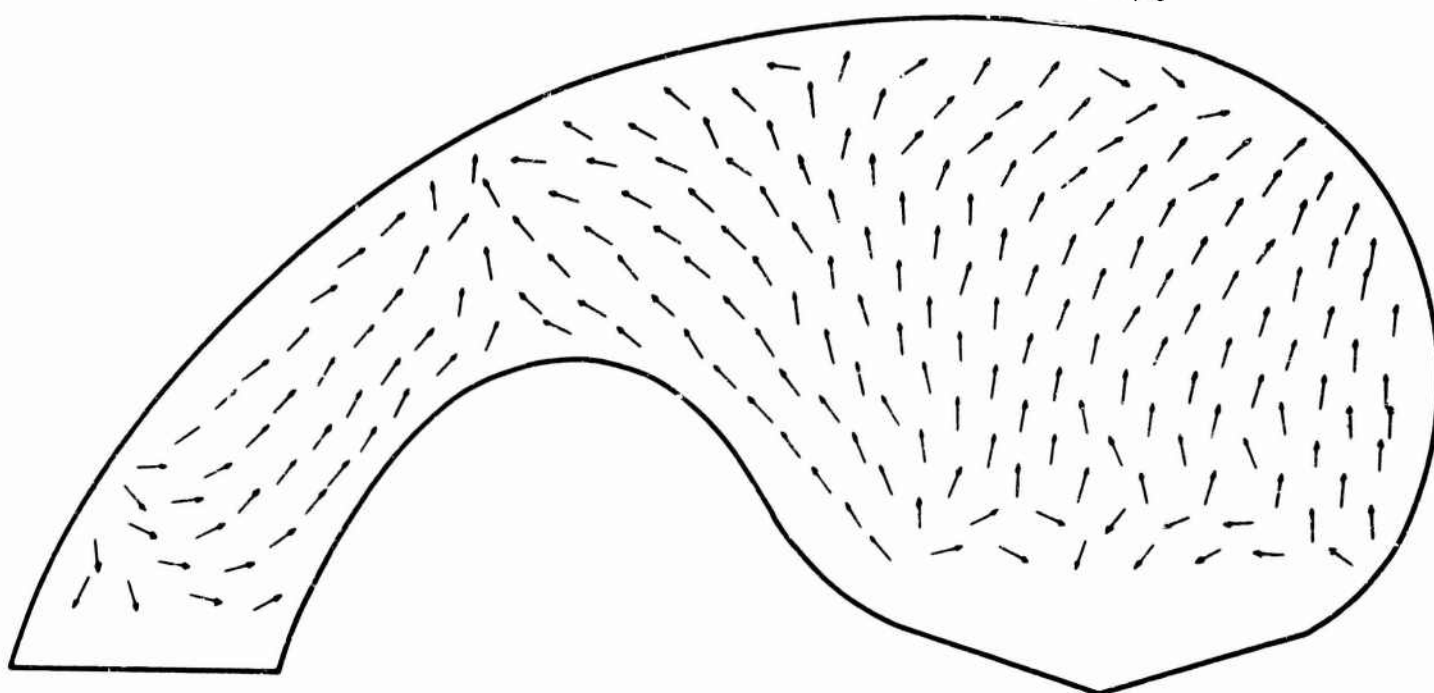
Fig. 87d

f - 1000 Mc/s

t - 4/10 T
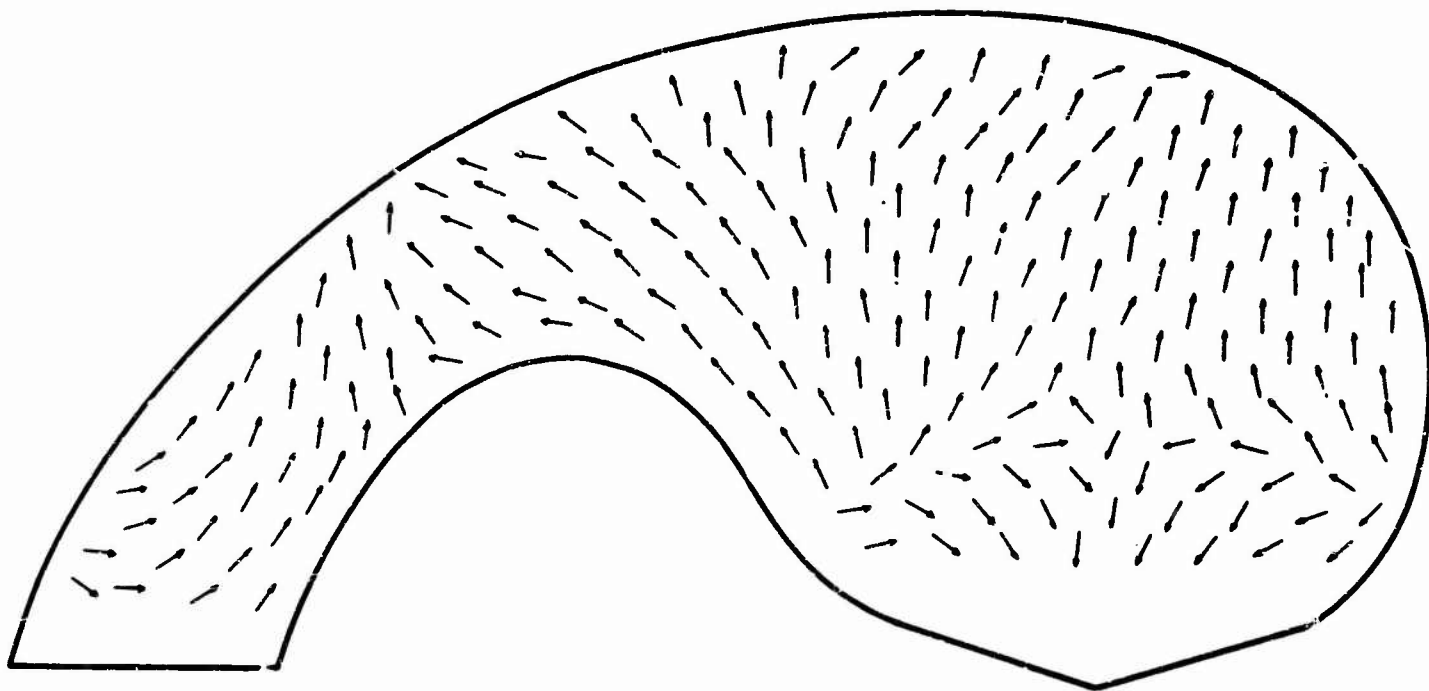
Fig. 87 e

current or H-field amplitudes in db

f = 1700 Mc/s   d/λ₀ = 1.8
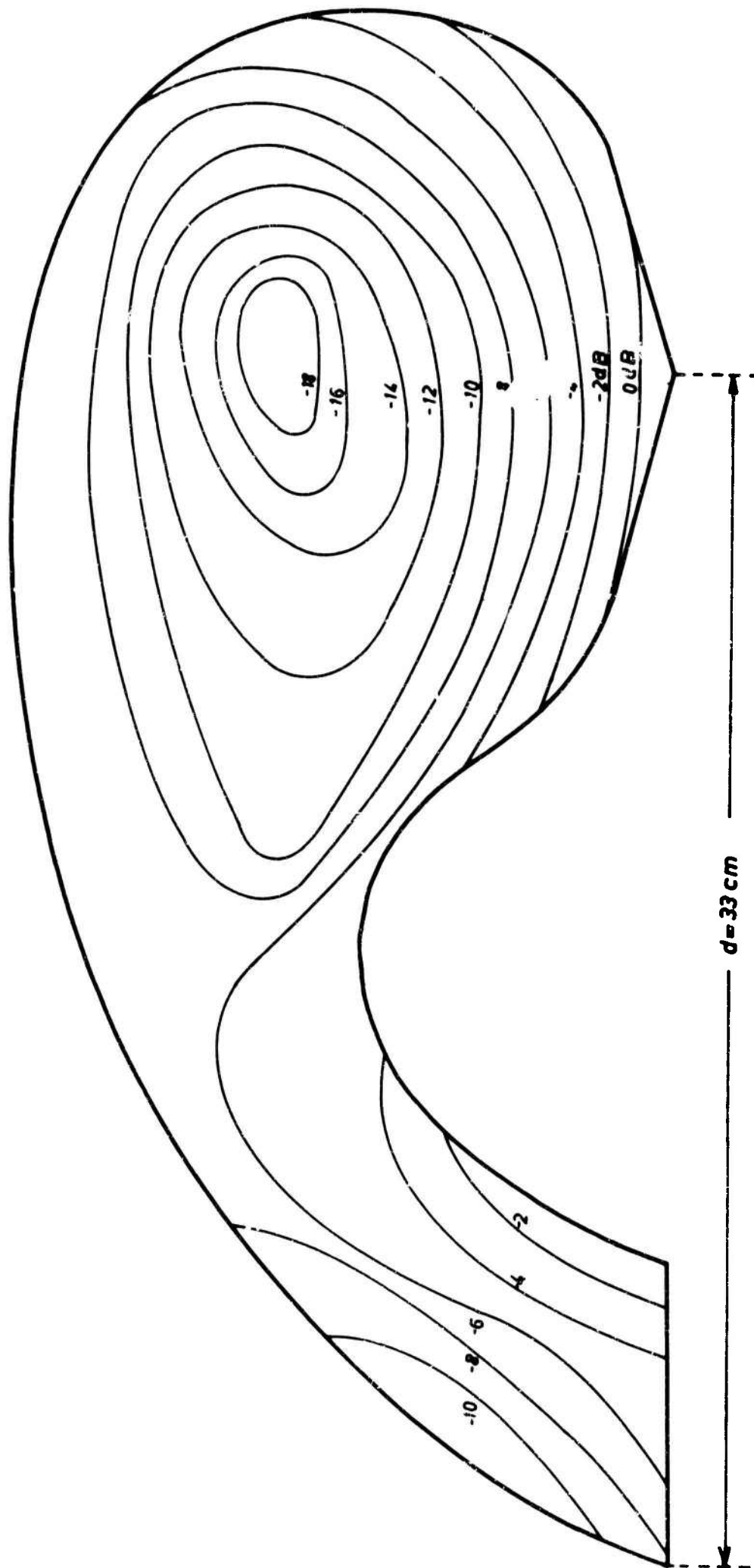
Fig. 88

Ellipses of current

f = 1700 Mc/s   d/λ = 1.8
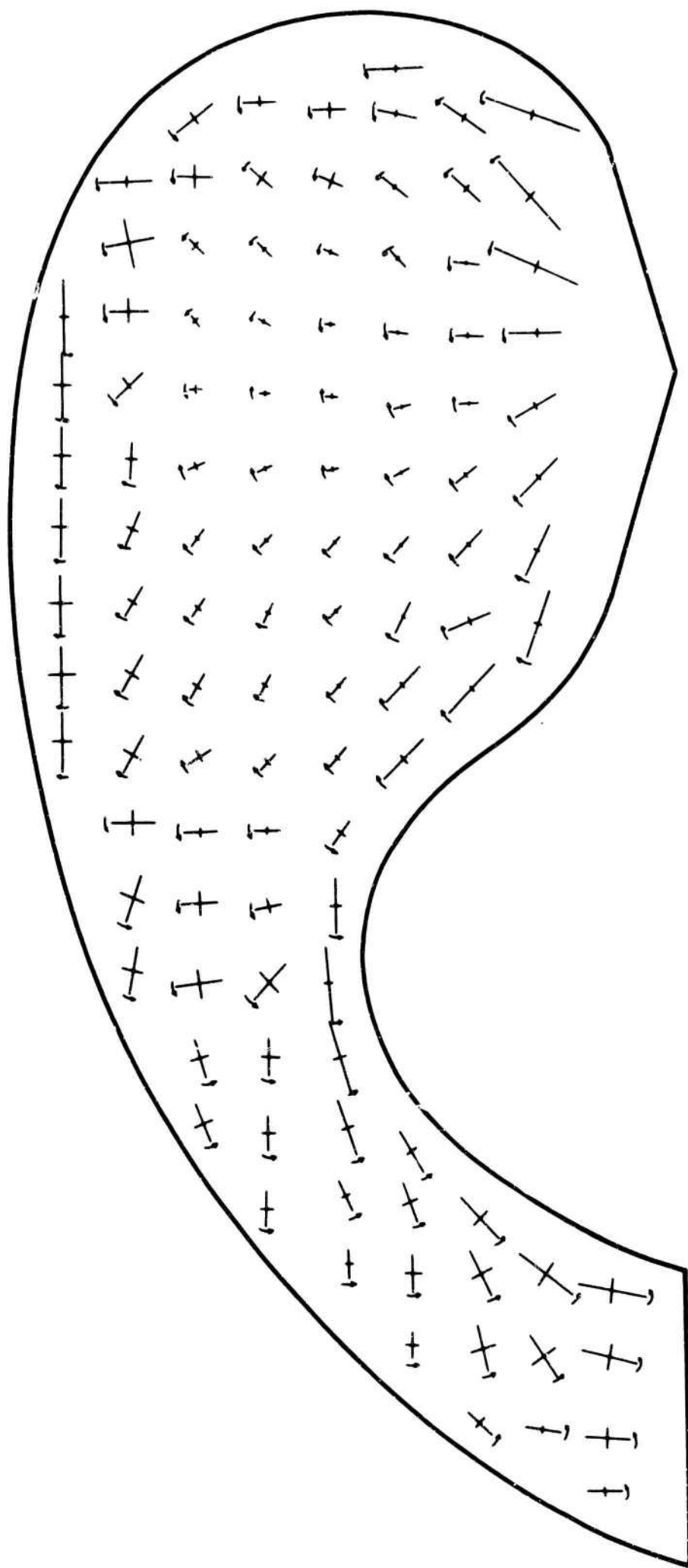
Fig. 89

Momentaneous picture of current
f = 1700 Mc/s
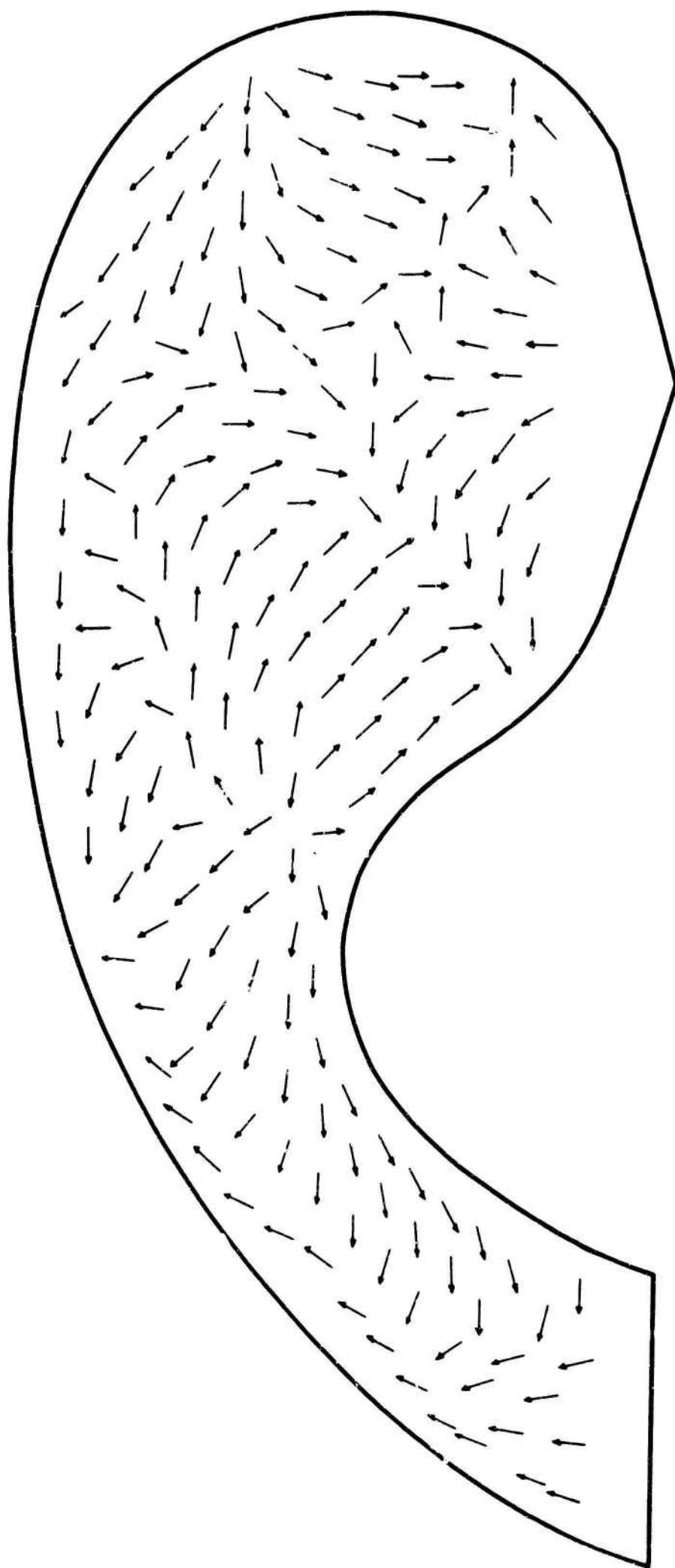
Fig. 90

Fig. 91   1000 Mc/s, $\frac{d}{\lambda} = 1.1$
current or H-field
amplitude in db

connection to
ground plane

feeding point

d = 33cm

Fig. 92 Ellipses of current on ground plane

f = 1000 Mc/s

Fig. 93a

VERTICALDIAGRAM
φ=0°   Θ var.
POLARIZATION E_φ

VERTICALDIAGRAM
φ=90°   θ var.
POLARIZATION E_ϕ

Fig. 93b

Fig. 93c

VERTICAL DIAGRAM
$\phi = 90°$ ϑ var.
POLARIZATION E_ϕ

0.728

1.82

0.546

1.45

d/λ
0.182

0.354

1.09

3.055

0.908

2.62

Fig. 93 d

HORIZONTALDIAGRAM
$\Theta = 86°$ ϕ var.
POLARIZATION E_Θ

0.728

1.82

0.546

1.45

0.364

1.09

3.055

d/λ
0.182

0.908

2.62

0,728

1,82

0,546

1,45

0,364

1,09

3,055

d/λ
0,182

0,908

2,62

HORIZONTALDIAGRAM
$\Theta = 0°$ ϕ var.
POLARIZATION E_Θ

Fig. 93 e

Bibliography

[1] K. Fujimoto: Analysis and Design of Tunnel Diode Dipole Antennafiers, Contract AF 33(657)-10386, 15 May 1963

[2] K. Fujimoto: Some General Properties of the Tunnel-Diode-Loaded Dipole Antenna, Contract AF 33(657)-10386, 15 February 1964

[3] H.H. Meinke: Research on Electrically Small Antennas, Final Report Contract AF 61(052)-506 30 April 1963

[4] E.E. Altschuler: The Traveling Wave Linear Antenna, Contract AF 19(604)-4118, 5 May 1960

[5] H.H. Meinke: Einführung in die Elektrotechnik höherer Frequenzen, Berlin 1961

[6a] H.H. Meinke, F.W. Gundlach: Taschenbuch der Hochfrequenztechnik, Berlin 1962, section H

[6b] H.H. Meinke, F.W.Gundlach: section C

[7] John R. Copeland, William J.Robertson: Antennaverters and Antennafiers, Contract AF 33(616)-6211, 15 December 1961

[8] K. Küpfmüller: Einführung in die theoretische Elektrotechnik, Berlin 1962, page 406

[9] G.S. Ajsenberg: Kurwellenantennen, Leipzig 1954

[10] E.M. Turner: US-Patent
     W.P. Turner:

[11] V.H. Ramsey: Frequency Independent Antennas,
                         IRE Nat. Conv. Rec..(March 1957)
                         page 114-118

Glossary of Symbols

a = distance of the rod antennas

$\ddot{a}$ = length of the short-circuited line

a' = length of the transmission line

α = attenuation constant; angle

b = length of the upper part of the antenna

β = phase constant

C_p = parallel capacity of the TD

D = diameter of the antenna rod

d = distance

E_z = electric field strength in the direction of the z-coordinate

η = efficiency

f = frequency

f_o = operation frequency

f_g = cut-off frequency

$-G_n$ = negative conductance of the TD

g_p = amplification factor

γ = α + jβ = complex transmission-line constant

H = magnetic field strength

h_o = total height of the antenna

h_1 = height of the lower part of the antenna

I = current

I_a = antenna current at the feeding point

k = coupling coefficient

L_s = series inductance of the TD

λ_o = wavelength in free space λ = wavelength

m = reciprocal value of VSWR

p = complex radian frequency

P = complex power

P_s = radiated complex power

P_w = real power

P_{sw} = radiated real power

r = reflection coefficient

ρ = radius

R_i = internal resistance

$-R_n$ = negative resistance of the TD

R_s = series resistance of the TD

R_s' = additional series resistance

$\left.\begin{matrix} R_{s11} \\ R_{s12} \end{matrix}\right\}$ = real part of the $\left\{\begin{matrix} \text{inherent} \\ \text{mutual} \end{matrix}\right\}$ radiation impedance

δ = real part of the complex radian frequency p

t = time

T = time for one period

U = voltage

W = impedance inserted in the antenna rod

ω = radian frequency

$\left.\begin{matrix} X_{s11} \\ X_{s12} \end{matrix}\right\}$ = imaginary part of the $\left\{\begin{matrix} \text{inherent} \\ \text{mutual} \end{matrix}\right\}$ radiation impedance

Y_i = internal admittance

Z_1 = input impedance

Z_2 = terminating impedance

Z_{11}, Z_{12}, Z_{21}, Z_{22} = parameters of the impedance matrix

Z_a = extermal impedance at the terminals of the TD

Z_e = input impedance

Z_i = internal impedance

Z_L = characteristic impedance of the transmission line

Z_o = wave impedance of free space = $120\pi\ \Omega$

Z_{s11}, Z_{s12}, Z_{s21}, Z_{s22} = radiation impedances

Z_T = input impedance of the TD

AF 61 (052) - 506

ASR

Electronics

Technische Hochschule
München, Institut für
Hochfrequenztechnik
30. Oktober 1964

RESEARCH ON ANTENNAS
Prof. Dr. H. H. Meinke

Abstract: Part I. Rod antennas with integrated tunnel diodes. A rod is cut in 2 parts and joined again by a complex impedance. This impedance is produced by a tunnel diode, shunted by a short circuited line of variable length. Current distribution and input impedance are calculated and measured. Amplification factor and mutual coupling between 2 parallel antennas are

---

---

treated theoretically. A method for measuring the mutual coupling is developed.

Part II. Scimitar antennas. For better understanding the radiation diagram, the electrical and magnetical near field and the current distribution on the scimitar is measured. To improve the broad-band matching of the input impedance and the radiation diagrams new forms of scimitars were tested (radiation diagram, input impedance, near field and current distribution).